International Journal of Advanced Engineering Research and Science

(IJAERS)

An Open Access Peer Reviewed International Journal

FOREWORD

I am pleased to put into the hands of readers Volume-4; Issue-8: 2017 (Aug, 2017) of **"International Journal of Advanced Engineering Research and Science (IJAERS) (ISSN: 2349-6495(P)| 2456-1908(O)"** , an international journal which publishes peer reviewed quality research papers on a wide variety of topics related to Science, Technology, Management and Humanities. Looking to the keen interest shown by the authors and readers, the editorial board has decided to release print issue also, but this decision the journal issue will be available in various library also in print and online version. This will motivate authors for quick publication of their research papers. Even with these changes our objective remains the same, that is, to encourage young researchers and academicians to think innovatively and share their research findings with others for the betterment of mankind. This journal has DOI (Digital Object Identifier) also, this will improve citation of research papers.

I thank all the authors of the research papers for contributing their scholarly articles. Despite many challenges, the entire editorial board has worked tirelessly and helped me to bring out this issue of the journal well in time. They all deserve my heartfelt thanks.

Finally, I hope the readers will make good use of this valuable research material and continue to contribute their research finding for publication in this journal. Constructive comments and suggestions from our readers are welcome for further improvement of the quality and usefulness of the journal.

With warm regards.

Dr. Swapnesh Taterh
Editor-in-Chief
Date: Sept, 2017

Vol-4, Issue-8, Aug 2017

Effect of Intermediate Quenching and Tempering on the Mechanical Behaviour of Low Carbon Steel

Sunday Chukwuyem Ikpeseni

Department of Mechanical Engineering, Delta State University, P.M.B. 1, Abraka, Oleh Campus, Delta State, Nigeria.

Abstract— This research has assessed the impact of intercritical annealing using the intermediate quenching technique and tempering on the mechanical properties of low carbon steel. The procedure involved austenitizing at 850°C for 1hour followed by quenching in water and thereafter annealed at 730°C, 750°C and 770°C (i.e. α + γ region) for 30 minutes and then quenched in water again. Some of the as-quenched samples were tempered at 320°C for 1hour and cooled in still air. Tensile, hardness and impact tests as well as microstructure characterization were conducted for samples from all the heat treatment schedules. It was observed from the results that martensite volume fraction increases almost linearly as a function of temperature. Ductility and impact decreased with increase in temperature. Tempering deteriorated the assessed mechanical properties. Hence, for a steel of this composition, intermediate quenching should not be followed by tempering.

Keywords— intermediate quenching, intercritical annealing, mechanical properties, martensite volume fraction, dual phase steel.

I. INTRODUCTION

The microstructure of steels can be altered by changing processing parameters, which ultimately affects their mechanical properties. These process parameters which can be altered include the base steel composition, mode of manufacture, type of heat treatment and parameters of heat treatment such as temperature, soaking time, heating and cooling rates, cooling media etc.

Intermediate quenching is one of the various types of heat treatment for developing dual phase (DP) steels. Over the recent years, DP steels have been widely used in the automotive industries because of good compromise between its high strength and reasonable ductility which enhances performance and crash safety as well as high fuel economy due to weight reduction as a result of the improve strength. This weight reduction also impacts positively on the environment because of drastic reduction in emissions to the environment. Apart from the automotive industry, DP steels have found applications in oil and gas industries, building and structural industries, earth moving equipment (yellow goods) etc. Furthermore, very tall structures in the form of skyscrapers are becoming common these days due high demand on land. Hence, the urgent need to provide common materials with ultra-high strength at reasonable cost cannot be over emphasized. This will help to militate against the frequent occurrence of collapsed buildings in the country. Again, the high demand for large diameter and high strength pipes for the conveyance of crude oil and petroleum productions requires materials with excellent formability, high strength and good weldability.

Hence, this research is intended to investigate the influence of intermediate quenching and tempering on the mechanical behaviour of low carbon steel. Intermediate quenching uses martensite microstructure as the starting or initial microstructure for the intercritical annealing heat treatment process. Bag*etal* have worked on intermediate quenching, step quenching and direct quenching using high strength low alloy (HSLA) steel. Ikpeseni *etal* had worked on step quenching and direct quenching using low carbon steel [17, 18]. A good number of researchers have worked on the effect of processing parameters on the properties of dual phase steels with encouraging results [1 – 20]. [1 – 3] examined the effect of cooling rates; the effect of alloying element on mechanical properties was investigated by [4 – 12]; while [13, 16,17] worked on the effect of the temperature. Furthermore, [14, 15, 17] examined strain or deformation effect while [15, 18 - 21] examined the impact of microstructure on mechanical properties of the investigated steels.

II. MATERIALS AND METHOD

2.1 Materials

The carbon steel used for this research was supplied by universal steel Lagos, Nigeria. Its chemical composition shown in Table 1was determined as documented in [17].

Table.1: Chemical Composition of the Investigated Steel

Element	C	Si	Mn	S	P	Cr	Ni	Cu	B	Ti	Fe
Weight (%)	0.23	0.20	0.73	0.03	0.03	0.12	0.10	0.27	0.001	0.001	98.28

2.2   Methods
2.2.1   Sample preparations
Standard samples for tensile test, impact test, hardness test and microscopic examination were prepared from the as-received 16mm diameter rod. All the samples were prepared following standard procedures.

2.2.2   Heat Treatments
All the samples were first of all normalized in a muffle furnace at 850^0C for 1hr in order to cancel the effects of previous mechanical, thermal or thermo-mechanical treatments. After normalizing some of the samples were left as control, while others were subjected to the intermediate quenching (an intercritical annealing) heat treatment. This involved austenitizing at 850^0C for 1hr and quenching in water to produce martensite which was used as the starting or initial microstructure for the intercritical annealing. Thereafter, all the samples were intercritically annealed at various temperatures of 730^0C, 750^0C and 770^0C (i.e. in α + γ region) for thirty minutes each, followed by quenching in water. Then some set of these sample were tempered at 320^0C for 1hr, while the others are left in their intermediate quenched state.

2.2.3   Mechanical Properties Testing
Tensile test: an instron Universal tensile testing machine was used to conduct the tensile test. The sample were tested at a cross head speed of 20mm/min and were all tested to fracture at room temperature (25 -27^0C). All the tensile properties data were captured by the interfacing computer system.
Impact test: The charpy impact tester (Avery) was used to determine the absorbed energy and thereafter the impact

strength (toughness) of the heat treated samples were evaluated. Again, all the samples were tested to fracture at room temperature. Thereafter the fractured surfaces were examined under the scanning electron microscope (SEM) in order to ascertain the mode of fracture.
Hardness test: The hardness property of samples from all the heat treatment schedules were examined using the Vickers hardness testing machine (LM 7 700AT Leco) with a dwell time of 10 – 15S. The hardness values are digitally displayed on the machine screen.

2.2.4   Microstructure Characterization
Nikon Eclipse (me 600) was used to examine the microstructures developed after the various heat treatment schedules. This was preceded by sample preparation using standard procedures. A combination of sylvert cloth and 0.2µ diamond paste was used to polish the samples while 2% NITAL was used as etchant. The standard grid point count technique was used to determine martensite volume fracture (MVF) as contained in Russ and Dehoff (1999) [22].

III.   RESULTS AND DISCUSSION
3.1   Microstructural Evolution of Intermediately Quenched Samples
Figures 1a - g show the microstructures developed after intermediate quenching and subsequent tempering. The structures revealed predominantly features of ferrite (light) and martensite (grey) with dispersion of carbide or retained austenite (dark) in some of the microstructures.

a

b   c   d

e   f   g
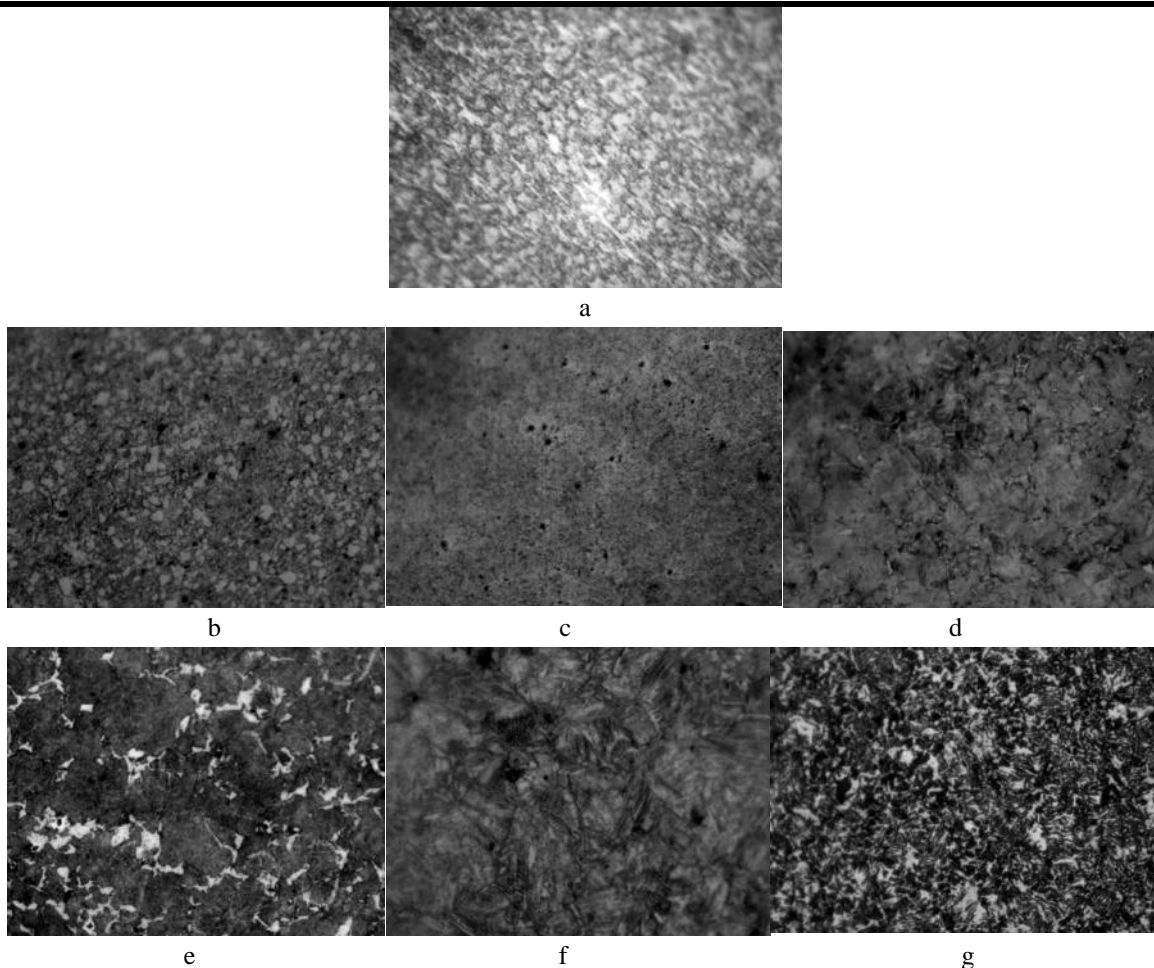
Fig.1: (a) Photomicrograph of A X400 i.e. Phase structure produced by normalizing at 850ºC for one hour. The structure reveals ferrite (light phase) and pearlite (alternate layers of ferrite - light and cementite – dark).(b) Photomicrograph of IQ730 X200. Sample intermediately quenched at 730ºC for 30 minutes. The structure reveals distribution of regularly shaped globular ferrite (light) and martensite (grey) with little dispersed carbide (dark).
(c) Photomicrograph of IQ730T X200. Sample intermediately quenched at 730ºC for 30 minutes and tempered at 320ºC for 1hour. The structure reveals distribution of ferrite (light) matrix, tempered martensite (grey) and dispersed fine carbide (dark).
(d) Photomicrograph of IQ750 X200. Sample intermediately quenched at 750ºC for 30 minutes. The structure reveals distribution of fine fibrous martensite (grey) in a ferrite (light) matrix. (e) Photomicrograph of IQ750T X200. Sample intermediately quenched at 750ºC for 30 minutes and tempered at 320ºC for 1hour. The structure reveals distribution of tempered martensite (gray) and nucleated ferrite (bright) mainly along grain boundaries in a network of ferrite (light) matrix.(f) Photomicrograph of IQ770 X500. Sample intermediately quenched at 770ºC for 30 minutes. The structure reveals lath martensite (grey), ferrite (light) and little dispersed carbide (dark). (g) Photomicrograph of IQ770T X200. Sample intermediately quenched at 770ºC for 30 minutes and tempered at 320ºC for 1hour. The structure reveals network of tempered martensite (gray), ferrite (light) and dispersion of plenty carbide (dark).

Figures 1(b, d and f) are the microstructure photographs of the as-quenched samples subjected to intermediate quench treatment.

Martensite (probably with very small percentage of retained austenite) formed as a product of quenching from the austenitizing temperature (850ºC) was used as the initial microstructure for this treatment. Intercritical annealing at

the various temperatures gradually transforms the formed martensite to austenite and ferrite. Austenite formation from martensite structure was observed to occur by classical heterogeneous nucleation at imperfect lattice sites like spheroids in ferrite, matrix /carbide interface, martensite lath boundaries, and prior austenite grain boundaries [20, 22]. The photomicrographs display tiny but numerous

globular/fibrous martensites after soaking for 30 minutes, with some carbide particles precipitated along prior austenite boundary, in a ferrite matrix in the microstructure (see Fig. 1b, d). Martensite volume fraction is noticed to increase as a function of intercritical annealing temperature. This is so because austenite nucleation at different sites mentioned above continued and increases at higher temperatures. Hence the microstructures became greatly enriched with more martensite on quenching. It was clearly shown (qualitatively) that martensite grain size remained fairly the same. Pinning down of the grain boundaries by precipitated carbide particles in prior boundaries of austenite must have been responsible for this. Honeycombe and Bhadeshia[23] stated that these are usually present in grain boundaries; as such an interaction occurs between the grain boundary and the particles. They explained that when there is replacement of a short length grain boundaries by particles, the interfacial energy help to maintain a stable configuration such that any attempt for the grain boundary to move away or separate from the particles, there is an increase in local energy; as a result the particle exerts a drag on the boundary.

3.1.1 Effect of Intercritical Annealing Temperature and Starting Microstructure on the Volume Fraction of Martensite (MVF)

Martensite was used as starting microstructure for the intermediate quenching intercritical annealing heat treatment to produce the dual phase (ferrite-martensite) structures. The intercritical annealing heat treatment was conducted at various temperatures in order to produce dual phase microstructures with varied proportions of martensite in a ferrite matrix. The effect of intercritical annealing temperature on MVF is presented in Fig. 2. As indicated, it

is clear that MVF increases almost linearly with intercritical annealing temperature. This is in agreement with the observation of earlier published research findings [19, 20,24] As intercritical annealing temperature increases, the amount of austenite increased which transformed to martensite upon quenching. The simulated (fitted) linear curve for the treatment schedule is shown in equation (1) as obtained from Fig. 2.

$$V_M = 0.325T - 203.4 \qquad (1)$$
$$R^2 = 0.953$$

where T = intercritical annealing temperature

V_M = martensite volume fraction

The high value of R^2 indicates a high correlation between the simulated and experimental data, which also indicates the validity and reliability of equation (1).

The high martensite volume fraction of intermediate quenched samples could be attributed to numerous sites for nucleation of austenite which transforms to martensite upon quenching. Some of these sites as suggested by Bag et al [20] include:

a. Prior grain boundaries of austenite
b. Carbide particles precipitated on prior grain boundaries of austenite
c. Spheroids in ferrite
d. Fine carbide arrays formed on the prior martensitic plate/lath boundaries.

The shape, size and distribution of martensite in the microstructures of the samples given the intermediate quenching treatment stems from the process of reversion of austenite from the tempered martensite. Austenite nucleation from the prior martensite could take place at various locations or sites as listed from a – d above.
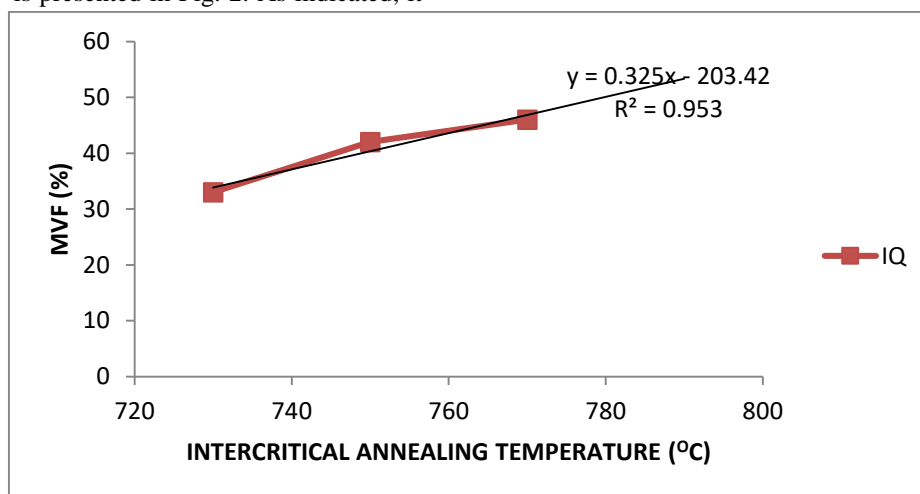
Fig.2: Martensite Volume Fraction vs Temperature

3.1.2 Effect of Tempering on the Microstructure of Intermediate Quenched Samples

On tempering, the as-quenched intermediate quenched samples at 320°C for 1hr, the microstructure consisted of fine grained tempered martensite and ferrite for IQ730T, with dispersion of fine carbide – Fig. 1c, while for IQ750T and IQ770T, the ferrite phase became well defined and coarse with plenty of carbide especially IQ770T as shown in Fig. 1e and g.

3.2.   Effect of Process Parameters on the Mechanical Properties

Figures 3 – 6 present the results of the mechanical properties which show the relationships between the mechanical properties and intercritical annealing temperatures.
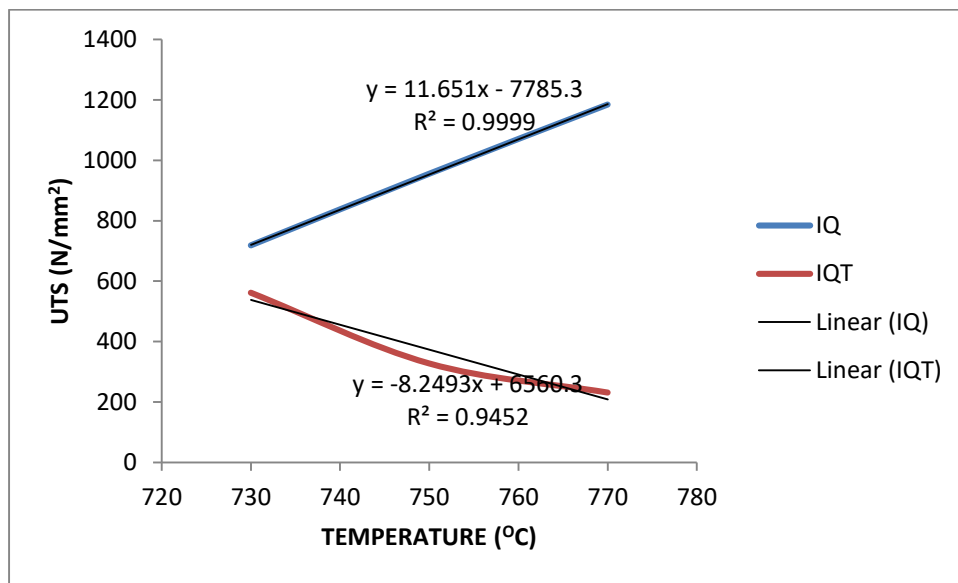
Fig. 3: Ultimate Tensile Strength vs Temperature
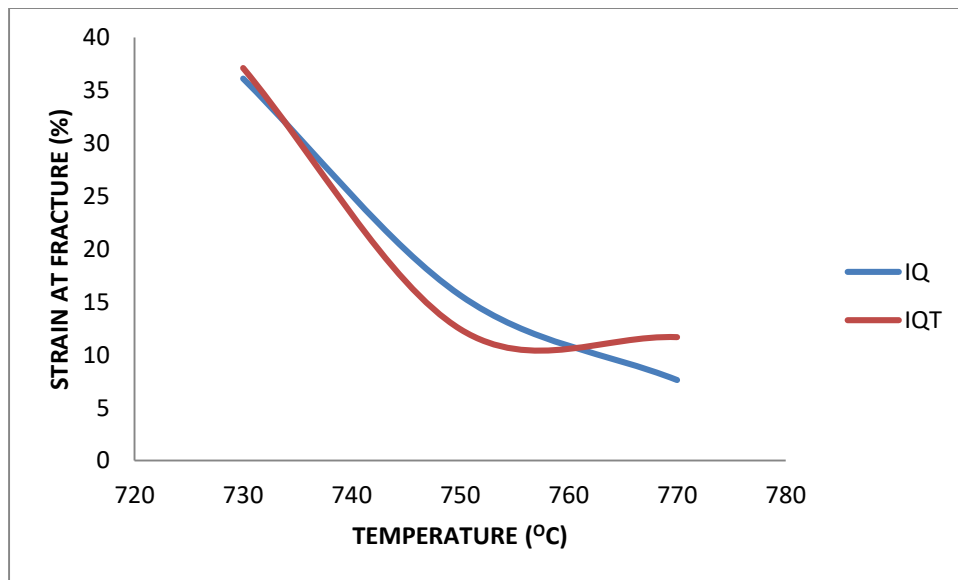
Fig. 4: Strain at Fracture vs Temperature
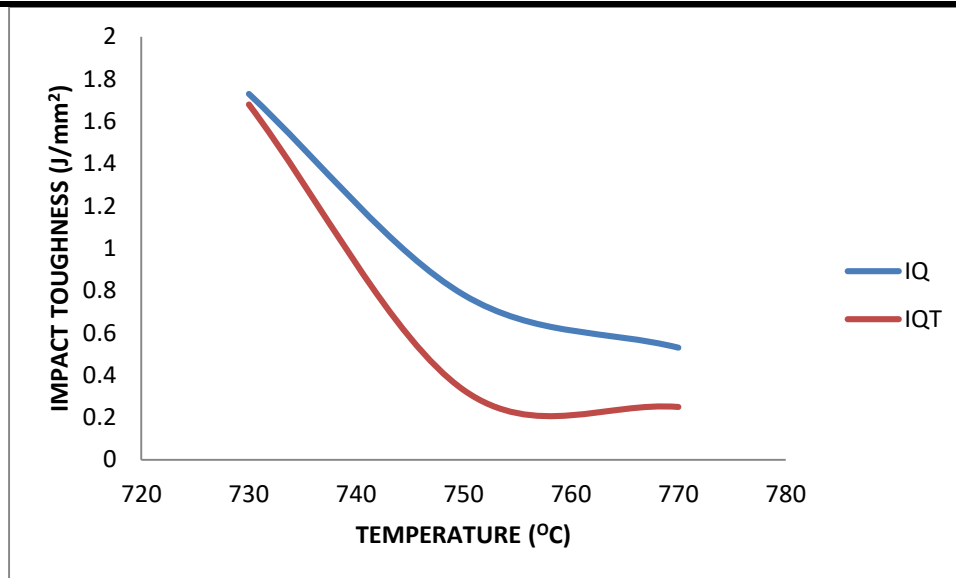
Fig. 5: Impact Toughness vs Temperature
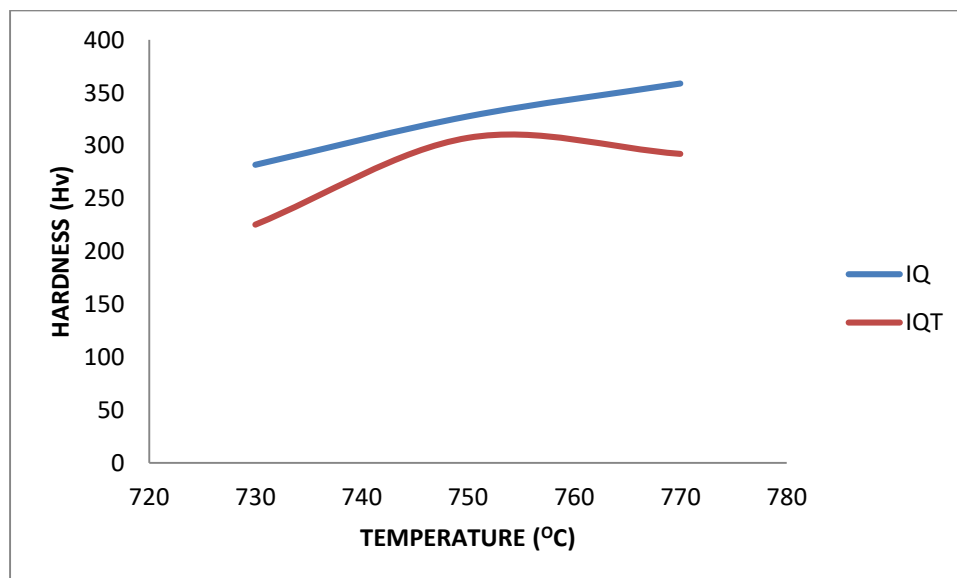
Fig. 6: Hardness vs Temperature

3.2.1 Effect of Annealing Temperature on the Mechanical Properties of Intermediate Quenched Samples

Variation of hardness value temperature for all the samples is presented in Fig. 6. The hardness of intermediate quenched samples increases steadily with rise in temperature within the investigation limit. The rise in hardness value is attributed to the increasing martensite volume fraction as intercritical annealing temperature increases (Fig. 1).

The ultimate tensile strength of samples given the intermediate quenching intercritical heat treatment, increased steadily with increasing temperatureas shown in

Fig. 3 (IQ series). The decrease in strain at fracture (i.e. ductility or total elongation) and impact strength could be traced to nucleation, growth and recrystallization of ferrite and austenite from the initial martensite structure, which upon quenching the nucleated austenite transforms to martensite. Consequently, strain at fracture and impact toughness of samples given this same treatment decreased as temperature increased (Fig. 4 and 5). Continuous yielding was observed for all the samples given this particular treatment, which is a common characteristic of regular dual phase steels. Austenite to martensite transformation involves volume expansion which introduces

residual stress on the surrounding ferrite as a result of the strain produced during the transformation [25,26, 27]. Davis (1979) [28] and Rigsbee*et al* (1979) [29] explained that this change in volume causes neighbouring ferrite grains to be plastically deformed, thus generates high density of mobile dislocations in the surrounding ferrite. This ultimately results to the generation of mobile dislocations. This could have increased the hardness and ultimate tensile strength, while ductility was decreased as a function of temperature. The fall in impact strength and ductility could also be attributed to decreased carbon content of the martensite at higher martensite volume fraction, because MVF increases with increase in temperature and at higher MVF carbon content of martensite decreases.

Optimum mechanical properties for intermediate quenched samples are observed at 730^OC (i.e. 33% martensite volume fraction). A comparison of improvement of properties showed that hardness, ultimate tensile strength, total elongation and impact strength are 74.4%, 7.2%, 64.7% and 33.1% respectively over the normalized samples. Summary of all the assessed mechanical properties is presented in Table 2.

Table.2: Summary of Mechanical Properties Results

SAMPLE	UTS(N/mm^2)	YS (N/mm^2)	YS/UTS	TEL (%)	IS (J/mm^2)	HARDNESS
A	670.55	385.96	0.56	21.97	1.30	161.7
IQ730	718.56	416.76	0.58	36.12	1.73	282.0
IQ750	955.70	583.00	0.61	15.65	0.78	327.8
IQ770	1184.64	805.55	0.68	7.63	0.53	358.9
IQ730T	561.28	325.54	0.58	37.11	1.68	225.3
IQ750T	327.50	-	-	12.43	0.33	307.4
IQ770T	231.31	120.28	0.52	11.67	0.25	292.2

3.2.2 Effect of Tempering on the Properties of Intermediate Quenched Sample

Fig.6 shows that tempering the as-quenched intermediately quenched sample at 320^OC for 1hr decreases hardness (IQT series). However, the hardness increased with temperature and reached a peak at 750^OC. The increased hardness with increase in martensite volume fraction can be attributed to the precipitation of carbide on tempering — see Fig. 1e and g. The decrease in value of hardness observed with tempered intermediate quenched (IQT) samples could be as a result of the coarsening of soft ferrite phase as shown in Fig. 1e and g respectively. This emanated from precipitation of more ferrite from martensite on tempering.

All the other properties equally deteriorated on tempering at 320^OC for 1hour.

Conventional stress – strain curve with discontinuous yielding was observed for IQ730T (i.e. sample intermediately quenched with 33% martensite volume fraction and tempered at 320^OC for an hour), while the others exhibited continuous yielding which is typical of conventional dual phase steel.

3.3 Fractography

Figure 7 shows the fractured surfaces of the failed impact test samples upon testing. Figures 7b, c and d present the fractured surfaces of IQ730, IQ730T and IQ750 samples respectively. They revealed predominantly dimple fibrous surface which is typical of materials with good combination of high strength, ductility and impact toughness. It showed that IQ730T has majorly dimple fibrous fractured surface with dislocations cutting across circular obstacles. On the other hand, Fig. 7e, f and g display the fractured surfaces of IQ750T, IQ770 and IQ770T respectively, which revealed majorly pure or quasi cleavage fracture, no wonder the low impact strength exhibited by these samples (Table 2).

a

b

c

d

e

f

g
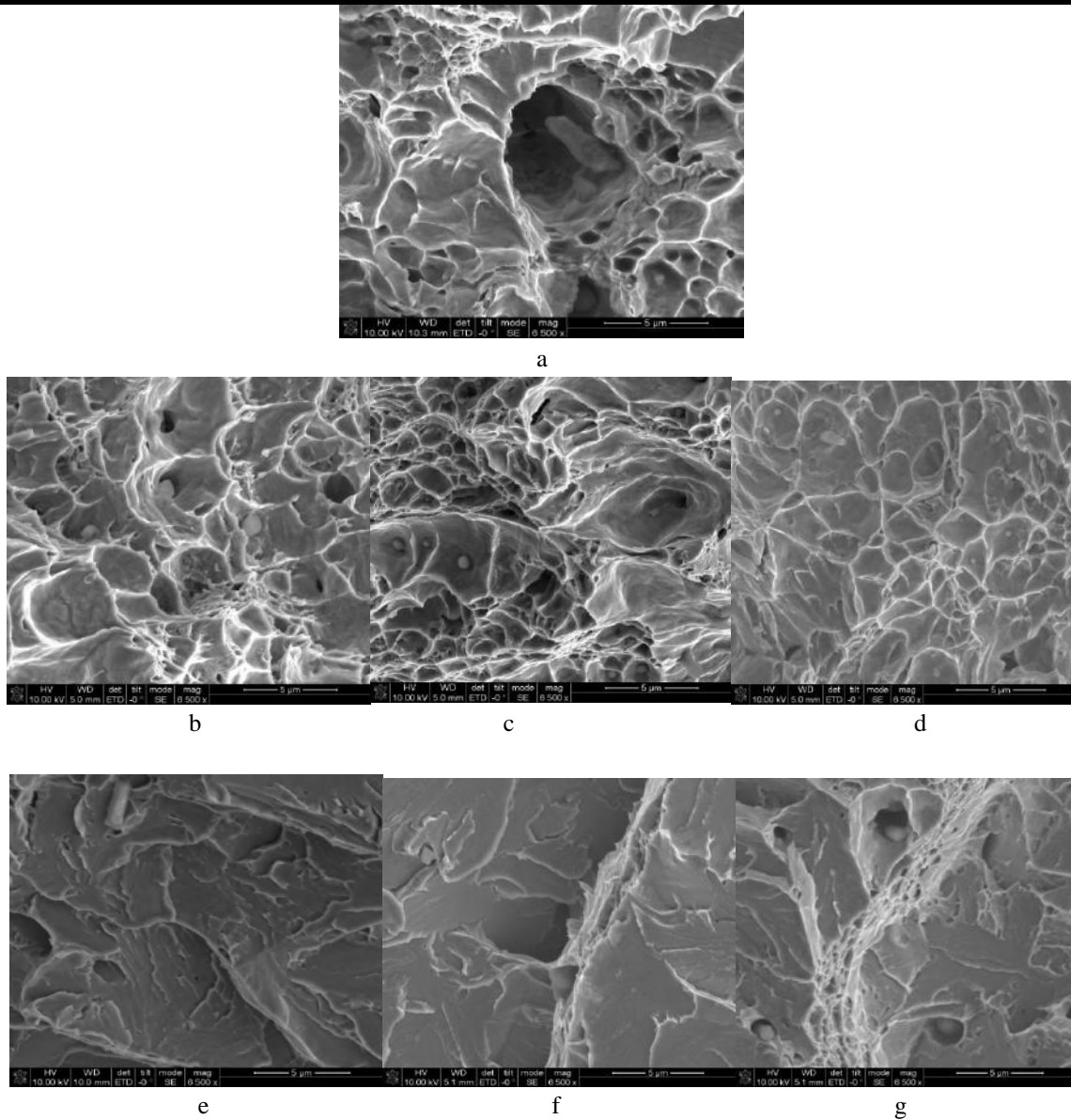
Fig. 7: (a)Impact fractured surface ofA (i.e. Sample normalised at 850°C for one hour). *Structure reveals fibrous surfaces with cavity.* ***(b)Impact fractured surface ofIQ730(i.e.Sample intermediately quenched at 730°C for 30 minutes).*** *Structure reveals fibrous surface.*

(c) Impact fractured surface of IQ730T (i.e. Sample intermediately quenched at 730°C for 30 minutes and tempered at 320°C for 1hour). *Structure reveals majorly dimple fibrous fractured surface with dislocations climbing on circular obstacles.* ***(d) Impact fractured surface of IQ750 (i.e. Sample intermediately quenched at 750°C for 30 minutes).*** *Structure reveals fibrous fractured surface.* ***(e)Impact fractured surface ofIQ750T(i.e.Sample intermediately quenched at 750°C for 30 minutes and tempered at 320°C for 1hour).*** *Structure reveals pure cleavage surface.* ***(f) Impact fractured surface of IQ770 (i.e. Sample intermediately quenched at 770°C for 30 minutes).*** *Structure reveals quasi cleavage fractured surface.* ***(g) Impact fractured surface of IQ770T (i.e.Sample intermediately quenched at 770°C for 30 minutes and tempered at 320°C for 1hour).*** *Structure reveals quasi cleavage fractured surface. Presence of some cracks across grain boundaries was also observed.*

IV.   CONCLUSION

From the analysis conducted in this research, it can be concluded that for intermediate quenching heat treatment:

i.   Increase in intermediate quenching temperature leads to increased MVF.

ii.   Tensile strength and hardness value of the as-quenched steel increased with increase in temperature and MVF while impact toughness and ductility decreases with increase in temperature and MVF.

iii. Tempering the as-quenched samples deteriorated all the properties assessed.

iv.   Ferrite/martensite microstructures associated with conventional DP steels was developed from the investigated low carbon steel using intermediate quenching intercritical annealing heat treatment.

It is therefore recommended that unlike the step quenching technique, for a carbon steel of this composition, it should not be tempered after intermediate quenching heat treatment.

REFERENCES

[1] Sakuma, Y.; Matsumura, O. and Takechi, H. (1991): Mechanical-Properties and Retained Austenite in Intercritically Heat-Treated Bainite-Transformed Steel and Their Variation with Si and Mn Additions. *Metallurgical Transactions A,* 22 (2): 489-498.

[2] Minote, T.; Torizuka, S.; Ogawa, A. and Niikura, M. (1996): Modelling of Transformation Behaviour and Compositional Partitioning in TRIP Steel. *ISIJ International,* 36 (2): 201-207.

[3] Speer, J. and D. Matlock (2002): Recent Developments in Low-Carbon Sheet Steels.*Journal of the Minerals, Metals and Materials Society,*54(7): p. 19-24.

[4] Bleck, W. and K. Phiu-On (2005): Microalloying of Cold-formable Multi Phase Steel Grades. *Journal of the Minerals Metals & Materials Society,* 54 (7): 19-24.

[5] Speich, G.R. (1990): Dual-Phase Steels, in ASM Handbook, *ASM International,*424-429.

[6] Llewellyn, D.T. and D.J. Hillis (1996): Dual phase steels.*Ironmaking and Steelmaking*, 23(6): 471-478.

[7] Verdeja, J.I., J.A. Pero-Sanz, and J. Asensio (2005): Multiphase Steels: Structure – Mechanical Properties Relationships in the Cold Rolled and Continuous Annealed Condition.*Microalloying for NewSteel Processes and Applications*, 500-501: 429-435.

[8] El-Sesy, I.A. and Z.M. El-Baradie (2002): Influence Carbon and/or Iron Carbide on the Structure and Properties of Dual-Phase Steels.*Materials Letters*, 57(3): 580-585.

[9] Oliver, S., T.B. Jones, and G. Fourlaris (2007): Dual Phase versus TRIP Strip Steels: Comparison of Dynamic Properties for Automotive Crash Performance.*Materials Science and Technology*, 23(4): 423-431.

[10] DeArdo, A.J.; Gray, J.M. and Meyer, L. (1984): Fundamental Metallurgy of Niobium in Steel. San Francisco, California, 685-759.

[11] Backe, L. (2009): Modeling the Microstructural Evolution during Hot Deformation of Microalloyed Steels. Ph.D. Thesis, Royal Institute of Technology, Stockholm.

[12] Yamamoto, S.; Ouchi, C. and Osuka, T. (1982): The Effect of Microalloying Elements on the Recovery and Recrystallization in Deformed Austenite. Thermomechanical Processing of Microalloyed Austenite, Pittsburgh, Pennsylvania, 613-639.

[13] Alaneme K.K., Ranganathan S. and Mojisola T. (2010): Mechanical Behaviour of Duplex Phase Structures in a Medium Carbon Low Alloy Steel, *Journal of Minerals and Materials Characterization and Engineering*, 9 (7): 621 – 633.

[14] Calcagnotto, M.; Ponge, D. and Raabe, D. (2008): Ultrafine Grained Ferrite/Martensite Dual Phase Steel Fabricated by Large Strain Warm Deformation and Subsequent Intercritical Annealing. *ISIJ International,* 48 (8): 1096-1101.

[15] Park, K.T.; Lee, Y.K. and Shin, D.H. (2005): Fabrication of Ultrafine Grained Ferrite/Martensite Dual Phase Steel by Severe Plastic Deformation. *ISIJ International,* 45 (5): 750-755.

[16] Hanzaki, A.Z.; Hodgson, P.D. and Yue, S. (1997): Retained Austenite Characteristics in Thermomechanically Processed Si-Mn Transformation-induced Plasticity Steels. *Metallurgical and Materials Transactions A,* 28 (11): 2405-2414.

[17] Ikpeseni S.C., Onyekpe B.O. and Momoh I.M. (2015): Effect of Tempering on the Microstructure and Mechanical Properties of Austenitic Dual Phase Steel. *International Journal of Physical Sciences,* 10(16): 490 – 497. DOI: 10.5897/IJPS 2015.4377

[18] Ikpeseni S.C., Onyekpe B.O. and Ovri H. (2015): Influence of Intercritical Annealing Temperature on Mechanical Properties and Microstructure of 0.23%C

Low Alloy Steel. *Nigerian Journal of Technology (NIJOTECH),* 349(3): 499 – 505. http://dx.doi.org/10.4314/njt.v34i3.11

[19] Majid P. (2010): Tensile Strength and Ductility of Ferrite – Martensite Dual Phase Steels, *Association of Metallurgical Engineers of Serbia (AMES)*, 187 – 194.

[20] Bag, A.; Ray, K.K. and Dwarakadasa, E.S. (1999): Influence of Martensite Content and Morphology on Tensile and Impact Properties of High-Martensite Dual-Phase Steels. *Metallurgical and Materials Transactions A*, 30 (5): 1193-1202.

[21] Ikpeseni S.C. (2016): The Effect Of Microstructure on the Mechanical Properties and Corrosion Susceptibility of Dual Phase Steel Developed from 0.234%C Steel. Ph.D. Thesis submitted to P.G. School, University of Benin, Benin City, Nigeria.

[22] Russ J.C. and Dehoff R.T. (1999): Practical Stereology. 2nd Ed, *Plenum Press,* New York.

[23] Honeycombe, R.W.K and Bhadeshia,H.K.D.H, (1995): Steels, Microstructure and properties,2nd ed., *Edward Arnold,* London.

[24] Dzupon M., Parilak L. Kollarova M. and Sinaiova I. (2007): Dual Phase Ferrite – Martensitic Steel Micro-Alloyed with V- Nb. *Metabk,* 46(1)15-20.

[25] Timokhina, I.B.; Hodgson, P.D. and Pereloma, E.V. (2004): Effect of Microstructure on the Stability of Retained Austenite in Transformation-Induced-Plasticity Steels. *Metallurgical and Materials Transactions A,* 35A (8): 2331-2341.

[26] Colla, V.; De Sanctis, M.; Dimatteo, A.; Lovicu, G.; Solina, A. and Valentini, R. (2009): Strain Hardening Behavior of Dual-Phase Steels. *Metallurgical and Materials Transactions A,* 40A (11): 2557-2567.

[27] Calcagnotto, M.; Ponge, D.; Demir, E. and Raabe, D. (2010): Orientation Gradients and Geometrically Necessary Dislocations in Ultrafine Grained Dual-Phase Steels Studied by 2D and 3D EBSD. *Materials Science and Engineering A,* 527 (10-11), 2738-2746.

[28] Davies, R.G. (1979): Early Stages of Yielding and Strain Aging of a Vanadium-Containing Dual-Phase Steel. *Metallurgical Transactions A,* 10 (10): 1549-1555.

[29] Rigsbee, J.M.; Abraham, J.K.; Davenport, A.T.; Franklin J.E. and Pickens, J.W. (1979): Structure and Properties of Dual-phase Steels. Eds. Kot, R.A. and Morris, J.W. *TMS-AIME,* New York, 304-329.

Cement Mortar Restorations and Disorders in the Archaeological Site of Chellah

Meriem Benharbit

Institut National des Sciences de l'Archéologie et du Patrimoine

Abstract— *The restoration works undertaken in the archaeological site of Chellah in the Sixties used cement for the consolidation of the Roman structures undercovered. They're mainly consisting of calcareous rocks, which density, porosity, and hardness are lower then cement, and they're clearly weakened. Indeed, the capillary increase to which are subjected the structures allowed to convey salts whose advance is blocked by the introduced cement mortar. Trapped in the calcareous rock, the salts contribute to the acceleration of its degradation.*

Keywords—Chellah, restoration, incompatibility, stone, cement.

I. INTRODUCTION

In the 1960s, Chellah's archaeological site saw the consolidation of masonry and structures following the discovery of buildings dating back to Roman times. As a result of this work, where the cement mortar was massively used to reinforce the masonry, important disorders appeared in the calcareous stone. The purpose of this article is to underline the incompatibility of the mortars used with the stone used for the construction of the Roman buildings and to identify the disorders and saline phases involved in the deterioration of the cut stone.

II. PRESENTATION OF THE ARCHAEOLOGICAL SITE OF CHELLAH

The archaeological site of Chellah, located 4 km away from the Atlantic coastline overlooks the Bou Regreg valley and occupies an intramural area of about 7 hectares. The site had a Phoenician occupation in the 6th century BC and Carthaginian in the 12th century BC. Later, the Romans settled there and founded a city mentioned by the Greek astrologer and astronomer Ptolemy under the name of Sala, and a river port serving as a Mediterranean counter (Basset H., and Levi-Provençal E., 1929, Basset H., and Terrasse H., 1932, Boube J., 1966). This prosperous Roman city surpassed the site of the Merinid precinct, which still encircles it in the direction of the river. Chellah was then deserted and abandoned before being occupied again by the Merinid sultans who built a necropolis named Al-Ribat Al

Mubarak. An inscription in kufic script on the front door indicates that the work was completed in 739 AD / 1339 AD. The surrounding walls of the Merinides encircle the remains of the Roman cities, including the capitol, the forum, the thermal baths, a nymphaeum and a triumphal arch. A mosque, a medersa, a mausoleum, rooms for ablutions and several funerary rooms remain. The site, property of the state, is protected since November 19, 1920 by the royal decree, which defines as national historical monument the whole complex of Chellah. Since 2012, Chellah is part of the the sites of Rabat inscribed on the list of World Heritage of UNESCO as cultural property.

Fig. 1: Localization of the archaeological site of Chellah in the town of Rabat – Morocco

Fig. 2: Panoramic view of the archaeological site of Chellah

III. CHARACTERIZATION OF MATERIALS USED IN CHELLAH

The cut stone used in the construction of the Roman structures, of plio-quaternary age, is outlined in the form of a system of elongated dune cords juxtaposed parallel to the line of the Atlantic coast from El Jadida to Larache. It corresponds to the local appellation of calcarenite of Salé. The rock, of beige color, shows stratification levels (So). The grain is predominantly millimetric. The petrographic study of the calcarenite shows a detrital fraction composed of rock debris and quartz grains and a bioclastic fraction (Lamellibranchiata, brachiopods and echinoderms shell fragments). These elements, which may present specific variations in terms of content and particle size, are linked by a mainly calcareous phase.

The mechanical strength of the salt stone is about 50 MPa (Asebriy L., 2010). It is in fact sufficient to allow its use as a building stone but remains relatively weak, making its extraction, size and sculpture quite easy compared to other massive rocks of the region.

The rock has an important porosity ranging from 25 to 35% (Rahmouni A., et al., 2013) releasing cavities of varying shape and size. This porosity conditions the sustainability of the rock in the long term: it regulates fluid transfers, gives the material a surface roughness for fixing pollutants, and also opens the way to biological colonization.

Fig. 3: Macroscopic aspect of the calcarenite of Salé

IV. STATEMENT OF THE DESORDS

The archaeological site of Chellah is an excellent exemple of natural site. The materials are exposed there to the severe weather, with the animal and vegetable biological breakdown, and the action of the man (Benharbit, 2017) . To these factors, the consequences of defective restoration works undertaken in the Sixties in order to consolidate the structures of the buildings, are added. There are also various figures of deterioration such as

illustrated in glossary ICOMOS (2008) going, from the least harmful, of simple efflorescences saltworks to more or less dense saline encrustings "fig. 4 and 5". However, other figures witnessing of more advanced disorders are also present: sandy disintegration "Fig.6", alveolation "Fig.7" and gullying "Fig.8".

Fig. 4: Damage Salt develops as encrustation covering the stone in interface with cement mortar

Fig. 5: Details of the saline efflorecences and encrusting on the calcarenite of Salé, at the interface stone-mortar

Fig. 6: Granular decomposition of a block of calcarenite, consequence of the use of a hard cement mortar. The rock has grown into a single alveolus.

Fig. 7: formation, on the stone surface, of deep interconnected cavities

Fig.8: In contact with cement mortar, the rock has deep grooves that hollow out the material highlighting the hardest levels

V. DETERMINATION OF SALINE PHASES

Sampling was carried out on the saline coverings developed at the stone-mortar interface and observed using the Moroccan Foundation for Advanced Science, Innovation and Research (MAScIR) environmental field emission electron microscope (FEG). Observations show that the surface of the rock is lined with deposits of potassium sulphate. "Fig. 9" and cracks propagating between the aggregates" Fig. 10 ".
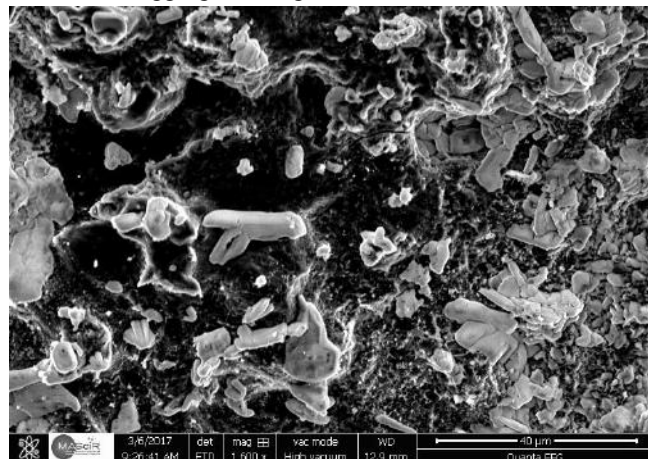
Fig.9: observation with the MEB (X 1600) of potassium sulphate deposits recovering the surface of the calcareous rock
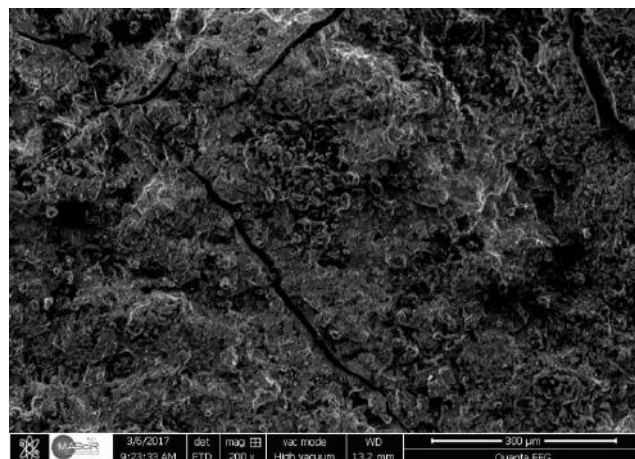
Fig.10: development of microcracks propagating on the surface of the rock

Analysis of the salt deposits formed shows the presence of potassium sulphate K_2SO_4. This salt is commonly used as a fertilizer, potassium being an element that promotes the accumulation of reserves in both raciness and fruit.
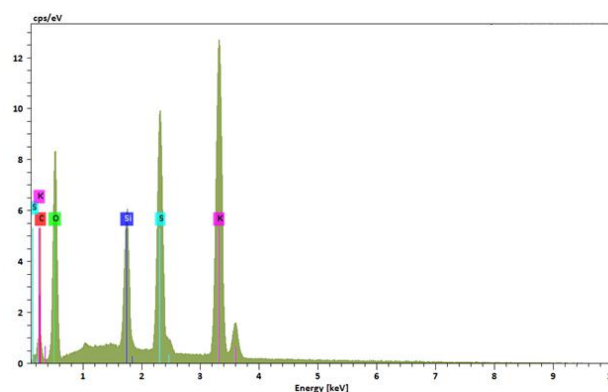
Fig.11: elementary spectrum of analysis obtained with the MEB of crystallizations saltworks showing of the potassium and sulphur peaks

In Chellah, masonries are not isolated at their base. The capillary increase of water since the ground convey these salts which forward owing to the porosity of the rock. The cement mortar used to joint the blocks of calcarenite constitutes an obstacle for the mobility of the fluids which concentrate and deposit, during evaporation, the elements dissolved in the porosity of the rock. These salts generate disorders which are studied since the the 19th century (Turner, 1833). The constraints exerted by salts in the course of growth on the walls of the porous network of the rocks (Scherer 2004, Putnis and Mauthe, 2001) can in the long term create and/or to widen cracks in the rocks.

VI. CONCLUSION

The restorations undertaken in the Sixties used the cement mortar to consolidate the structutres of the buildings going back to the Roman occupation. Cement's higher quality supposed then, dependening on its hardness and to the promptitude of the catch, had contributed to its very broad use in the field of the restoration. This hardness is unfortunately not the pledge of durability desired for masonries. Indeed, the strong sealing of the ciment mortar forbid the water contained in the stone to migrate in the mortar and to evaporate. Salts are trapped on the level of the porous calcareous rock contributing thus to the acceleration of its degradation. Various facies of degradation developed on the site: efflorescences saltworks, sandy disintegration and gullying of the blocks of rock under the effect of the pressures of crystallization which lead to the progressive unsetting of the components of the calcarenite.

The analyzed superficial saline efflorescences indicated potassium sulphates used like fertilizer and which forward in the rock owing to capillary lift.

REFERENCES

[1] Basset H., et Lévi-Provençal E., Chella : une nécropole mérinide, E. Larose éditeur, Paris, 1929.

[2] Basset H., et Terrasse H., Sanctuaires et forteresses almohades, coll. Hesperis, I.H.E.M., Larose éditeur, Paris, 1932.

[3] Boube J., « Fouilles archéologiques à Sala : problèmes de la recherche historique au Maroc » dans Hespéris - Tamuda, T. 7, 1966, p. 23-32.

[4] Asebriy L., 2010. Les monuments historiques de la ville de Rabat: étude des processus d'altération et propositions de solutions durables de prévention et de restauration. Workshop International Patrimoine géologique et Développement durable de la Région de Rabat Salé Zemmour Zaer, du 14 au 16 Décembre 2010 à Rabat.

[5] Rahmouni, A., Boulanouar, A., Boukalouch, M., Géraud, Y., Samaouali, A., Harnafi, M. & Sebbani, J. 2013. Prediction of Porosity and Density of Calcarenite Rocks from P-Wave Velocity Measurements. International Journal of Geosciences, 4, 1292-1299.

[6] Benharbit M., « Le site archéologique de Chellah, panorama des facteurs de dégradation », 95p. 1ère édition : juillet 2017. Top Presse Edition-Rabat.

[7] ICOMOS-ISCS : Illustrated glossary on stone deterioration patterns Glossaire illustré sur les formes d'altération de la pierre ISBN :978-2-918086-00-0 EAN :9782918086000 Impression septembre 2008, Ateliers 30 Impression,Champigny/Marne,France

[8] Turner E., « Report on a lecture on the chemistry of geology ». London and Edimburgh Philosophical magazine, Journal of Science. 1833. Vol. 3, n°21.

[9] Scherer G. W., « Stress from crystallization of salt », Cement and Concrete Research, 34, 2004, p. 1613-1624.

[10] Putnis, A. and Mauthe G., The effect of pore size on cementation in porous rocks, Geofluids, 1, 2001, pp.37-41

Behavior of the Physiochemical Parameters of Raw Milk Stored in Temporary Horizontal Storage Tanks

Maria Regina Thomaz, Francieli DalCanton, Josiane Maria Muneron de Mello, Sideney Becker Onofre

Universidade Comunitária da Região de Chapecó - UNOCHAPECÓ - Center of Exact and Environmental Sciences - CEA - Graduate's Program in Technology and Innovation Management - PPGTI - Av. Senador Attílio Fontana, 591-E EFAPI - 89809-000 - Chapecó - Santa Catarina - Brazil. E-mail: beckerside@unochapeco.edu.br.

Abstract—*Milk is a product with a high nutritional value, and it may appear in daily meals in its natural form or processed and transformed into various milk products. To be processed in industry, milk must have the proper quality conditions for its consumption, and the levels of its constituents must fall within the standards indicated by Normative Instruction no. 62 (2011). Due to its composition, its constituents tend to separate when at rest. In this context, the objective of this work was to evaluate the behavior of the physiochemical parameters of chilled raw milk stored in temporary horizontal storage tanks. With the milk at rest in the tank, collections were made of the milk at the times of 0, 60, 120, 180, 210, 240, 270 and 300 minutes. These collections were performed at two points of the tank: at the top collection point (Ps) and the bottom collection point (Pi) of the tank. After the collection of the samples, the following parameters were determined: fat (G), non-fatty solids (SNF), density (D), cryoscopic index (95), protein (P), lactose (L) and solids (SI). After completion of the tests, it was possible to verify that the solid constituents of the milk showed different behaviors, since the fat separated completely at 210 minutes promoting a stabilization in the separation of the fat. This same behavior was found for Density and the Cryoscopic Index. The other solid constituents of the milk didn't separate, maintaining themselves stable in both the bottom and top of the tank. As such, the conclusion can be drawn that fat is the only physiochemical compound that separates from milk at rest, thus affecting its Density and Cryoscopic Index.*
Keywords - Fat, milk, rest, storage, temporary horizontal tank.

I.   INTRODUCTION

Milk is a white and opaque liquid. It's appearance is the result of the reflection of light by fat globules, insoluble phosphates and casein, with variations ranging from cream to bluish. It has a slightly sweet taste because of the presence of lactose, sodium chloride, fats and proteins. It is a homogeneous mixture with a high nutritional value and it plays a fundamental role in human nutrition, in addition to providing energy and nutrients for subsistence (Koblitz, 2011; Gonzaga *et al.,* 2015).

According to the Normative Instruction no. 62/2011 of the Ministry of Agriculture, Livestock and Food Supply (MAPA), milk is the product arising from the complete and uninterrupted milking of healthy. well-nourished and rested cows in hygienic conditions (Brazil, 2011).

Controlling the physiochemical and microbiological quality of the milk arriving in industrial and processing units is crucial to ensure the health of the population and should be a routine procedure (Tronco 2008; Azevedo 2014).

To be processed in industry, the milk must have the proper quality and consumption conditions and levels within the standards indicated by the Normative Instruction No. 62 of December 29, 2011 from the Ministry of Agriculture, Livestock and Food Supply (MAPA), whose parameters are used as indicators to provide the conditions in which the milk was obtained and processed or to identify any fraud of the product (Brazil, 2011).

When the milk arrives at the reception platform of the dairy industry, milk samples should be collected directly in the truck and go through a series of analyses through rapid tests. Standing out as one of the main analyses required by legislation are the acidity, density, color, smell and texture tests, but the most important factor to be analyzed is the temperature of the milk. This temperature should remain in a range of 7ºC to 10ºC (Brazil, 2011). The minimum quality requirements that refrigerated raw milk in rural properties must comply with, and which can be considered as the acceptable contamination limits of milk, are: a fat content of at least 3% titratable acidity between 0.14 and 0.18 g of lactic acid, density at 15°C between 1.028 and 1.034 g/cm³, dry degreased extract

(ESD) of at least 8.5g/100g, cryoscopic index of - 0.530°H to -0,550°H, equivalent to -0,512°C and 0.531°C, and a minimum of 2.9 g of proteins (Brazil, 2011; Moura *et al.,* 2013; Liu *et al.,* 2016).

Dairy industries pay producers not only for the volume of milk, but also for its quality, where a low TBC (Total Bacteria Count), a low SCC (Somatic Cell Count), and high levels of protein and fat contribute to more remuneration (Rezende *et al.,* 2012; Almeida, 2013).

The physiochemical characteristics of milk and their inter-relationships are a valuable tool to evaluate the productive performance of dairy cattle, to provide information about the physiological state of the lactation, and to diagnose metabolic disorders and their possible impacts on the industrial processing and the final quality of milk products (Rowbotham and Ruegg, 2016).

In the tanks of the trucks arriving at the dairy industry, samples are collected for laboratory tests, which must be taken after agitation for five to ten minutes by means of an agitator of the total volume of the tank (Di Domenico, 2009; Ponce, 2009; Bittante *et al.,* 2012; Tonini, 2014)

The fat globules are suspended in water and have a lower density than it. This causes the formation of a fat layer on top of the rest of the milk, which must be constantly stirred to prevent the formation of a too thick layer of fat at the top. In milk that hasn't been sufficiently homogenized, differences show up in the composition of the milk removed from the bottom of the cooler, through the tap, and from the top, with the aid of the collection ladle (Durr *et al.,* 2001; 2014; Buza *et al.,* 2014).

Due to the differences in the chemical composition of the milk, the exact behavior of the physiochemical parameters of the milk stored in the isothermal tanks of the trucks waiting for analysis in the platform of dairy industries so its quality can be determined, is not known. In this context, the objective of this work was to evaluate the behavior of the physiochemical parameters of chilled raw milk stored in temporary storage tanks.

II. MATERIALS AND METHODS
2.1 MILK SAMPLES

This study used chilled raw milk 'in natura' granted by a dairy producer located in the city of Chapecó - Santa Catarina. The milk samples supplied by the dairy producer were of milk collected on the same day as the analysis. These samples were transported in a cold chamber to the test laboratories of the Universidade Comunitária da Região de Chapecó - Unochapeco. The official analyses were performed in the Food Technology Laboratory of the Chapecó Campus.

The samples were kept in the temporary horizontal tank, in a controlled temperature environment of 7.00 ºC ± 2.0, as determined by the Normative Instruction no. 62

(Brazil, 2011) of the Ministry of Agriculture, Livestock and Food Supply - MAPA, which establishes that chilled raw milk in Brazil must pass through an analysis to assess its quality. All analyses were performed in triplicate.

2.2 STORAGE TANK

In order to carry out this experiment, an isothermal, horizontal temporary storage tank was designed and built with a capacity of 33 liters of milk, with similar characteristics as the truck tanks used for the transport of milk in bulk to the dairy industries. The tank was built in stainless material and jacketed according to Figure 1, allowing it to maintain the temperature of the milk under ideal conditions, thus complying with IN 75/2003 and IN 62/2011 of the Ministry of Agriculture (Brazil, 2003; Brazil, 2011).

Fig. 1: Tank used in the experiments

The tank was constructed with two collection points for the milk samples, called: Top Collection Point (Ps) and Bottom Collection Point (Pi). These points allowed for the collection of milk samples during the evaluation times. At each collection point, a faucet was installed to perform the collection without contaminating the rest of the stored milk. The faucets used are in accordance with sanitary legislation.

2.3 BEHAVIOR OF THE MILK'S SOLID CONSTITUENTS

With the milk at rest in the tank, collections were made of the milk at the times of 0, 60, 120, 180, 210, 240, 270 and 300 minutes. These collections were performed at two points of the tank: at the top collection point (Ps) and the bottom collection point (Pi). After the collection of the samples, the following parameters were determined: fat (G), non-fatty solids (SNF), density (D), cryoscopic index (95), protein (P), lactose (L) and solids (SI).

The centesimal composition of the milk's constituents was determined through the Master Mini milk analyzing equipment from AKSO, which uses ultrasound

technology to analyze the samples. The method is based on an ultrasound spectroscopy based on the undulating movement that propagates in the medium where the product is inserted.

The deformations of the milk molecules indicate if it was altered in its composition. In addition, the physiochemical analysis of the milk through ultrasound spectroscopy has advantages over traditional methods since samples don't need to be prepared, minimal volumes of the intact samples need to be used, no chemical reagents or specific glassware are necessary and results can be obtained in few minutes.

Before the analyses, the equipment was properly calibrated and cleaned according to the manufacturer's instructions. After adding a milk sample to a 25 ml cuvette, the device sucks in the quantity of milk needed for analysis and shows the values of the constituents of the milk under analysis on the screen (Ponsano *et al.,* 2007).

2.4 STATISTICAL ANALYSIS

The Microcal Origin software, version 7.0 (Microcal Software Inc., Northamptomn, MA, USA), was used for the statistical data analysis, ANOVA using the Tukey test, with a significance level of 5%, was used for the analysis of variance. The physiochemical parameters were evaluated by the difference of the sample means according to the Normative Instruction no. 62 (2011). All activities were performed in triplicate.

III.   RESULTS AND DISCUSSION

The behavior of the physiochemical parameters of the milk stored in a temporary horizontal tank is presented in Table 1, 2 and 3. In Table 1 and Figure 2 the fat behavior can be seen.

Table.1: Behavior of the fat in storage tanks in 8 evaluation times.

Time (Minutes)	Mean Top Collection Point	Mean Bottom Collection Point
0	3.85±0.05aA	3.75±0.05aA
60	4.95±0.05abA	3.85±0.05aA
120	9.70±0.60bA	3.05±0.05aB
180	13.60±0.20bA	3.15±0.05aB
210	15.75±0.15cA	2.75±0.05bB
240	15.85±0.05cA	2.85±0.05bB
270	16.25±0.05cA	2.70±0.10bB
300	16.67±0.05cA	2.70±0.20bB

* Means and deviations followed by the same small case letter in the vertical axis and capital letters on the horizontal axis do not differ statistically between themselves by the Tukey test at the level of probability of 5%.

The analysis of the data in Table 1 reveals that there were variations in the fat levels, both in the samples collected from the top point and those collected from the bottom point. One can see that at the starting time (zero minutes), the observed levels in both points were of 3.85±0.05 and 3.75±0.05 for the top and bottom evaluation points, respectively. As can be seen, the levels don't differ significantly among themselves at the level of 5% in Tukey's Test.

After the 60 minute mark of the milk at rest, one can see that the fat levels increased until the time of 210 minutes, with values of 4.95±0.05, 9.70±0.60, 13.60±0.20 and 15.75±0.15 at the times of 60, 120, 180 and 210 minutes, respectively. As can be seen, the levels found differ significantly among themselves at the level of 5% in Tukey's Test. This behavior can be observed in the curves for the fat separation from the milk, shown in Figure 2.
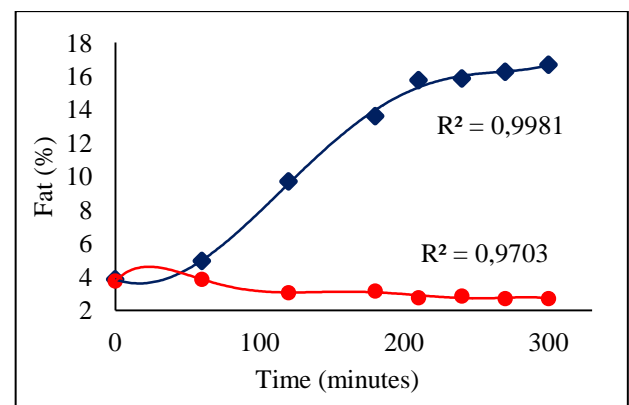
Fig. 2: Separation of the fat in milk stored in a temporary horizontal tank.

After 210 minutes, a stabilization of the fat levels can be observed, because the values found were 15.85±0.05, 16.25±0.05 and 16.67±0.05 at the times of 240, 270 and 300 minutes, respectively. When these data are analyzed, they show that there is no statistically significant differences between the data at the evaluation times. This behavior suggests that the movement of the fat from the lower to the higher regions of the tank stabilized. One can therefore infer that the time of separation of the fat and milk when stored under the conditions of this study is 210 minutes, or 3.5 hours.

In a study conducted by Wangdi, Vijchulata and Chairatanayuth (2014), in Thailand, the characteristics were investigated of the separation by gravity of the fat globules in chilled milk. Similar to this study, the milk samples collected from the tanker truck remained at rest for a period of 8 hours, with five samples being taken, which remained at rest for the times of 0, 2, 4, 6 and 8 hours, in a place with a temperature of 4 °C. While in the present study samples were collected at the top and

bottom points through a faucet, in Thailand the milk samples were collected by means of a pipette at the top (between 250 and 200 ml), middle (between 150 and 100 ml) and lowest point (between 50 and 0 ml) of the container in which the sample was stored.

In the Thai study, there was a significant influence of time on the fat levels, starting at the top point, where the fat content increased from 3.85 to 5.07%, an increase of about 31.69% after a time interval of 2 hours. The fat content continued to increase in the top sample and at the end of the 8 hours of the milk at rest, the fat content increased to 7.07%, consisting in a total increase of 83.63% compared to the initial fat content of 3.85%. This is corroborated in the present study, where in 120 minutes (2 hours), the fat content increased from 3.85 ± 0.05 to 9.70 ± 0.60, an increase of 152% from the initial value of 3.85% and the value continued to increase, but the rate of change decreased with the increase of time intervals.

The behavior of the fat content obtained from the samples collected at the bottom collection point (Pi) is the opposite of the one obtained from the samples collected at the top collection point (Ps), because as the analysis time progresses, the fat content of the collected samples can be seen to decrease after 180 minutes of storage, moving from 3.15 ± 0.05 to 2.75 ± 0.05% at 210 minutes. As such, one can see that there is a statistically significant difference between the two means in these times. It is also clear that from 210 minutes to 300 minutes of rest, there was a stabilization in the fat content, going from 2.75 ± 0.05 at 210 minutes to 2.70 ± 0.20 at 300 minutes.

As shown in Table 1 and Figure 2, there was a gradual reduction of the fat content at the bottom collection point and one can see that the largest value occurred at 120 minutes (2 hours), which was 81.33%, going from 3.75 ± 0.05 to 3.05 ± 0.05. Just as in the work by Wandi, Vijchulata and Chairatanayuth (2014), who found a gradual reduction in fat content in the middle and lowest points, with an average decrease of around 8.05% and 12.99% for the medium and lower fractions, respectively. After 8 hours of the milk at rest, the decrease in fat content was around 20.8% in the middle and 28.80% at the bottom.

Servello *et al.,* (2004) developed an extensive study to define the optimal time of agitation and, in his work, a fat loss rate of around 30% was observed at the bottom of the tank after three hours of the milk at rest. Jackson (1981), on the other hand, observed a fat loss rate of 60%, but in 1.5 hours. This difference may be due to the different methods used in the collection of the samples.

In the evaluation of the quality of chilled raw milk as a function of the transportation and storage conditions in isothermal tanks and industrial silos performed by Brazil *et al.,* (2012), the fat content in the milk stored in a refrigerated tank was 3.53% and in the silo 3.45%, lower than the values found in this work.

The data found here are in agreement with the recommendations of IN no. 62/2011, which established that the fat content in milk should be 3.0 g/100 g of milk (Brazil, 2011), with the composition of milk varying widely between breeds and in lesser intensity between animals of the same breed. It hover around 35g/liter. The fat contributes to a better palatability of the product. It is responsible for a large number of essential fatty acids. Each gram of fat provides 9 calories. The nutritive value of fat is due to the fat-soluble vitamins (A, D, E and K) and the presence of the carotene precursors of vitamin A (Tronco, 2008).

According to Foschiera (2004), the fat is formed by globules of different sizes, suspended in the aqueous phase. Each globule is surrounded by a phospholipid membrane and it is this layer that prevents the union of all the globules. According to Koblitz, (2011), maintaining the milk at rest leads to the separation of this component, forming a top layer. Since it is less dense than water, the fatty matter floats when the milk is at rest, forming the so-called cream layer, the main component of the milk sub-products butter and cream (Florião, 2013).

Cunha *et al.,* (2013) found no significant differences in the mean levels of lactose, protein, fat and SCC of the milk samples collected before and after the training of transporters. Although no statistical difference was found in the mean levels of fat between the collection times, the coefficient of variation (CV) of the data was 10.09%, which was a greater value than the CV for lactose and protein levels, which were 2.92 and 4.18%, respectively. According to Goodrigge *et al.,* (2004), the collection in the lower or top layers from the milk tank may explain the variations concerning fat contents, since the fat globules tend to concentrate on the top layer of chilled milk.

Regarding the density of the milk measured according to storage time, one can see that the values obtained are similar in all samples, both in samples collected at the top collection point (Ps) and in samples collected at the bottom collection point (Pi). These data can be seen in Table 2.

The values obtained reveal a density of 1.039 ± 0.05 for the collection at Ps at the beginning of the process, time zero, and a density of 1.014 ± 0.35 at the time of 210 minutes. The analysis of these data, although very similar, show they are statistically significantly different by the Tukey test at a probability of 5%. From the time of 210 up to the time of 300 minutes, an equilibrium in the density could be seen, since the values went to 1.012 ± 0.70. These density values, therefore, are no different, when evaluated. The same behavior was observed in the samples taken from the bottom collection point (Pi) for

the density values across the test times. The density can be modified by adding water or prior skimming, because water has a higher density than fat, $1g/cm^3$ and $0,9301g/cm^3$, respectively.

The behavior of density in this study is corroborated by the literature, which points out that the higher the fat content, the lower the density, with skimmed milk having a higher density than whole milk, because according to Castro (2005), density is the relationship that exists between the mass and volume of a body. As such, one can see the relationship between the solids and the solvent in milk.

This study revealed that in the 300 minutes of storage, the samples collected in Ps and Pi had a density of 1.012 ± 0.70 and 1.045 ± 0.20, respectively. It should be emphasized that these samples show levels of 16.67 ± 0.05 and $2.70\pm0.20\%$ for fat in the samples collected at the time of 300 minutes in the Ps and Pi, respectively.

Table 2: Physiochemical parameters of the milk - Non-fatty solids - SNF, Density and Cryoscopic Index (Means followed by Standard Deviation)

Time*	SNFs[1]	SNFi[2]	Ds[3]	Di[4]	ICs[5]	ICi[6]
0	8.25±0.50aA[#]	8.80±0.05aA	1.039±0.05aA	1.039±0.30aA	-0.545±0.002aA	-0.548±0.004aA
60	8.33±0.13aA	8.86±0.05aA	1.037±0.05aA	1.039±0.55aA	-0.542±0.001aA	-0.549±0.005aA
120	8.83±0.55aA	8.72±0.10 aA	1.028±1.30aA	1.040±0.05 aAB	-0.542±0.004aA	-0.544±0.005aA
180	8.50±0.10 aA	8.95±0.05aA	1.020±0.60 aAB	1.041±0.20aB	-0.545±0.005aA	-0.543±0.004aA
210	8.14±0.10 aA	8.71±0.10 aA	1.014±0.35bB	1.045 ± 0.08bA	-0,553±0.015bA	-0.520±0.000bB
240	8.14±0.00aA	8.77±0.05aA	1.013±0.25bB	1.044±0.30bA	-0.554±0.005bA	-0.528±0.002bB
270	8.18±0.10aA	8.93±0.16aA	1.012±0.75bB	1.044±0.05bB	-0.552±0.001bA	-0.524±0.006bB
300	8.49±0.25aA	8.91±0.18aA	1.012±0.70bB	1,045±0,20bA	-0.553±0.027bA	-0.523±0.003bB

* Time in Minutes. [1]Non-fatty solids (SNF) Top Point. [2]Non-fatty solids (SNF) Bottom Point. [3]Density - Top Point. [4]Density - Bottom Point. [5]Cryoscopic Index - Top Point.[6]Cryoscopic Index - Bottom.

 # Means and deviations followed by the same small case letter in the vertical axis and capital letters on the horizontal axis do not differ statistically between themselves by the Tukey test at the level of probability of 5%.

Table 3: Physiochemical parameters of the milk - Proteins, Lactose and Solids (Means followed by Standard Deviation)

Time	Ps[1]	Pi[2]	Ls[3]	Li[4]	SIs[5]	SIi[6]
0	3.03±0.05aA[#]	3.41±0.05aA	4.52±0.04aA	4.69±0.15aA	0.70±0.00aA	0.70±0.00aA
60	3.12±0.03aA	3.42±0.05aA	4.51±0.11aA	4.74±0.31aA	0.70±0.00aA	0.70±0.00aA
120	3.24±0.20aA	3.40±0.05aA	4.89±0.30aA	4.62±0.11aA	0.70±0.00aA	0.70±0.00aA
180	3.12±0.05aA	3.43±0.06aA	4.68±0.05aA	4.82±0.04aA	0.70±0.00aA	0.70±0.00aA
210	2.98±0.09aA	3.42±0.04aA	4.46±0.20aA	4.59±0.12aA	0.70±0.00aA	0.70±0.00aA
240	2.99±0.06aA	3.42±0.06aA	4.45±0.05aA	4.65±0.04aA	0.70±0.00aA	0.70±0.00aA
270	3.01±0.10aA	3.44±0.03aA	4.47±0.05aA	4.79±0.08aA	0.70±0.00aA	0.70±0.00aA
300	3.10±0.05aA	3.43±0.05aA	4.69±0.15aA	4.78±0.04aA	0.70±0.00aA	0.70±0.00aA

* Time in Minutes. [1]Proteins - Top Point. [2]Proteins - Bottom Point. [3]Lactose - Top Point. [4]Lactose - Bottom Point. [5]Solids - Top Point. [6]Solids - Bottom.

#Means and deviations followed by the same small case letter in the vertical axis and capital letters on the horizontal axis do not differ statistically between themselves by the Tukey test at the level of probability of 5%.

The density of the milk may be associated to the Cryoscopic Index (IC), a test serving to control the volume of water present in the milk, recommending the addition of water or removal of its components, or even the addition of some compound to mask a problem (Tronco, 2008; Botaro and Santos, 2016).

The cryoscopic point is defined as the temperature at which the milk passes from a liquid to a solid state. The freezing temperature of milk is lower than water due to the substances contained in it, such as lactose and mineral salts. The freezing point can vary depending on the season of the year, feed, breed, health status, age, among others (Alberton, 2012). The higher the freezing point, therefore, the greater the water content in the milk (Robim *et al.,* 2012).

The behavior of this parameter on the data obtained in this study corroborate the fat content found in the samples taken at the established times in each collection point.

The data show that the higher fat rate, the lower the density and the higher the cryoscopic index. At 300 minutes of storage, therefore, the fat contents off in Ps were 16.67±0.05%, the density was 1.012±0.70 g/mL and Cryoscopic Index was-0,553±0,027H (Degrees Hortvet ºH), thus showing a clear correlation between these three parameters. The samples taken at the same time of 300 minutes in the Pi, on the other hand, had the opposite behavior.

Castro and Luz (2015) evaluated the quality of chilled raw milk before and after 30 and 60 days of freezing. As a result of all samples under different conditions, they obtained a mean density ranging from 1029.8 to 1031.0 g/cm3 and a cryoscopic index that remained between -0.530 and -0.544ºH, values complying with the standards of current legislation. The fat and protein contents remained between 3.5 and 4.0% and 2.90 and 3.19% and the results obtained for ESD remained within a range of 8.46 and 8.77% for the Degreased Dry Extract per formula and 8.19 to 8.90% for the gravimetric Degreased Dry Extract.

The Non-Fatty Solids (SNF), or Degreased Dry Extract (ESD), comprise all the elements of the milk minus the water and fat. They also include, therefore, the solids (SI), also known as ashes, the lactose (L) and the proteins (P).

For the dairy industry, the fat, protein, lactose, total dry extract (EST) and degreased dry extract (ESD) contents are criteria used to pay producers, assign raw material within the processes and to predict industrial yield (Beloti *et al.,* 2008; Costa, 2014).

With respect to these evaluated parameters, one can see that they didn't show variations in relation to storage time, not undergoing sedimentation or flotation and remaining stable, therefore.

It should be emphasized that the lactose content found was 4.52% at time zero and 4.69% at 300 minutes of storage. No significant differences (p<0.05) were therefore observed in the Ps and Pi at the evaluated times.

The lactose values of this study were similar to the results obtained by Teixeira (2003), who found 4.66% while studying the lactation of Holstein cows. The results obtained here were similar to those in a study performed by Machado (2000), who obtained a mean lactose level of 4.51% in milk samples from expansion tanks (Oliveira and Santos, 2012).

In the study by Brazil *et al*., (2012), the lactose levels were 4.52% for the milk stored in a isothermal tank and 4.51% for the milk stored in a silo, very similar to this study, but higher than the result of Silva (2008), who reported a lactose level of 4.41% in the period, while Alberton (2012), studying the % lactose in different seasons of the year, observed higher values (4.47 %) in summer and smaller (4.40 %) in fall.

Lactose is the sugar found only in milk, being a disaccharide composed of glucose and galactose ($C_{12}H_{22}O_{11}H_2O$) that is of technological importance in all milk acidification, lactic fermentation, processes, which is the basis of the manufacture of yogurts, fermented butters, cheeses, and the most stable constituent of milk, with virtually no variation between the bovine breeds (Mendes, 2010). The lactose isolated from milk in powder form serves as a raw material in the pharmaceutical industry. It should be noted that the IN-62 from MAPA (Brazil, 2011) does not determine minimum or maximum limits for the milk.

From a qualitative and quantitative point of view, proteins are the noblest nitrogenous compounds found in milk, which are essential in the formation of tissues and the foundation of animal life. It is also the main component in animal and human nutrition since the beginning of life (Koblitz, 2011; Santos et al., 2011).

The protein content of milk has become valuable and is considered in the paymen- by-quality programs because it is a nutrient that promotes the quality of raw materials and the industrial yield of milk derivatives. IN 62/2011 determines a minimum total protein content of 2.9 g/100 g of milk (Brazil, 2011), but there can be variations in protein content and the other nutrients in milk as a function of the season, breed, genetics, nutrition and lactation stage (Glantz *et al.,* 2010; Barbosa *et al.,* 2012; Ye *et al.,* 2013).

The data collected in this study revealed that the quantified protein levels had higher values than the requirements of IN-62 from MAPA, which requires values higher than 2.9%. When analyzing these data, one can see that the protein levels determined in the Ps samples in relation to the levels of the Pi samples did not have significant differences at the level of probability of p<0.05.

Brazil *et al.,* (2012) studied the storage of milk and found protein contents of 3.34% in a isothermal tank and of 3.35% in an industrial silo, while Castro and Luz (2015) found that the protein contents remained between 2.90 to 3.19%, values in accordance with the IN 62 (2011) and considered excellent for chilled raw milk, similar to this work.

Several environmental factors influence the protein composition of milk, especially breed, feed and disease management, followed by season of the year, lactation stage and age of the cow. An unbalanced and nutritionally poor diet can cause changes in the composition of the milk, especially regarding the fat and protein levels and the saline balance, causing, for example, low yields in the production of cheeses and a decrease in the milk's thermal stability (Silva, 2009).

The results obtained in this study can serve as support for the technical departments of dairy industries to monitor and qualify the raw material and consequently improve the industrial yield.

It is also hoped that this work will strengthen the commercial relations system between economic agents acting in the milk production chain. It is also expected that Milk Production Associations can use this information as indicators and to assist in the interface between primary production, industry and the consumers of the product.

IV. CONCLUSION

Through this study analyzing the solid constituents of milk, one can conclude that only the fat separates completely from the other constituents, concentrating on the top of the cold milk.

Milk samples taken improperly or without homogenization from the isothermal tanks awaiting unloading of the milk on reception platforms, may compromise the quality of milk and the physiochemical and microbiological characteristics of the product.

Payment by quality is a motivating factor for the producer, but it is not enough that the milk leaves the property in compliance with standard IN 62 (2011). If the sample taken on the platform does not match the sample from the property, the producer will be penalized.

REFERENCES

[1] Alberton, J. (2012). O estudo da qualidade do leite de amostras obtidas de tanques de resfriamento em três regiões do estado do Paraná. Arquivos de Ciências Veterinárias e Zoológicas da Unipar, 15(1): 5-12.

[2] Almeida, T. V. (2013). Parâmetros de qualidade do leite cru bovino: contagem bacteriana total e contagem de células somáticas. Goiânia: Seminários Aplicados.

[3] Antos, G., Lopes, M. A. (2014). Indicadores econômicos de sistemas de produção de leite em confinamento total com alto volume de produção diária. Ciência Animal Brasileira, 15(3): 239-248.

[4] Azevedo, C. S. (2014). Ocorrência de leite instável não ácido (LINA) na região da Grande Florianópolis-SC (Monografia de Graduação). Universidade Federal de Santa Catarina, Florianópolis.

[5] Barbosa, R. S., Fischer, V., Ribeiro, M. E. R., Zanela, M. B., Stumpf, M. T., Kolling, G. J., Júnior, J. S., Barros, L. E., & Egito, A. S. (2012). Caracterização eletroforética de proteínas e estabilidade do leite em vacas submetidas à restrição alimentar. Pesquisa Agropecuária Brasileira, 47(4): 621-628.

[6] Beloti, V., Ribeiro Júnior, J. C., Tamanini, R., Yamada, A. K., Cavaletti, L., Shecaira, C. de L., Novaes, D. G., & Silva, F. F. (2011). Qualidade microbiológica e físico-química do leite cru refrigerado produzido no município de Sapopema/PR. Revista Científica Eletrônica de Medicina Veterinária, 9(16).

[7] Bittante, G., Penasa, M., & Cecchinato, A. (2012). Invited review: Genetics and modeling of milk coagulation properties. Journal of Dairy Science, 95(12): 6843-6870.

[8] Botaro, B., & Santos, M. V. (2016). Entendendo a variação da crioscopia do leite. Piracicaba: Milkpoint. Disponível em: https://www.milkpoint.com.br/. Acesso em: 20 de dezembro 2016.

[9] Brasil, R. B., Silva, M. A. P., Carvalho, T. S., Cabral, J. F., Nicolau, E. S., & Neves, R. B. S. (2012). Avaliação da qualidade do leite cru em função do tipo de ordenha e das condições de transporte e armazenamento. Revista do Instituto de Laticínios Cândido Tostes, 389(67): 34-42.

[10] Brasil. (2002). Instrução Normativa n. 75, de 28 de outubro de 2003. Regulamento Técnico para Seleção, Projeto, Fabricação e Manutenção de Tanques Isotérmicos Destinados à Coleta e ao Transporte de Leite e Derivados Fluidos. Brasília, DF. Secretaria de Inspeção de Produto Animal. Diário Oficial da República Federativa do Brasil.

[11] Brasil. (2011). Instrução Normativa n. 51, de 29 de dezembro de 2011, que altera o art. 1º, da Instrução Normativa MAPA nº 51, de 18 de setembro de 2002. Diário Oficial da República Federativa do Brasil.

[12] Brasil. (2011). Instrução Normativa n. 62, de 29 de dezembro de 2011, que altera o art. 1º, da Instrução Normativa MAPA nº 51, de 18 de setembro de 2002. Diário Oficial da República Federativa do Brasil.

[13] Buza, M. H., Holden, L. A., White, R. A., & Ishler, V. A. (2014). Evaluating the effect of ration composition on income over feed cost and milk yield. Journal of Dairy Science, 97(5): 3073-3080.

[14] Castro, A. D., & Luz, R. (2015). Avaliação da qualidade do leite in natura antes, pós 30 e 60 dias de congelamento (Monografia de Graduação Tecnológica). Centro Universitário Univates, Lajeado.

[15] Castro, P. S. (2005). Apostila de aulas práticas: tecnologia de leites e derivados. Goiás: Universidade Católica de Goiás.

[16] Costa, J. F. (2014). Atributos de qualidade associados à ocorrência de proteólise em leite cru

granelizado (Dissertação de Mestrado). Universidade Federal de Juiz de Fora, Juiz de Fora.

[17] Cunha, A. F., Parreira, D. S., Silva, S. Q., & Cerqueira, M. M. O. P. (2013). Efeitos do treinamento de transportadores de leite na determinação da qualidade do leite cru refrigerado. Acta Veterinaria Brasilica, 7(3): 241-246.

[18] Di Domenico, Q. (2009). Acompanhamento da rotina de análises do laboratório de recepção e leite: avaliação dos resultados das amostras de qualidade do leite de uma indústria de produtos lácteos (Monografia de Graduação). Universidade do Estado de Santa Catarina, Chapecó.

[19] Durr, J. W. (2012). Como produzir leite de qualidade (4. ed.). Brasília: SENAR.

[20] Durr, J. W., Fontaneli, R. S., & Moro, D. V. (2001). Determinação laboratorial dos componentes do leite. In F. H. D. González, J. W. Durr, & R. S. Fontaneli (Ed.), Uso do leite para monitorar a nutrição e o metabolismo de vacas leiteiras (p. 23-29). Porto Alegre: UFRGS.

[21] Florião, M. M. (2013). Boas práticas em bovinocultura leiteira com ênfase em sanidade preventiva. Niterói: Programa Rio Rural.

[22] Foschiera, J. L. (2004). Indústria de laticínios: industrialização do leite, análises, produção de derivados. Porto Alegre: Suliani.

[23] Glantz, M., Devold, T. G., Vegarud, G. E., Lindmark Månsson, H., Stålhammar, H., & Paulsson, M. (2010). Importance of casein micelle size and milk composition for milk gelation. Journal of Dairy Science, 93: 1444-1451.

[24] Gonzaga, N., Daniel, G. C., Mareze, J., Marioto, L. R. M., Tamanini, R., & Beloti, V. (2015). Evolução da qualidade microbiológica e físico-química do leite pasteurizado. Semina, 36(1): 47-54.

[25] Goodridge, L. D., Hill, A., & Lencki, R. (2004). A review of international standards and the scientific literature on farm milk bulk tank sampling protocols. Journal Dairy Science, 87: 3099-3104.

[26] Jackson, A. C. (1981). Agitation and sampling of tankers and storage tanks. Journal Society Dairy Technology, 34: 98-103.

[27] Koblitz, M. G. B. (2011). Matérias-primas alimentícias: composição e controle de qualidade. Rio de Janeiro: Guanabara Koogan.

[28] Liu, S., Zhang, R., Kang, R., Meng, J., & Ao, C. (2016). Milk fatty acids profiles and milk production from dairy cows fed different forage quality diets. Animal Nutrition, 2: 329-333.

[29] Machado, P. F., Pereira, A. R., & Sarries, G. A. (2000). Composição do leite de tanques de rebanhos brasileiros distribuídos segundo sua contagem de células somáticas. Revista Brasileira de Zootecnia, 29(6): 1883-1886.

[30] Mendes, C. G. (2010). Análises físico-químicas e pesquisa de fraude no leite informal comercializado no município de Mossoró, RN. Ciência Animal Brasileira, 11(2): 349-356.

[31] Moura, J. F. P., Pimenta Filho, E. C., Gonzaga Neto, S., & Candido, E. P. (2013). Avaliação tecnológica dos sistemas de produção de leite bovino no Cariri da Paraíba. Revista Brasileira de Saúde e Produção Animal, 14(1): 121-131.

[32] Oliveira, E. N. A., & Santos, D. C. (2012). Avaliação da qualidade físico-química de leites pasteurizados. Revista do Instituto Adolfo Lutz, 71(1): 93-197.

[33] Ponce, P. (2009). Composición láctea y SUS interrelaciones: expresión genética, nutricional, fisiológica y metabólica de La lactación en las condiciones del trópico. Revista Salud Animal, 31(2): 69-76.

[34] Ponsano, E. G. H., Perri, S. H. V., Madureira, F. C. P., Paulino, R. Z., & Camossi, L. G. (2007). Correlação entre métodos tradicionais e espectroscopia de ultra-som na determinação de características físico-químicas do leite. Arquivo Brasileiro de Medicina Veterinária e Zootecnia, 59(4): 1052-1057.

[35] Rezende, E. S. J., Pinto, S. M., Pereira, J. L. A. R., & Labigalini, I. (2012). Qualidade higiênico-sanitária do leite cru em três mesorregiões de Minas Gerais. Revista do Instituto de Laticínios Cândido Tostes, 67(387): 64-69.

[36] Robim, M. S., Cortez, M. A. S., Silva, A. C. O., Torres Filho, R. A., Gemal, N. H., & Nogueira, E. B. (2012). Pesquisa de fraude no leite UAT integral comercializado no estado do Rio de Janeiro e comparação entre os métodos de análises físicoquímicas oficiais e o método de ultrassom. Revista do Instituto de Laticínios Cândido Tostes, 67(389): 43-50.

[37] Rowbotham, R. F., & Ruegg, P. L. (2016). Association of bedding types with management practices and indicators of milk quality on larger Wisconsin dairy farms. Journal of Dairy Science, 98(11): 7865-7885.

[38] Santos, N. A. F., Lacerda, L. M., & Ribeiro, A. C. (2011). Avaliação da composição e qualidade físico-química do leite pasteurizado padronizado comercializado na cidade de São Luís, MA. Arquivos do Instituto Biológico, 78(1): 109-113.

[39] Servello, V., Hill, A. R., & Lencki, R. W. (2004). Towards an optimum mixing protocol for on-farm

bulk milk sampling. Journal Dairy Science, 87(9): 2846-2853.

[40] Silva, M. A. P. (2009). Influência do transporte a granel na qualidade do leite cru refrigerado. Revista do Instituto Adolfo Lutz, 68(3): 381-387.

[41] Tonini, C. B. (2014). Avaliação da qualidade do leite e caracterização de laticínios do estado do Espírito Santo (Dissertação de Mestrado). Universidade Federal do Espírito Santo, Alegre.

[42] Teixeira, N. M., Freitas, A. F., & Barra, R. B. (2003). Influência de fatores de meio ambiente na variação mensal da composição e contagem de células somáticas do leite em rebanhos no Estado de Minas Gerais. Arquivo Brasileiro de Medicina Veterinária e Zootecnia, 55(4): 491-499.

[43] Tronco, M. (2008). Manual para Inspeção da Qualidade do Leite (3. ed.). Santa Maria: UFSM.

[44] Venturoso, P. C., Almeida, K. E., Rodrigues, A. M., Damin, M. R., & Oliveira, M. N. (2007). Determinação da composição físico-química de produtos lácteos: estudo exploratório de comparação dos resultados obtidos por metodologia oficial e por ultra-som. Revista Brasileira de Ciências Farmacêuticas, 43(4): 123-129.

[45] Ye, R., & Harte, F. (2013). Casein maps: effect of ethanol, pH, temperature, and $CaCl_2$ on the particle size of reconstituted casein micelles. Journal of Dairy Science, 96(2): 799-805.

[46] Wangdi, J., Vijchulata, P., & Chairatanayuth, P. (2014). Gravity Separation Characteristics of Cows' Raw Milk Fat Globules. International Journal of Innovation and Applied Research, 2(10): 13-22.

Functionalized up conversion rare earth nanoparticles for bio imaging of cancer cells

Chávez-García D.[1], Juárez-Moreno K.[2,3], Campos C. H.[4], Alderete J. B.[4], Hirata G.A.[2]

[1]Centro de Enseñanza Técnica y Superior. Campus Ensenada. Camino a Microondas Trinidad S/N Km. 1, Moderna Oeste, Ensenada, Baja California, C.P. 22860, México. E-mail: dalia.chavez@cetys.mx

[2]Centro de Nanociencias y Nanotecnología, Universidad Nacional Autónoma de México, Carretera Tijuana-Ensenada. Km. 107, Ensenada, Baja California, C.P. 22860, México. E-mail: kjuarez@cnyn.unam.mx, hirata@cnyn.unam.mx

[3]CONACYT ResearchFellow at Centro de Nanociencias y Nanotecnología, Universidad Nacional Autónoma de México, Carretera Tijuana-Ensenada. Km. 107, Ensenada, Baja California, C.P. 22860, Mexico.E-mail: kjuarez@cnyn.unam.mx

[4]Facultad de Ciencias Químicas, Universidad de Concepción. EdmundoLarenas 129, Concepción, Chile. E-mails: ccampos@udec.cl; jalderet@udec.cl

Abstract—In recent yearsupconversion nanoparticles (UCNPs)have being investigated due to their potential applications in biomedicine such as fluorescent biolabels, among many others. The luminescence of this kind of NP's are effectively activatedby near infrared radiation (NIR) and upconvertto luminescence in the visible region. Besides, their luminescence is not faded as compared with organic dyes and fluorescent proteins. In this study, UCNPs made of Y_2O_3:Yb^{3+}, Er^{3+} (1%, 10% mol) and Gd_2O_3:Yb^{3+}, Er^{3+} (1%, 10% mol) were functionalized with aminosilanes and folic acid (UCNP-NH_2-FA) and characterized with transmission electron microscopy (TEM), Fourier transform infrared spectroscopy (FTIR) and luminescence measurements. Moreover, cytotoxicity was analyzed via colorimetric assays MTT (methy-134 thiazolyltetrazolium) in two cancer cell lines: cervical adenocarcinoma cells (HeLa) and breast cancer cells MB-MDA-231. It is found that the functionalized UCNPs were non-cytotoxic in all cancer cell lines. Confocal images revealed that UCNP-NH_2-FA conjugates as a target to attract cells with overexpressed folate receptor (FR). The UCNPs offer a great potential to be used as bio labels because their fluorescence was clearly localized into cell cytoplasm.

Keywords— luminescence, nanophosphors, lanthanide, biomedical

I. INTRODUCTION

Nanotechnology has arisen with different types of nanoparticles and nanomaterials for several applications in biomedicine. Our special interest is in bioimaging applications, using upconversion nanoparticles(UCNPs) to identify certain types of cancer cells [1,2]. The nanoparticles can upconvert the near infrared (NIR) energy (λ= 980 nm) into visible light[3]. In this context, the UCNPs of Y_2O_3:Yb^{3+}, Er^{3+} (1%, 10% mol) and Gd_2O_3:Yb^{3+}, Er^{3+} (1%, 10% mol) were synthesized by sol-gel method[4], the hosts were the oxides Y_2O_3 and Gd_2O_3 and they were combined with two rare earth ions $Er^{3+}$and Yb^{3+}. The ion Yb^{3+} receives the energy from the NIR laser at 980 nm wavelength and it shows high quantum yield. The excited Yb^{3+} ion transfers the energy to the Er^{3+} ions, which results in their excitation to a higher level $^4I_{11/2}$. The ions have a non-radiative decay to $^4I_{13/2}$ level and further radiative decay to theground state with 661 nm of wavelength emission (red) this event is called energy transfer upconversion (ETU)[5]. The color of the emission varies according with the percentage of dopants elements [6].One of the challenges of the biolabels, is the chemical durability of the UCNPs, in this study theyhave a silica core shell that is useful because we prevent possible cytotoxicity into the cells[7]. Also, the functionalization of the UCNPs with specific ligands is necessary to label specific cancer cells.There are different types of biological ligands; in this case, folic acid has been use for several authors with successful results with cervical adenocarcinoma cells (HeLa) and breast cancer cells MB-MDA-231[8]. After the UCNPs were coated with a thin silica shell by Stöber method[9], they were functionalized with amine group (APTES/TEOS) to enable folic acid (FA) conjugation[10]. The FAare able to bind to the folate receptor (FR) available on cancer cells surface.Further this bindingprovoke the internalization of the NPs into the cytoplasm via endocytosis[11]. The FR has three isoforms (α, β and γ), the studied cells have FR-α overexpressed[12].The cytotoxicity of the UCNPs was tested by a cell viability assay based on the reduction of the MTT reagent (methy-134

thiazolyltetrazolium) for HeLa and trypan blue assay for MB-MDA-231. They were characterized before and after functionalization. The UCNPs presented an average size of 50 nm for the $Gd_2O_3:Yb^{3+}$, Er^{3+} and 70 nm for the $Y_2O_3:Yb^{3+}$, Er^{3+}, showed strong luminescence emission and they were non-cytotoxic.

II. MATERIALS AND METHODS

2.1 Sol-gel synthesis and ultrasonication

The precursors used were: $Y(NO_3)_3$ (Alfa Aesar 99.9965%) or$Gd(NO_3)_3$ (Alfa Aesar 99.99%) with$Yb(NO_3)_3$ (Alfa Aesar 99.9%) and$Er(NO_3)_3$ (Alfa Aesar 99.9%). Theywere prepared by sol-gel synthesis and the annealing temperatures were 1200°C for Y_2O_3 and 900°C for Gd_2O_3[4, 6]. The UCNPs were ultra-sonicated with high intensity ultrasonic processor (Sonics & Materials, Inc.) at 70% of the amplitudefor about 30 min with 20 ml of isopropanol/ethanol [6].

2.2 Silica and Aminosilane functionalization

The biolabels must accomplish specific characteristics in order to target onto a specific tumour; the size has to be less than a 100 nm and the surface need to have the proper ligands that bind to the surface of the cells.The UCNPs were functionalized with aminopropyltrimethoxysilane (APTES)[8], the amino groups (NH_2) formed on the surface of the UCNPs are easily able to bind with folic acid (FA). TheFAcan be linked with the folic acid receptors on the cell surface (FR).It was found that when FA was chemically linked with amine or c-carboxyl groups, its FR binding affinity were hardly affected[13].The UCNPs were coated with a thin silica shell; we used the Stöber synthesis[9]. The UCNPswere coated with the TEOS technique (Tetraethyl orthosilicate, Sigma Aldrich 98%) [14]. They were ultrasonicated after the coating and then the aminosilane functionalization (UCNP-NH_2) was done mixing the coated UCNPswith ethanol, 0.02 ml of 3-Aminopropyl-trimethoxysilane (APTES, 98% Sigma Aldrich), 0.14 ml of TEOS and 0.2 ml of ammonium hydroxide, for 4 hours.Theywere dried and collected [8, 14].

2.3 Folic acid conjugation

Folic acid is also known as folate and it has a high affinity binding reagent that could recognize folate receptor (FR). The cancer cells studied have a tumor marker over-expressed on the surface[8]. The UCNPs were functionalized with folic acid ligands; the reaction was prepared on a Schlenk system. The solution was agitatedinto the darkness. The resulted UCNP-NH_2-FA were centrifuged (6000 rpm for 15 min), washed with DMSO (3 x 45 ml) and ethanol (5 x 45ml). Finally they

were vacuum dried overnight at 30°C. The UCNP-NH_2-FA turned into a yellow color [15].

2.4 Characterization

To study the crystallinity of the UCNPs we did the X-Ray diffraction (XRD) analysiswith the Phillips X'Pert-MPD, equipped with Cu Kα radiation (λ= 0.15406 nm). The results obtained were compared with the database PCPDFWIN [6]. To study the morphology and the nanoparticle size we used the transmission electron microscopy (TEM) brand JEOL JEM-2100-F. We used the fluorescence spectrometer (PL, Hitachi® FL-4500) with 980 nm for excitation to analyze the photoluminescence of the UCNPs. FTIR analysis was done to confirm the aminosilane-folic acid functionalizationin the range of 400–4000 cm^{-1}(Thermonicolet 1700).

2.5 Cell culture

We obtained from American Type Culture Collection (ATCC) the human cervix carcinoma HeLa cells (ATCC CCL-2) and breast cancer cells (MDA-MB-231). Theywere cultivated in RPMI-1640 media supplemented with 10% Fetal Bovine Serum (FBS, BenchMark, Gemini Bio Products), 1% Penicillin streptomycin (Sigma-Aldrich), 1% L-glutamine and 1.5 g/l sodium bicarbonate. Cells were propagated in growth medium and maintained at 37°C and 5% CO_2.

MCF7 cells were cultured in Dubelcco's Modified Eagle Media (DMEM, Sigma Aldrich, MO, USA) supplemented with 10% SFB, 1% antibiotic/antimicotic, 1% L-glutamine, 1.5. g/l sodium bicarbonate and 0.01 mg/ml of human recombinant insulin. Cells were propagated in growth medium and maintained at 37°C with 5% CO_2.

2.6 Cytotoxicity assay

The evaluation of the cell membrane integrity is one of the most common ways to measure cell viability and cytotoxic effects. The assay based on the reduction of the MTT reagent (methy-134 thiazolyltetrazolium) measures the reducing potential of the cell using a colorimetric reaction. The viable cells reduce the MTT reagent to a colored formazan product. The bare UCNPs and functionalized UCNP-NH_2-FA were tested using the TOX1 in vitro toxicology assay kit (Sigma-Aldrich). The test was done in a 96-well plate containing 10,000 cells per well. The UCNPs were ultrasonicated and diluted at 0.001 μg/mL to 1 μg/mL in RPMI-1640 media. Hela cells were incubated for 24 hr at 37°C and 5% CO_2. The positive control was the incubation of cells in complete RPMI-1640 media without UCNPs, simulating cell behavior under ideal conditions. DMSO (Dimethyl sulfoxide) was used to induce cell death for negative control. After incubation time, cells were

washed with phosphate buffer solution pH 7.4 (PBS 1x) and MTT reagent was added to the plate. Cytotoxicity was evaluated by absorbance measurements with an ELISA plate reader (Thermo Scientific, USA) at 570 and 690 nm. All data obtained from incubated UCNPs were normalized to data from three positive control wells with no UCNPs in three independent experiments[16].

2.7 Trypan blue assay

Vital dyes, such as trypan blue, are normally excluded from the inside of healthy cells; but if the cell membrane has been compromised, they cross the membrane and stain intracellular components. This staining method is described as a dye exclusion method, because cells are very selective in the compounds that pass through the membrane, the trypan blue is not absorbed by viable cells however, it traverses the membrane in a dead cell.Thetrypan blue assay was used to measure the cytotoxicity of the UCNPs (bare and functionalized) with breast cancer cells (MB-MDA-231).The cell viability was calculated as the number of viable cells divided by the total number of cells within the grids on the hemacytometer. The cells are considered non-viable if they take up trypan blue. The solution of trypan blue was prepared with 0.4% solution of in buffered isotonic salt solution pH 7.4 (PBS 1x) and 0.1 mL of trypan blue stock solution to 1 mL of cells. The cells were loaded on the hemacytometer and examined immediately under a microscope at low magnification. The quantities of blue staining cells were counted and the number of total cells was also verified [17]. All experiments were done in triplicate and the results were expressed as mean ± standard deviation of three independent experiments. The data were evaluated by analysis of variance (ANOVA), followed by Tukey's Multiple Comparison Test, using Graph Pad Prism 6.0 software. The results were considered statistically significant when $p < 0.05$.

2.9 Confocal microscopy cell imaging

In this study, the nucleus of the fixed cells was strained withthe fluorescentstainDAPI (4', 6-diamidino-2-phenylindole). This dye binds strongly to A-T (adenine-thymine) rich regions in DNA and it is used extensively in fluorescence microscopy.We seeded 300,000 cells in RPMI-1640 media and incubated overnight at 37 °C and 5 % CO_2 into a culture Petri dishes coated with Poly-d-lysine (Mat-Tek P35GC1.5-10C). The HeLa and breast cancer cells (MB-MDA-231) wereincubated with 1 µg/mL of UCNP-NH_2-FA for 24h at 37 °C and 5 % CO_2. After incubation, the cells were rinsed with PBS 1x and fixedwith 4 % formaldehyde-PBS solution at 4 °C for 15 min.Then they were permeabilized with 0.5 % Triton X/PBS 1x for 15 min at 4 °C. The nuclear staining was achieved by incubated the cells with DAPI at 0.5 ng/µL in darkness for 10 min at RT, followed by five washes with PBS. Nuclear staining with DAPI was also visualized with an inverted laser-scanning microscope OlympusFluoView FV1000 (Japan) using an argon ion laser for excitationat 405 nm wavelength and filters for emission of DAPI. UCNPsfluorescent was detected using the NIR laser (980 nm) and RFP (red fluorescent protein) filter channel (excitation at 487 nm and emission at 610 nm). Cells were visualized with a $63 \times$ (DIC), 1.4 N.A. planapochromaticoil immersion objectives. The imaging parameters used produced no detectable background signal from any source other than from UCNPs and DAPI. The MetaMorph software for Olympus was used to capture the images [18].

III.   RESULTS

3.1 TEM images of UCNPs

The compositions obtained for the UCNPs synthesized by the sol-gel method wereand $(Y_{0.89}Yb_{0.1}Er_{0.01})_2O_3$ and $(Gd_{0.89}Yb_{0.1}Er_{0.01})_2O_3$ respectively.In figure 1 are shown the TEM images of bare and functionalized UCNPs of Y_2O_3:Er^{3+}/Yb^{3+} (1%, 10% mol) and Gd_2O_3:Er^{3+}/Yb^{3+} (1%, 10% mol). The form of the UCNPs is mostly spherical. The average size of UCNPs Y_2O_3:Er^{3+}/Yb^{3+} were 70 nm (+/- 10 nm) and 50 nm for Gd_2O_3:Er^{3+}/$Yb^{3+.}$ We observed agglomerates in all the UCNPs. The silica shell is approximately of 5 nm thick.
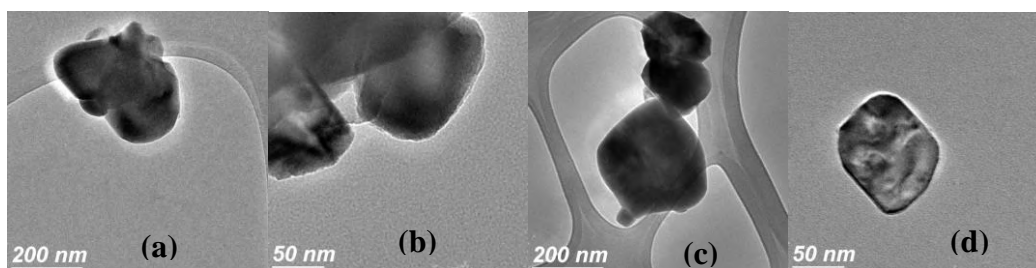
Fig.1: *TEM images of UCNPs Y_2O_3: Er^{3+}/Yb^{3+} (1%, 10% mol) (a) bare and (b) functionalizedUCNP-NH_2-FA.TEM images of Gd_2O_3: Er^{3+}/Yb^{3+} (1%, 10% mol) (c) bare and (d) functionalized UCNP-NH_2-FA.*

3.2 Upconversion luminescence

In figure 2 are shown the upconversion luminescence spectra of bare and functionalized UCNP-NH$_2$-FA with 980 nm laser excitation. The red emission of the nanoparticles Y$_2$O$_3$:Er^{3+}, Yb^{3+}(1%, 10% mol) was at 661 nm of wavelength(figure 2-a) and also the same fluorescence applying for the Gd$_2$O$_3$:Er^{3+}, Yb^{3+}UCNPs (figure 2-b), with

the electronic transitionof the Er^{3+} ion in the level^{4}F$_{9/2}$→^{4}I$_{15/2}$ (660 nm). This is because the UCNPs have the same dopants in different hosts, so the luminescence effects are the same due to the energy transfer process from Yb^{3+} ion to the Er^{3+} ion. The difference between both UCNPs is the size; the Y$_2$O$_3$ UCNPs are bigger due to the size of the lattice.
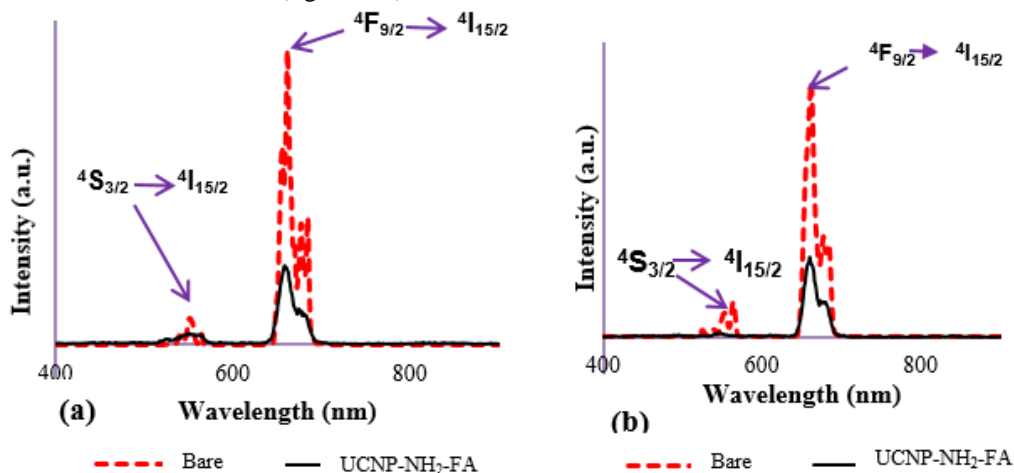
Fig.2: The upconversion emission spectra with 980 nm excitation for bare and functionalized UCNPs of (a) Y$_2$O$_3$:Er^{3+}/Yb^{3+} (1%, 10% mol) and (b) Gd$_2$O$_3$:Er^{3+}/Yb^{3+} (1%, 10% mol)

3.3FTIR analysis

The Fourier transform infrared spectroscopy analysis (FTIR) was used to verify the functionalization UCNP-NH$_2$-FA. With this technique, we verify thepresence of the amine groups and folic acid on the surface of the

nanoparticles with an infraredspectrum of absorption or emission.The figures4-aand 4-c show the FTIR spectra of bare UCNPs. Figures 4-b and 4-dshow the aminosilane-folic acid functionalization (UCNP-NH$_2$-FA).

(c)   **(d)**
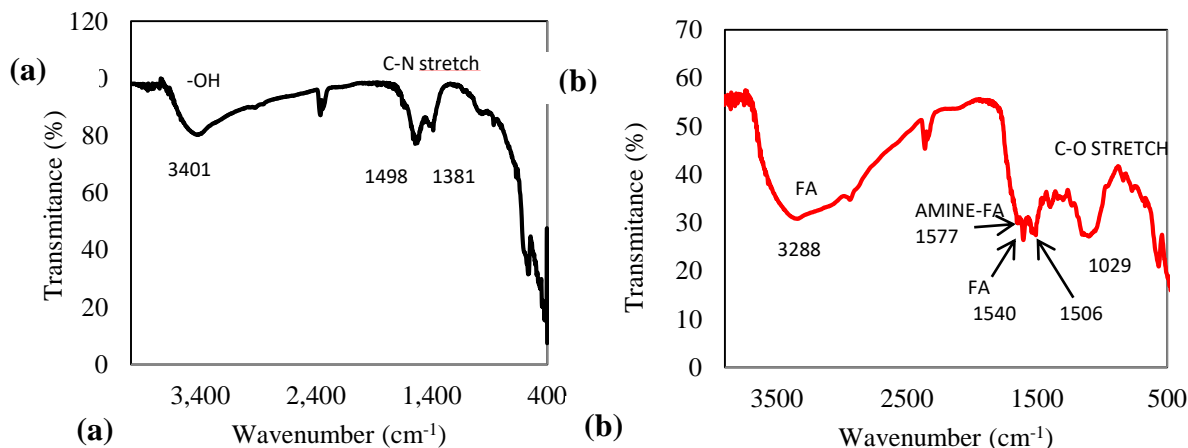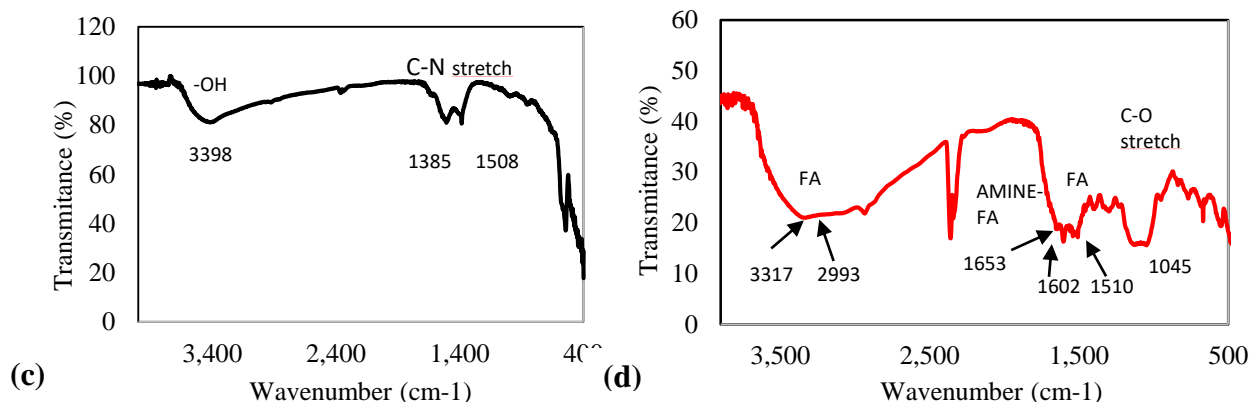
Fig.4: FTIR spectra of (a) bare UCNPs Y_2O_3:Er^{3+}/Yb^{3+}(1%,10% mol), (b) UCNPs with aminosilane functionalization, (c) bare UCNPs Gd_2O_3:Er^{3+}/Yb^{3+}(1%,10% mol), (d) functionalized UCNP-NH_2-FA.

3.4 Cytotoxicity assay and cellular imaging.

The cytotoxicity results with the MTT assay for bare and functionalizedUCNP-NH_2-FAincubated on HeLa are shown in figure 5.The UCNPs tend to agglomerate and precipitate after the addition to the well of the 96-well plate, even after been ultrasonicated, this reason causes interference with the absorbance reading of the plate.The results for Y_2O_3:Er^{3+}, Yb^{3+} are on figure 5-afor HeLa cellsand Gd_2O_3:Er^{3+}, Yb^{3+} are in figure 5-b. On both assays the functionalized UCNPs showed no cytotoxicity on both cancer cell lines.

(a)   **Nanoparticles concentration µg/mL**   **(b)**   **Nanoparticles concentration µg/mL**
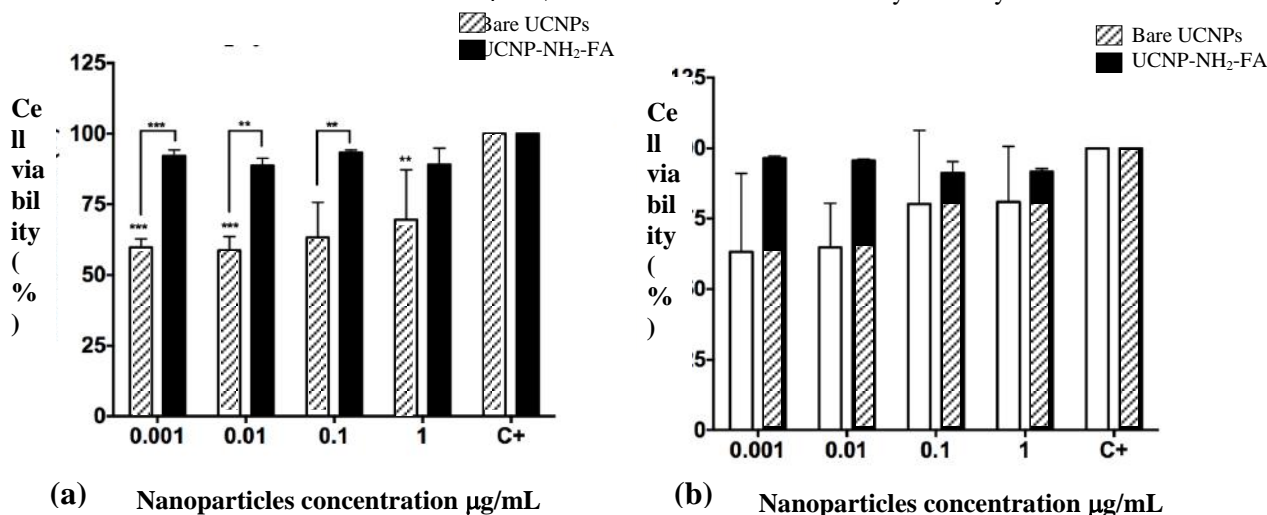
Fig.5: Cell viability assay of (A) bare UCNP Y_2O_3:Er^{3+}/Yb^{3+} (1%,10%) (lined bars) and functionalized UCNP-FR (black bars) with HeLa cells, (B) bare UCNP Gd_2O_3:Er^{3+}/Yb^{3+} (1%,10%) (lined bars) and functionalized UCNP-FR (black bars) with HeLa cells.

The cell viability for breast cancer cell MB-MDA-231 is shown in figure 6 shows with trypan blue assay with 0.1 and 1 µg/mL of UCNPs concentration. The results indicated in figure 6-a for UCNPs Y_2O_3:Er^{3+}, Yb^{3+} that there are no cytotoxicity of functionalized UCNPs with 65.71 % and 80.56% of cells viability. For the UCNPs Gd_2O_3:Er^{3+}, Yb^{3+}, the cell viability is more than 83% on both concentrations, as shown in figure 6-b.

(a)   **(b)**
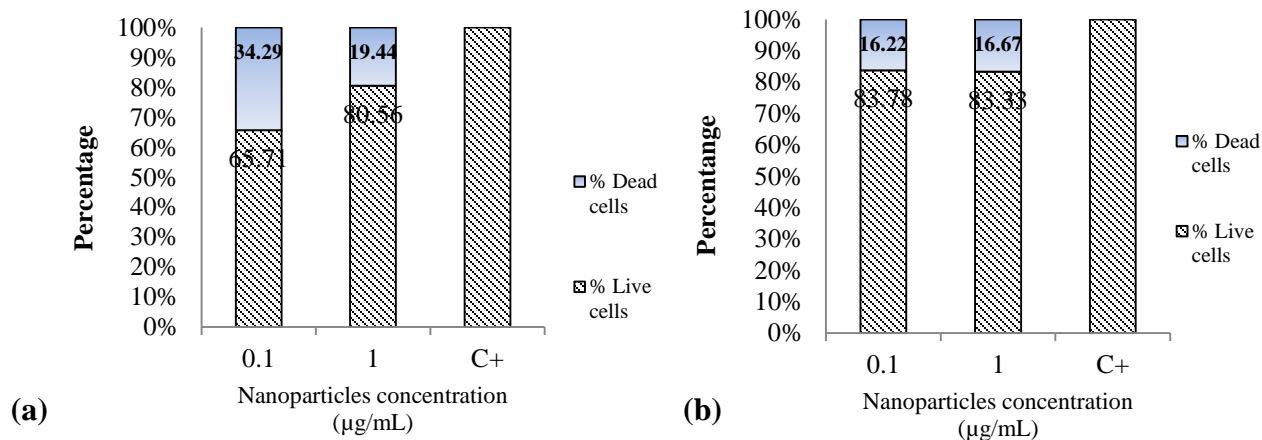
Fig.7: Results of trypan blue assay for breast cancer cells (MB-MDA-231) with the incubations of UCNP-NH$_2$-FA of (a) Y$_2$O$_3$:Er^{3+}/Yb^{3+}and (b)Gd$_2$O$_3$:Er^{3+}/Yb^{3+}with two different concentrations.

3.5 Cancer cell imaging with UCNPs

The UCNP-NH$_2$-FAwere excited with a 980 nm laser in cell culture medium with the characteristic green upconversion emissions; they were incubated in both cancer cell lines with a concentration of 1 µg/mL for 24 hours into the cells, then they were properly fixed and prepared in order to obtain imaging with the confocal microscope. The nucleus (N)stained with DAPI, was excited with 405 nm to obtain 461 nm of emission (blue) of the DAPI dye, shown in figures 8-a, 8-d, 9-a and 9-d. Figure 8 shows the UCNPsinto

HeLa cells and figure 9 shows UCNPs into breast cancer cells (MB-MDA-231). In figures 8-b, 8-e, 9-b and 9-e it is seen the localization of functionalized UCNPs only excited with NIR 980 nm +RFP (red fluorescent protein) 8-c, 8-f, 9-c and 9-f shows the merge of the images. The UCNPs were clearlylocalized in the cytoplasmic region as expected, since folic acid ligands were used for UCNPinternalization.The confocal images of the UCNPs into the cells were observed in the laser-scanning microscope Olympus FluoView FV1000 (Japan).
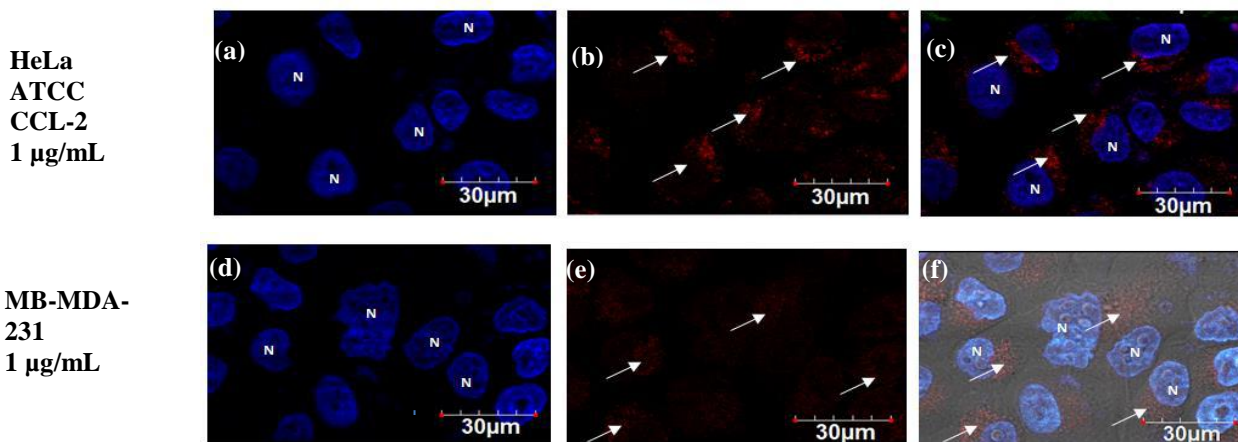
Fig.8: Fluorescence redemission by Y$_2$O$_3$:Er^{3+}/Yb^{3+} (1%,10% mol) incubated with ℍeLa cells (concentration 1 µg/mL) for 24 h. (a) Staining with DAPI show nuclei of HeLa, Мʙ-MDA-231 and MCF-7 cells labeled as "N" (b) Laser NIR 980 nm + RFP shows the functionalized UCNPs into the cell. (c) Overlay DAPI, Laser 980 nm +RFP localize the UCNPs activity in the cytoρiasm of the cells (white arrows).

Fig.9: *Fluorescence red emission by Gd_2O_3:Er^{3+}/Yb^{3+} (1%,10% mol) incubated with HeLa cells (concentration 1 µg/mL) for 24 h. (a) Staining with DAPI show nuclei of HeLa, MB-MDA-231 and MCF-7 cells labeled as "N" (b) Laser NIR 980 nm + RFP shows the functionalized UCNPs into the cell. (c) Overlay DAPI, Laser 980 nm +RFP localize the UCNPs activity in the cytoplasm of the cells (white arrows).*

IV. DISCUSSION AND CONCLUSIONS

The UCNPs synthesized by the sol-gel methodwith the hosts Y_2O_3 and Gd_2O_3 co-doped with Er^{3+} and Yb^{3+}had a shape mostly spheroidal with an average diameters of 70 nm and 50 nm (±10 nm) respectively.The photoluminescence analysis showed outstanding optical properties for bare and functionalized UCNPs, they have a stable luminescence, photostability and long lifetimes of excited states, so they overcome the problems of the currently used organic dyes. The UCNPs showed red emission spectra (660 nm). The FTIR spectra showed the prescence of the amine-folic acid bonds (NH2-FA) on the surface of the UCNPs (1612 to 1512 cm-1), the FA ligands (3331 cm-1) and the wagging –NH2 (669-793 cm-1).We evaluated the viability of the cells with bare and functionalized UCNPs with the MTT assay. The ability of the cells to reduce MTT is an indicator ofmitochondrial integrity and its functional activity is interpreted as measure of cell viability after exposure to the UCNPs evaluated.The HeLa cells incubation with different bare Y_2O_3:Er^{3+}/Yb^{3+} and G_2O_3:Er^{3+}/Yb^{3+}at 0.001 and 0.01 µg/mLconcentrations caused a 40% of cell death. But,with UCNP-NH_2-FA, all the cells had more than 80% of viability, thus the cell death and the cytotoxic effect was reduced for all of the tested concentrations. For breast cancer cells MB-MDA-231, trypan blue assay showed more than 80% cell viability for the tested concentrations, confirming that the UCNPs are non-cytotoxic.The studies with the confocal microscope showed the UCNPs localized into the cell cytoplasm with no cytotoxicity effects to other possible cells, which confirms that they can be used as biolabels for the cancer

cells studied. Further studies with *in vivo* murine models with breast and cervix cancer need to be tested to be considered as an important tool to diagnostic cancer.

V. ACKNOWLEDGEMENTS

REFERENCES

[1] Wang M., Abbineni G., Clevenger A.: Upconversion nanoparticles: synthesis, surface modification and biological applications.*Nanomedicine.***7**, 710–729 (2011).

[2] Min L., Ying Z., Shu W., Ming L., Duan Z., Chen Y., Li Y., Xu F., Lu T.: Recent advances in synthesis and surface modification of lanthanide-doped upconversion nanoparticles for biomedical applications. *Biotechnol. Ad.***30**, 1551-1561 (2012).

[3] Matsuura D.: Green and blue upconversion luminescence of trivalent-rare-earth ion-doped Y2O3 nanocrystals. *Appl. Phys. Letters.* **81**, 4526-4528 (2010)

[4] Taxak V., Khatkar S., Han S., Kumar R., Kumar M.: Tartaric acid assisted sol gel synthesis of Y_2O_3:Eu^{3+} nanoparticles. *J. Alloys Compds.* **469**(1), 224-228 (2009).

[5] Blasse G., Grabmaier B. Luminescent Materials, Telos, Berlin, Springer-Verlag (1994).

[6] Chávez D., Contreras O., Hirata G.: Synthesis and upconversion luminescence of nanoparticles Y_2O_3 and Gd_2O_3 Co-doped with Yb^{3+} and Er^{3+}. *Nanomaterials and Nanotechnology,***6**, 7-17 (2016).

[7] Da Costa M., Doughan S., Han Y., Krull U.: Lanthanide upconversion nanoparticles and applications in bioassays and bioimaging: A review. *Anal. Chim. Acta,***832**, 1–33 (2014).

[8] Sudimack, J., Lee, R.J.: Targeted drug delivery via the folate receptor. *Adv. Drug Deliv.Rev*. **41**, 147–162 (2000).

[9] StöberW., Fink A., Bohn E.: Controlled growth of monodisperse silica spheres in the micron size range.*J. of Colloid and Interface Science,***26** (1), 62-69 (1968).

[10] Sounderya N., Zhang Y.: Upconversion Nanoparticles for Imaging Cells. *Proceedings* **23**, 741–1744 (2009).

[11] Lu, Y., Sega, E., Leamon, C.P., Low, P.S.: Folate receptor-targeted immunotherapy of cancer: mechanism and therapeutic potential. *Adv. Drug Deliv. Rev*. **56**, 1161–1176 (2000).

[12] Yee, K., Seow, E, Zhang, Y., Chyn, Y.: Biomaterials Targeting CCL21 e folic acid e upconversion nanoparticles conjugates to folate receptor- a expressing tumor cells in an endothelial-tumor cell bilayer model. *Biomaterials.* **34**, 4860–4871 (2013).

[13] Ai J., Xu Y., Li D., Liu Z., Wanga E.: Folic acid as delivery vehicles: targeting folate conjugated fluorescent nanoparticles to tumors imaging. *Talanta*. **101**, 32–37 (2012).

[14] Chávez D., Juárez-Moreno K., Hirata G.: Aminosilane functionalization and cytotoxicity effects of upconversion nanoparticles Y_2O_3 and Gd_2O_3 Co-doped with Yb^{3+} and Er^{3+}. *Nanobiomedicine*. **3,** 1-7 (2016).

[15] Chávez-García D., Juárez-Moreno K., Hirata G.A.: Synthesis, aminosilane-folic acid functionalization and cytotoxicity of the upconversion nanoparticle Y2O3+:Er3+, Yb3+ for cancer cell detection. *RIIT*. **4,** 24, 1-11 (2017).

[16] Hemmer E., Yamano, Kishimoto, Venkatachalam, Hyodo, Soga: Cytotoxic aspects of gadolinium oxide nanostructures for up-conversion and NIR bioimaging.*ActaBiomaterialia.***9**, 4734-4743 (2013).

[17] Strober W.: Trypan blue exclusion test of cell viability.*Pub med.***3** (2001).

[18] Sanchez-Sanchez L., Tapia-Moreno A., Juarez-Moreno K., Patterson D., Cadena-Nava R., Douglas T. and Vazquez-Duhalt R.: Design of a VLP nanovehicle for CYP450 enzymatic activity delivery", *J. Nanobiotechnol.***13**, 66-76 (2015).

Analysis of fire extinguisher gauge level using OpenCV

Gayatri Behera

Abstract— *Computer Vision domain holds the promise of finding solutions to the most arduous issues of today. Analyzing and deciphering an image clearly with the aim of gathering more insight, especially without any human intervention is the ideal goal. With this aim in mind, it would be highly desired to have an autonomous detector that measures the reading given by a fire gauge which is mounted off a fire exterminator.*

Keywords— *Feature extraction, image processing, OpenCV.*

I.   INTRODUCTION

This problem is primarily focused in the domain of disaster-averting; with an inclination towards fire-fighting.

Any fire can be controlled by making use of fire extinguishers that help douse out a flame by spray out CO2 (carbon-dioxide). These fire extinguishers are installed at multiple locations in any establishment depending on the number of people frequenting the place, size of the establishment, nature of work conducted at the establishment etc. These cylinders have a dimension of about 30cm – 50 cm and typically weigh around 2.5kg – 18kg or so. The fire extinguishers are typically mounted with a fire gauge meter that helps track the pressure exerted on carbon dioxide still pending within the cylinder.

Regular maintenance work involves the monitoring of these gauges manually by maintenance workers to ensure that the content level is up to the mark. This would involve regular up-keep and monitoring by the said personnel at regular fixed intervals. This is a necessity, not just to get an estimate of the content level but also to ensure that proper health of the cylinder is being maintained. Such measures may not be entirely feasible if and when the establishment in question is very vast in size or lacks sufficient number of people to man the premises. This could create unimaginable difficulties in that, if a particular cylinder is partially full or not fully equipped to douse out a flame then it could lead to substantial loss of property and worse - injury as well as loss of life.

An ingenious work around could be to utilise the CCTV (closed circuittele-vision) cameras installed at such places to maintain the up-keep of cylinders installed at such premises. In fact, the inclusion of CCTV systems in manning them can help in taking daily as well as weekly updates.

A brief manner in which this can be done would involve taking snapshots of the video stream gathered from these cameras at regular, predefined intervals. Further processing and filtering of the image. Segmenting out the image to determine the features and areas of interest i.e. the fire gauge meter section. Ultimately, this would help in reaching a conclusion.

II.   WORKING

The abstract code would involve writing code in Python, utilizing OpenCV - Python's feature-rich library that caters exclusively to the computer vision domain.

The initial steps would involve procuring images of a certain preset dimension. Allowances can be made later on, to accommodate live video feed too.

The steps would involve:-

1. Fetching of the image of pre-defined configurations
2. Implementation of initial, filtering on the images to convert the image from a colored image to a gray-scale image
3. Smoothening of the image to remove noise, blurring effects from these images.
4. Performing color identification to identify particular color pixels in a certain region.
5. Cropping out or segmenting this region.
6. Drawing a conclusion.

System Flow:

Make use of OpenCV library by Python to read and perform filtering of the images. ThePython version used would be - 2.7 on Windows 8.1/10 environment. IDEused was Visual studio 2015 community edition - which provides support for installation of all other Python packages through the IDE itself, namely - Numpy, Matplotlib and OpenCV (but provided Python 2.7 has been installed before).

OpenCV: It provides certain in-built commands such as imread(), imshow() to take in as well as display images. cvtColor() to convert images from one color scale to another. Also, support for certain filters for edge detection, blurring etc. is provided.

Numpy: It helps in reading the image as an array of numbers. That helps in identifying important features that can be further isolated and which would aid in classification. For instance - the Numpy value of an image provides information not just about the image dimension and size, but also about particular pixel values which in turn indicate the presence of a certain color. Each pixel in an image has an RGB component – which denotes the extent of the colors – Red, Green and Blue. In case of the fire extinguisher cylinder, the pressure gauge measures the pressure exerted in psi on the pressurized gas.The gauge meter is separated into two color-coded regions i.e green and red. Green indicates the "Safe" zone and Red that the pressure is well within the normal range.

Fig.1: Standard fire extinguisher pressure gauge image

Conversion of this image to the it's gray-scale equivalent yields the below result –

Fig.2: (a) Standard fire extinguisher pressure gauge image on gray-scale conversion. (b) On segmenting out the red-colored region.

Segmenting the image based on the pixel values that would identify the region based on it's underlying color.

III.   RESULTS

Utilizing this approach helped identify fire extinguishers which would not function as expected in the advent of a fire emergency. The relative position of the dial on the particular color region indicates the health of the fire extinguisher. In this case, it came out to lie in the "danger" or red zone, so the fire extinguisher could be duly replaced or repaired before-hand.

REFERENCES
[1] www.opencv.org/
[2] http://ieeexplore.ieee.org/document/6240859/?reload=true
[3] http://www.pyimagesearch.com/

A Secure IoT Data Integration in Cloud Storage Systems using ABAC Access Control Policy

Ismail Chahid, Abderrahim Marzouk

IR2M Laboratory, Faculty of Science and Technology, University Hassan 1st Settat, Morocco

Abstract— Internet of Things has become one of the most emerging technologies now days, which is growing rapidly in the telecommunications field. It is as a network of physical objects, peoples, vehicles, buildings, and other items, which are having a unique identity and are able to interchange data using embedded electronics, sensors, and software equipment to reach common goals. The large scale of real time data collected and exchanged between objects in IoT grows exponentially which represent a big challenge in term of storing and processing. Cloud Computing has emerged as a key technology to solve the problem of IoT data storage and processing by offering multiple choices of resources provided by cloud service provider, including storage, processing, memory and network bandwidth. Nevertheless, as many other technologies, Cloud computing has some issues regarding IoT data storage. One of the major issues is Security and Privacy. In this paper, we will present a proposed architecture for a Secure IoT data integration in Cloud Storage Systems.

Keywords— Cloud Computing; Internet of Things; Security; Data.

I. INTRODUCTION

In the recent years, Internet of Things (IoT) has become one of the most promising technologies in the telecommunication field. It represent a new paradigm in which interconnected and heterogeneous entities such as physical objects, peoples, vehicles, devices, buildings and other objects are having a unique identity (ID) and are able to interchange data using embedded electronics, sensors, and software equipment to reach common goals [1]. This new step in technology sector will have a high impact on different areas including smart homes, assisted living, e-health, industrial manufacturing and environmental monitoring. The main technologies parts involved in Internet of Things are Wireless Sensor Networks (WSN), Radio-frequency identification (RFID), machine-to-machines interfaces (M2M), micro-electromechanical systems (MEMS) and Internet. All this technologies combined with different entities in IoT environment will increase the amount of data collected exponentially which represent a big challenge in term of processing and Storing. Cloud Computing appear to be an ideal choice to solve the

problem of processing and storing data collected from different IoT devices [2], since it provide a multiple choice of resources including high performance processing, storage, memory and network bandwidth that are accessible on demand anywhere [3]. However, Cloud Computing technology comes with some issues that are Security and Privacy concerns [4]. Many organizations, companies and individuals are using sensitive and confidential data in their transactions. This data is collected from IoT devices and moved into cloud storage to be processed using different computing techniques like virtual machines. Many security challenges can be encountered during this process like accessibility vulnerability, and virtualization vulnerability. which makes it hard for organisations to adopt this technology due to previous mentioned concerns. This paper is organized as follows. In section 2, we present the previous released research that deal with the topic of IoT data security in Cloud Storage. Section 3 discuss the IoT architecture and the authentication of IoT devices to the Cloud. Moreover, in section 4 we discuss the ABAC Access Policy and finally we present the proposed architecture for IoT Data integration to the Cloud.

II. RELATED WORK

Security issues is on of big concerns in term of storing processing and managing data in both IoT and Cloud environment. In [5] authors presented a survey on secure integration of IoT and Cloud Computing, and then they proposed a model for securing this integration. A secure storage system was proposed for storing IoT data in [6], the authors applied a Role Based Access Control policy (RBAC) combined with AES/RSA encryption to manage authenticity and data security, but Role-based access controls (RBAC) may not suffice in the IoT because of the lack of flexibility.. In [7] an authentication model was described based on different access use case scenarios in IoT Clouds. A multi-layer cloud architectural model was proposed in [8] for IoT-based smart homes, the main idea focus on the development of a Public cloud that collect data from different private cloud vendors using Ontology-based security service framework.

III. IOT DATA INTEGRATION IN THE CLOUD

A. *Internet of Things Architecture*

IoT architecture can be represented with four categories of interconnected systems such as things, gateways, network and cloud as showed in Figure 1.

Things: Today large amounts of things are found in industrial and commercial settings, it is also in users mobile and home. Already, cars, device sensors, and mobile phones are accessing the Internet through broadband wireless networks. IoT technology solution requires intelligent things capable of filtering and managing data locally and connecting to gateways easily.

Gateways: The majority of existing things are not capable to connect to the internet to share data with the cloud because of their design. To solve this issue, gateway act as intermediate between internet and things.

Network Infrastructure: Internet is a complex system of interconnected IP networks that links billions of computers together. Network infrastructure comprises gateways, routers, repeaters, switches and other devices that controls the data traffic and connect with cable and telecom networks operated by different service providers

Cloud: Cloud contains huge number of interconnected virtualized servers and standard servers connected together. To support the IoT environment cloud infrastructure runs different applications, which are capable to analyse the data collected from different devices and sensors to make the correct decision.
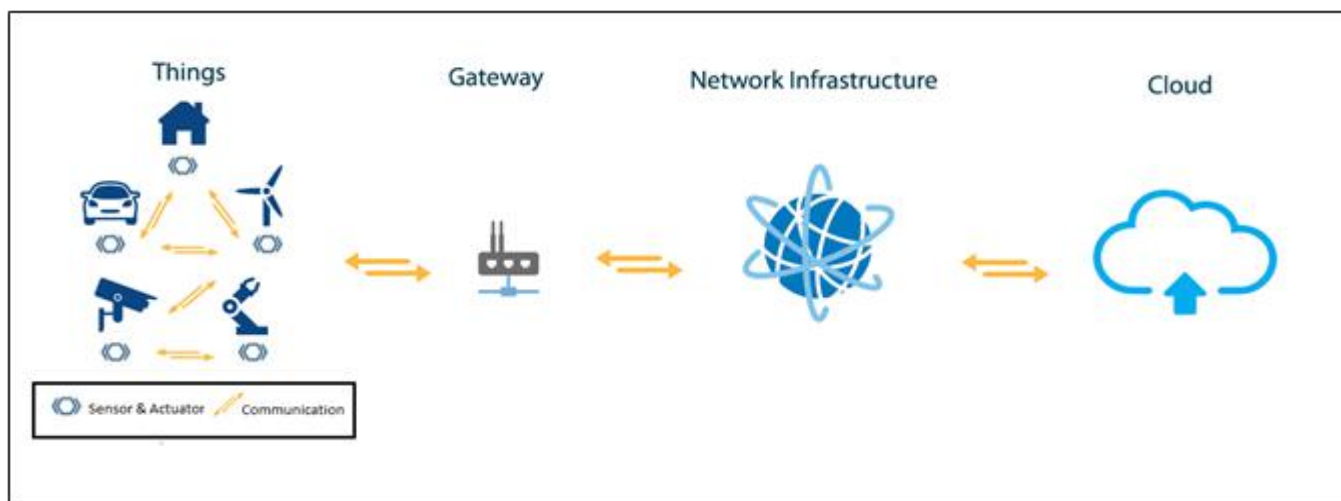
Fig. 1: IoT Architecture

B. *Cloud Computing Architecture*

According to the official NIST definition, "cloud computing is a model for enabling ubiquitous, convenient, on-demand network access to a shared pool of configurable computing resources (e.g., networks, servers, storage, applications and services) that can be rapidly provisioned and released with minimal management effort or service provider interaction."

Cloud Service Providers (CSP) offer their "services" according to standard models defined by NIST, are Infrastructure as a Service (IaaS), Platform as a Service (PaaS), and Software as a Service (SaaS) Figure 2.
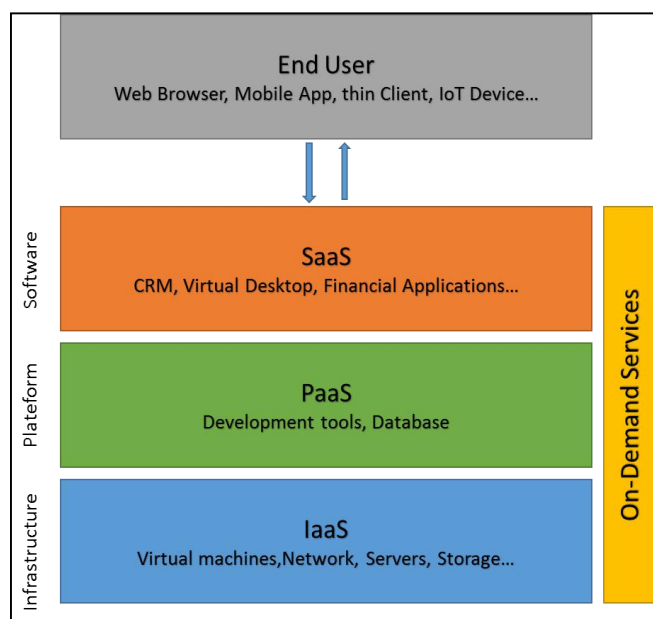
Fig. 2: Cloud Computing Layers

C. Authentication for IoT Clouds

Nowadays, Cloud Computing can provide access to IoT-based resources through special designed applications with specific interconnected structures. Thus, a new iteration in the "as-a-service" model is added to Cloud Concept, which is IoT as a Service or simply (IoTaaS). This new model requires a complex authentication scheme. Authentication refers specifically to verifying the identity of a device. It aims to prove that all entities are what they claim to be. This ensures that communications are only transmitted to the intended recipient; The authentication completely reassures the recipient on the origin of the communication. In the IoT universe, several scenarios are possible: authentication of devices on cloud services, users on devices, objects on objects.

In IoT development field, Authentication standards are a major requirement to execute operations in the efficient way. There is a variety of competing standards. One of them is Fast Online Identity (FIDO) alliance and the other one is M2M. They are both growing authentication and access architectures intended for all IoT markets.

To maintain security, trust, privacy and confidentiality of the integrated data, Internet of Things requires a solid and proven approach.

PKI infrastructure is an interoperable and standard-based technology that has been used in IoT. It comes with a specific scheme to provide main security assessments like privacy data integrity and authentication [9]. The design of PKI infrastructure makes it easily adapted for IoT requirements in term of diversity, velocity and volume. There are many models of integration of the PKI Infrastructure in IoT, one of the models is the hardware based cryptographic device TPM which is a ship that needs to be integrated to the device.

Enabling strong identities at the hardware level protects against identity theft and the compromise of keys that would endanger the entire interconnected system. If a change occurs, the entire ecosystem is notified and the administrators can respond accordingly.

IV.   ABAC ROLE BASED ACCESS POLICY

Access control is based on the identity of a user requesting execution of a capability to perform an operation (e.g., read) on an object (e.g., a file). This can be done directly either as in Discretionary Access Control or Mandatory Access Control or through predefined attribute types, such as roles or groups assigned to that user as in Role Based Access Control or RBAC.

Role-based access controls (RBAC) by themselves may not suffice in the IoT because they are not flexible enough. An RBAC-only system would increase risks in IoT systems and services that possess the following characteristics:

- Unpredictable environments: IoT services within unpredictable environments, such as those environments dealing with many people at once. Where crowd dynamics and emotions can create responses to different conditions that are very hard to project.

- Contrary functions: IoT services with dramatically different, or even opposite, functional requirements under abnormal versus normal conditions—for instance, a fire door during an actual fire (abnormal condition) that must open, versus the same door under non-fire conditions that must sound alarms and not open easily.

RBAC cannot effectively account for these sorts of properties alone, and in the IoT, with the increasing prominence of the logical-kinetic/cyber-physical interface, attributes will play an important role in authorization exercises.

Attribute-based access control (ABAC) is an access control method where subject requests to perform operations on objects are granted or denied based on assigned attributes of the subject, assigned attributes of the object, environment conditions, and a set of policies that are specified in terms of those attributes and conditions [10].

ABAC has three main functional points, which is as follows:

The PEP or Policy Enforcement Point: is a component that serves for protecting apps & data in which ABAC is applied. The PEP inspects the request and describe the user's attributes to the Policy Decision Point PDP.

The PDP or Policy Decision Point is the component that makes the determination of whether a user's request is authorised or not by evaluating incoming requests against policies it has been configured with. The PDP returns a Permit / Deny decision. The PDP may also use PIPs to retrieve missing metadata

The PIP or Policy Information Point serves as the retrieval source of attributes and bridges the PDP to external sources of attributes e.g. LDAP or databases.

The proposed architecture for the authentication of things in IoT-Clouds is a combination of ABAC Technology and PKI Infrastructure (Figure 3). It forces a smart object in IoT to pass a double check authentication system to ensure that the data is collected from the correct IoT object and not from a fake one. For the users that needs to get access the IoT data stored in the cloud, we used another multi authentication factor which is the mobile two factors authentication MPTFA [11].
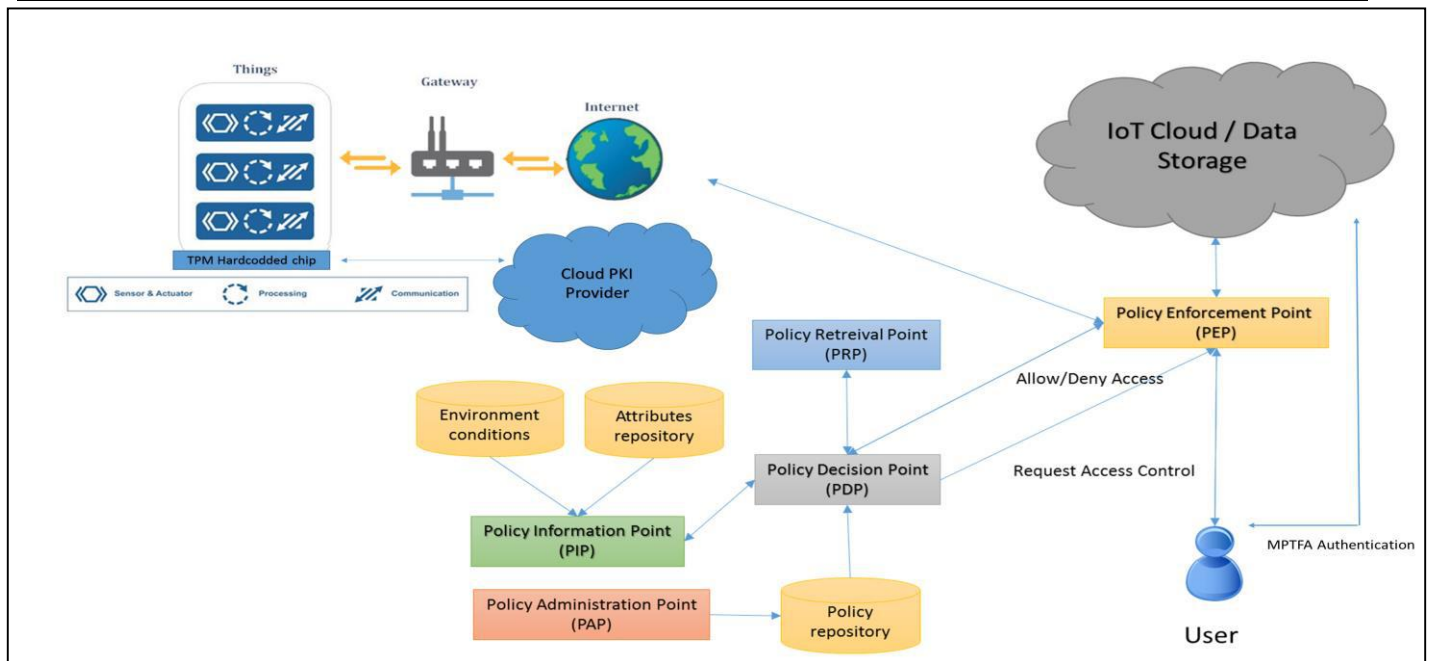
Fig. 3: Proposed Architecture

IV.

CONCLUSION & PERSPECTIVES

In our proposed architecture, we tried to make it possible for storage systems in IoT-Cloud infrastructures to ensure that data collected from things and smart objects is authentic and secure by combining three different authentication technologies: ABAC Access Control, PKI Infrastructure system, and MPTFA.

In our future work, we will try to implement an adoptable cryptosystem in the proposed architecture to increase the security level in cloud storage systems.

REFERENCES

[1] Luigi Atzori , et al The Internet of Things: A survey, doi:10.1016/j.comnet.2010.05.010
[2] The intel IoT platforme, white paper, intel 2015
[3] NIST SP 800-145, The NIST Definition of Cloud Computing, 2011
[4] Amit SangroyaSaurabh Kumar Towards Analyzing Data Security Risks in Cloud Computing Environments, DOI: 10.1007/978-3-642-12035-0_25
[5] C Stergiou, et al., Secure Integration of IoT and Cloud Computing, Future Generation Computer Systems (2016), DOI: 10.1016/j.future.2016.11.031
[6] Jayant D. Bokefode et al., Developing A Secure Cloud Storage System for Storing IoT Data by Applying Role Based Encryption. doi: 10.1016/j.procs.2016.06.007.
[7] Luciano Barreto et al., An Authentication Model for IoT Clouds, DOI: 10.1145/2808797.2809361.
[8] Ming Tao, Jinglong Zuo et al., Multi-layer cloud architectural model and ontology-based security service framework for IoT-based smart homes, DOI: 10.1016/j.future.2016.11.011
[9] Aysha Albarqi et al, Public Key Infrastructure: A Survey Journal of Information Security, 2015, 6, 31-37 TPM
[10] Guide to Attribute Based Access Control (ABAC) Definition and Considerations, NIST Special Publication 800-162,
[11] Ayu Tiwari, Sudip Sanyal, Ajith Abraham, Svein Johan Knapskog, Sugata Sanyal, "A Multi-Factor Security Protocol for Wireless Payment – Secure Web Authentication Using Mobile Devices", *IADIS*, *International Conference Applied Computing*, pp. 160- 167, 2007.

Incompatibility stone-mortar Influence of pH on the sensitivity of rocks to saline alterations

Meriem Benharbit

Institut National des sciences de l'Archéologie et du Patrimoine, Rabat, Maroc

Abstract—This paper discusses incompatibilities between stones and mortars. The aim is to understand the evolution of rocks of acid nature, sandstones in this case, in the presence of mortars of an alkaline nature, such as cement mortars used for jointing or coatings. Accelerated aging tests combining alkaline alteration and salt alteration were simultaneously carried out in order to study the synergy between these two processes of degradation. The degradation process is follow-up by observing the induced alteration patterns, the identification of the newly appeared mineral phases and the evolution of the ultrasonic propagation speed of the materials tested. The obtained results allow showing that the pH-salt crystallization synergy is particularly aggressive towards the studied materials and that the sustainability of the rocks subjected to circulations of basic solutions due to the proximity of mortars of alkaline nature is seriously reduced.

Keywords— durability, incompatibilities, mortar, pH, stone, salts.

I. INTRODUCTION

The aim of this work is to study the behavior of monument stones through an approach based on accelerated cycles of aging in a research theme aiming to study the influence of the chemical nature of mortars on the durability of implemented stones. The juxtaposition in a masonry of materials with different mechanical and chemical qualities can be an additional source of disorders and degradations. The problem of compatibility between waxes stones and mortars is essential [1]. It is indeed necessary to define the behavior of the "stone-mortar" assembly with regard to the factors of alteration in order to improve the durability of the structures. Among the agents of alteration, the soluble salts, which pass through the masonry by means of capillary ascents or rainwater, play a preponderant role in the degradation of the stones used. In fact, accelerated aging tests were carried out to analyze the behavior of materials in the laboratory. The aim of this study is to subject rock samples to the simultaneous action of salts and alkaline solution to see to what extent the alkaline mortars can weaken the stones with which they are associated. The

building stones studied are red vosgian sandstone, beige vosgian sandstone, coal sandstone and molière sandstone.

II. MATERIALS STUDIES

The studied sandstones, of varied provenances, are used in many historical monuments and in particular in the construction of the famous Strasbourg Cathedral with respect to the vosgian sandstones in particular. Coal sandstone comes from the coal basin of the Cevennes. It constitutes the bulk of the waste rock from the coalfields dating from the Stephanian. The molière sandstone comes from the Permian lands of the Montredon-Labessonié region in the Tarn. The Beige and Red Vosgian sandstones come from the Formation of the "Sandstone at lower Voltzia" of the upper Buntsandstein of the Triassic of the Vosges.

The characterization of the studied materials (Fig. 1) was determined by various analytical techniques including optical microscopy (Figs. 2, 3, 4, and 5) for the petrographic aspect. The characterization of the porous space was done by mercury porosimetry.
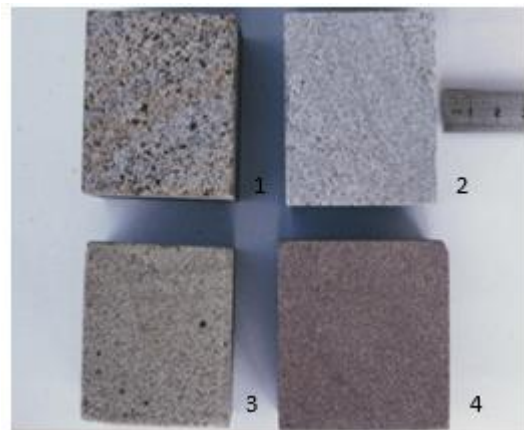
Fig. 1: Macroscopic aspect of sandstone materials, reflecting the differences in mineralogical composition and matrix that gives the rocks their specific color, 1-molière sandstone, 2-coal sandstone, 3- beige vosgian sandstone, 4- red vosgian sandstone.

The apparent volumetric mass, the compressive strength and the propagation velocity of the ultrasound defined the mechanical cohesion of the materials. The characteristics of the studied stones are grouped in Table 1.
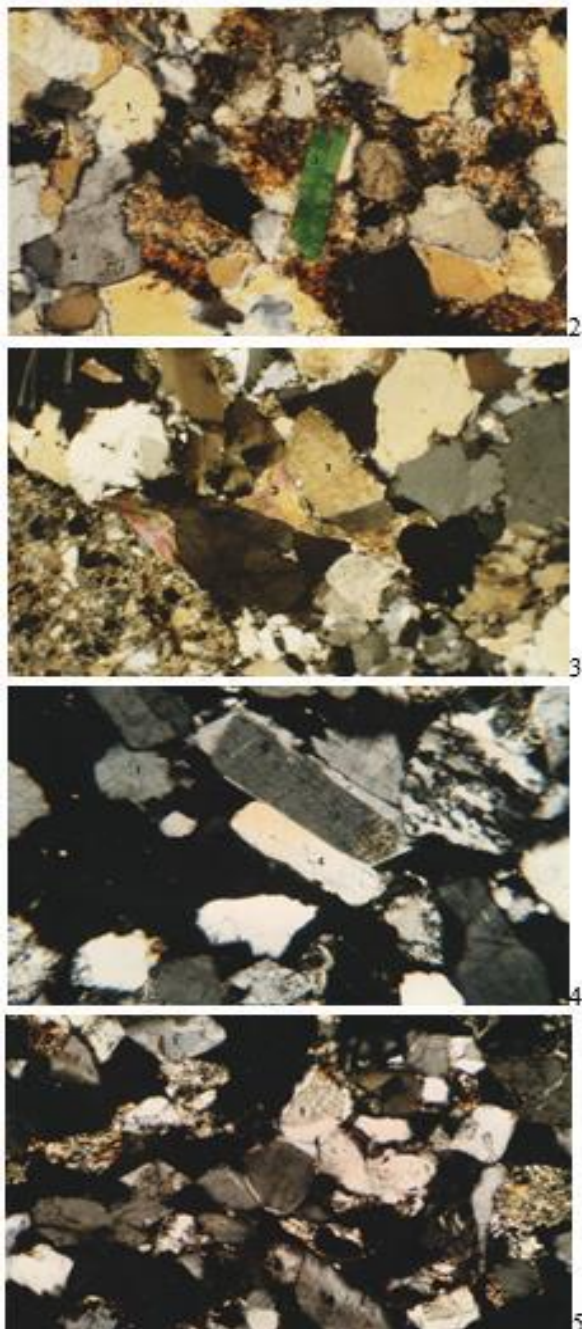
Fig. 2-3-4-5: Optical microscopy of sandstones. The molière sandstone (1) presents aggregates of microcrystalline quartz, detrital quartz, and muscovite flakes bathed in a clay-ferruginous matrix ; Coal sandstone (2) shows fragments of detrital and polycrystalline quartz, muscovite flakes and a clay matrix ; Beige vosgian sandstone (3) shows fragments of detrital quartz, quartz fed by secondary silica, fragments of metamorphic rock and muscovite ; The red vosgian sandstone (4) has elements of secondary feeding detrital quartz, aggregates of micrograiny quartz and a hematite rich matrix.

Table.1: Main characteristics of studied sandstone

	coal sandstone	*molière sandstone*	*beige vosgian sandstone*	*red vosgian sandstone*
Mercury porosity	13.6 %	13.9 %	3.6 %	6.5 %
Apparent volumetric mass (g/cm^3)	2,3	2,22	1,82	1,99
Mechanical resistance (MPa)	⊥ au lit : 60	⊥ au lit : 60	⊥ au lit : 24	⊥ au lit : 37
Ultrasonic propagation speed (m/s)	2760	2870	1840	1890

III.   EXPERIMENTAL PROCEDURE

The experimental protocol adopted is as follows: sandstone samples are subdivided into two batches. The first batch is first subjected to an alkaline bath for 28 days at 60 °C in a saturated solution based on calcium hydroxide imparting a pH of 12.6 similar to that of the solutions passing through the alkaline mortars .

In a second step, samples of control rock and those of the batch treated at pH 12.6 are then subjected to an accelerated aging test by salt alteration according to the experimental protocol recommended by RILEM [1]. The salt used is sodium sulfate. The immersion solution is prepared from 14% sodium sulfate decahydrate with a concentration of 14 g of salt for 86 g of water. Samples are subjected to repeated cycles of consecutive imbibition and drying. Samples are immersed in the saline solution for 2 hours at room temperature. The second phase of the cycle consists of desiccation for at least 16 hours under conditions of high relative humidity at the beginning of drying. This phase makes it possible to reach the saturation of the solution and then the crystallization of the salts.

IV.   RESULTS

The observation of thin plates of rocks of the treated batch at pH 12.6 shows the development of an important microcracking of the quartz grains constituting the sandstones. The microcracking revealed is generalized to all the materials studied (Figs. 6-7-8-9-10-11-12-13). Such disturbances have already been noted [2] in sandstones, granites and mortars, and attributed to the synergy of several processes: thermal effects (variations in temperature), hydric (successions of humidification-drying cycles, chemicals (dissolutions) and mechanical (saline crystallizations).
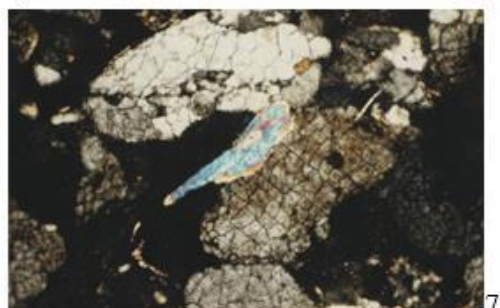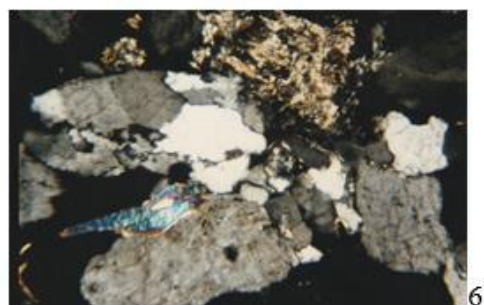
Fig.6-7: Observation of thin blade of the coal sandstone before (6) and after (7) treatment with pH 12.6
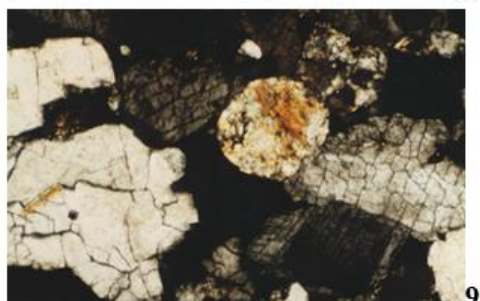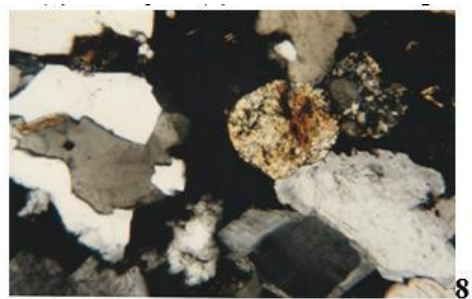
Fig. 8-9: Observation of thin blade of the red vosgian sandstone before (8) and after (9) treatment with pH 12.6
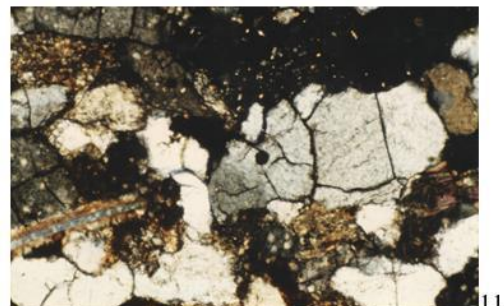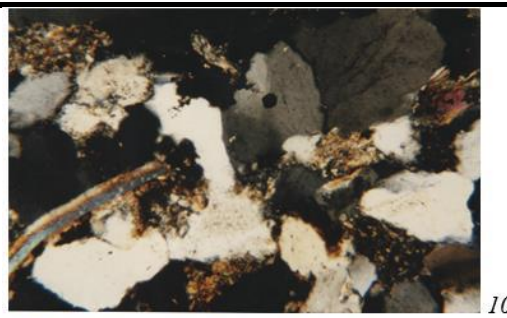
Fig. 10-11: Observation of thin blade of the molière sandstone before (10) and after (11) treatment with pH 12.6
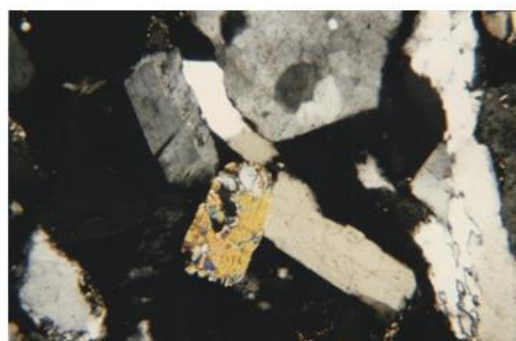
Fig. 12-13: Observation of thin blade of the beige vosgian sandstone before (12) and after (13) treatment with pH 12.6

Following the accelerated aging test by the salts, the two batches of samples studied show, over the course of the cycles, a high granular disintegration leading to the complete degradation of the test tubes (Fig. 14). The results obtained confirm the abundant data in the literature concerning the problem of the saline alteration of the stones used in the historical monuments [3], [4], [5], [6].
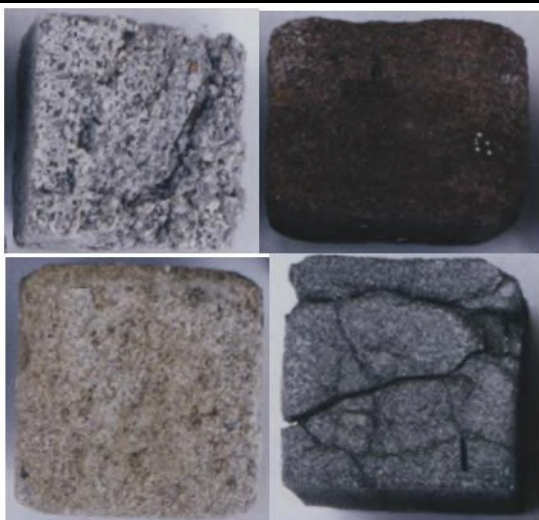
Fig.14: Illustration of facies of alteration of sandstone under the effect of saline crystallizations.

The alteration process is monitored by measurements of the propagation speed of the ultrasound. This measure, which has the advantage of being non-destructive, reflects the degree of cohesion and compactness of the materials [7]. Regardless of the studied material, ultrasonic propagation velocity measurements could not be carried out during last cycles, whereas the rock maintained a state of cohesion allowing the test to continue. The attenuation of the waves at this stage is such that no readable signal can cross these materials. The degradation of the specimens following saline crystallization is accompanied by the progressive fall in the propagation speed of the sound.

The results are plotted in the figures (15-16-17-18) where $\Delta V(\%)$ represents the variation of the ultrasonic velocity as a function of the saline alteration cycles.

$$\Delta V (\%) = 100 (Vc - Vx) / Vc \text{ with:}$$

Vc = ultrasonic propagation velocity measured through the samples of the control batch;

Vx = ultrasonic propagation velocity measured through the materials after x cycles.
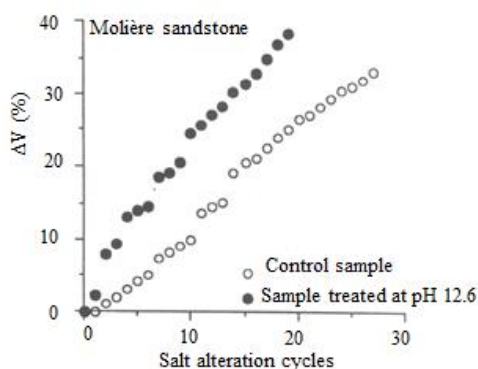
Fig.15: Variation according to salt alteration cycles of rate of loss of ultrasonic speed of the control and treated samples at pH 12.6 for 28 days at 60°C.
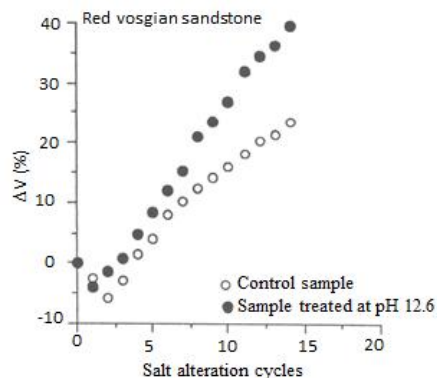
Fig.16: Variation according to salt alteration cycles of rate of loss of ultrasonic speed of the control and treated samples at pH 12.6 for 28 days at 60°C.
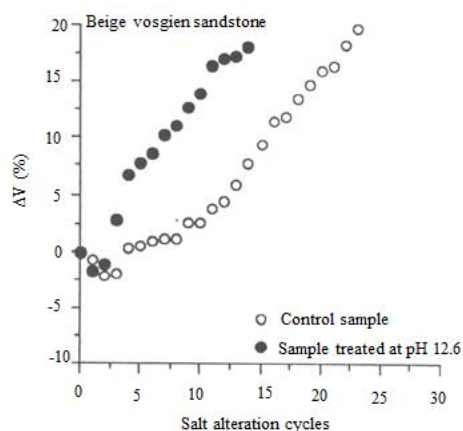
Fig. 17: Variation according to salt alteration cycles of rate of loss of ultrasonic speed of the control and treated samples at pH 12.6 for 28 days at 60°C.
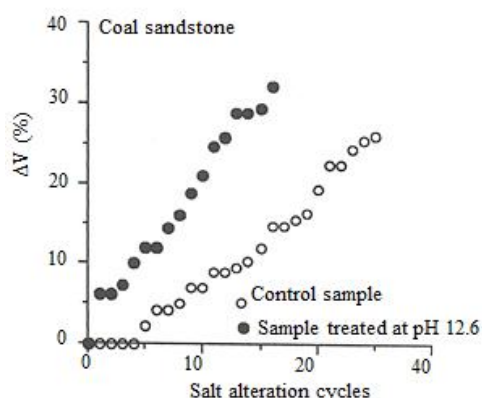
Fig.18: Variation according to salt alteration cycles of rate of loss of ultrasonic speed of the control and treated samples at pH 12.6 for 28 days at 60°C.

It should be noted that the batch treated with the basic pH shows a reduction in the propagation speed of the sound that is greater than the control samples, for all classes of rocks combined. These results can be attributed to the microcrack network revealed in quartz crystals following the alkaline attack. The play of the dilation and the

growth of salts in this microporosity (fig.19) further weakens the rocks by accentuating the observed disorders.
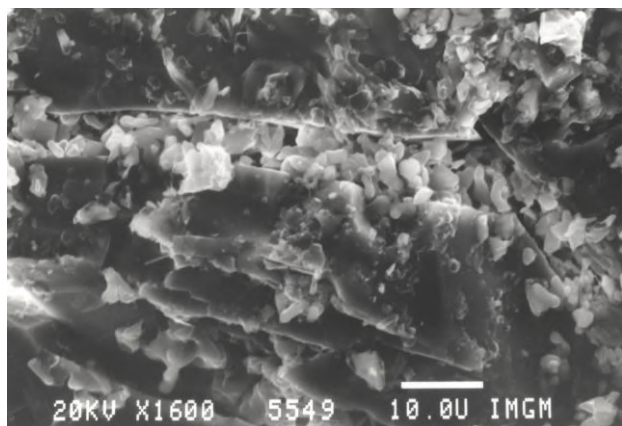
Fig. 19: SEM observation of crystallizations of mirabilite (Na₂SO₄ · 10 H₂O) in the cracks of quartz crystals previously induced

To these mechanical factors are added particularly interesting chemical mechanisms to the quartz: certain salts (NaCl, Na_2SO_4 ...) are able to generate chemical alteration of the quartz grains by sequences of dissolution-precipitation [8], as well as the presence of salts leads to an increase in the dissolution rate of silica [9].

It also appears that the mineralogical nature of saline crystallizations varies according to the nature of the batch of samples. If, in the batch of control samples, the crystallization of the mirabilite is observed, the batch treated at pH 12.6 also shows the appearance of ettringite (FIG. 20), calcium sulfate and hydrated aluminum, of formula: $Ca_6Al_2(SO_4)3$ $(OH)12.26H_2O$. The calcium introduced during the alkaline treatment reacts in the presence of the sodium sulphate of the saline immersion solution to give ettringite, known salts for its swelling properties [10], [11].
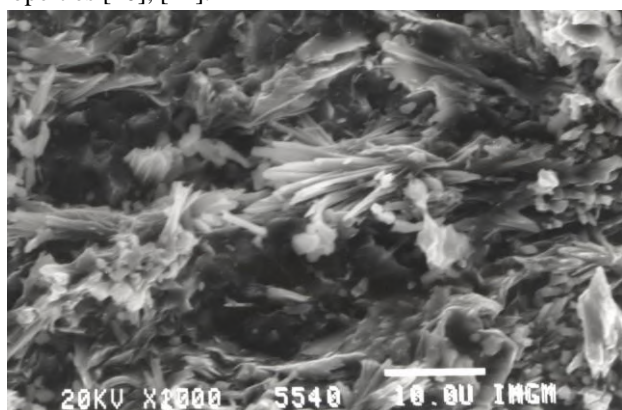
Fig.20: Observation in the SEM of crystallizations of ettringite (Ca₆Al₂ (SO₄) 3(OH) 12.26H₂O) in the samples treated simultaneously in pH 12.6 then in the cycles of ageing by salt alteration.

The simultaneous presence of these two salts further accelerates degradation processes and reduces the number of cycles tolerated by the materials (Table 2).

Table.2: Number of saline alteration cycles performed as a function of the initial state of the materials

	Number of cycles	
	Samples treated at pH 12.6	control samples
Coal sandstone	24	35
Molière sandstone	24	34
Beige vosgian sandstone	22	30
Red vosgian sandstone	15	19

V. CONCLUSION

In order to follow the evolution of sandstone rocks in the presence of a basic mortar, simulations of alkaline attack were carried out in order to simulate the potential role of the portlandite of these mortars. These tests made it possible to identify the nature of the reaction mechanisms involved, namely the alkali-silica reactions. These reactions lead to a profound disorganization of the microstructure of the sandstone rocks, in particular by the embrittlement of the major constituent elements of the sandstones, namely crystals of quartz. The pre-existing defects in these minerals are then revealed and accentuated following dissolution reactions. The consequences of the disorders due to the proximity of basic media also have repercussions on the resistance of the sandstones to the conventional alteration agents such as salt crystallizations. Indeed, the synergy pH-crystallizations saline was particularly harmful in the case of the sandstones studied. By creating an important porosity by revelation and accentuation of microcracks within the quartz, the basic solutions multiply the risks of alteration by alternating dissolutions and saline crystallizations. The durability of these materials is considerably reduced. The enrichment of the environment with calcium ions constitutes an additional degradation factor: in combination with the elements dissolved in rock and sulfur, calcium promotes the crystallization of ettringite known for its swelling properties.

Thus, the proximity of mortar joints in a structure can, by modifying the chemical equilibria, cause a weakening of the intrinsic structure of the sandstones and thereby their durability in a global manner.

REFERENCES

[1] RILEM, Commission 25-PEM, Essais recommandés pour mesurer l'altération des pierres et évaluer l'efficacité des méthodes de traitement. Matériaux de construction, V.13, N. 75, p. 175-252.

[2] Quénné B., " Transformations minéralogiques et texturales de matériaux rocheux, mortiers et bétons d'ouvrages variés-Approche de la cinétique des mécanismes et identification des facteurs responsables". Thèse Université de Nancy I, 1990.

[3] El-Gohary M., "Chemical deterioration of egyptian limestone affected by saline water", International Journal of Conservation Science, Vol. 2, n° 1, Janvier-mars 2011, p. 17-28

[4] Verges-Belmin V., Bromblet Ph., « Altération de la pierre par les sels », Monumental, 2001, p. 226-233

[5] Deneker M. F. C., "Le rôle des sulfates de sodium dans l'altération des pierres du patrimoine bâti : méthodes indirectes d'identification pour l'approche expérimentale". Thèse de l'université de Cergy-Pontoise, 2014.

[6] Angeli M., "Multiscale study of stone decay by salt crystallization in porous networks". Thèse de l'université de Cergy-Pontoise. 2007

[7] Ahmad Abdelraheem A., Pamplona M., Simon S., "Ultrasonic testing for the investigation and characterization of stone, a non-destructive and transportable tool ", Reviews in conservation, 2009, n° 10, p. 43-53

[8] Magee A.W., Bull P.A., and Goudie A.S., "Before rock decay, chemical weathering of constituent grains by salts". Symposium international d'Athènes sur « la géologie de l'ingénieur appliquée aux travaux anciens, monuments et sites historiques » V. 2, p. 779-786. 1988.

[9] Morris R.C. and Fletcher A.B., "Increased solybility of quartz following ferrous-ferric iron reaction". Nature, 330, 551-561.1987 ;

[10] Brunetaud X., "Etude de l'influence de différents paramètres et de leurs interactions sur la cinétique et l'amplitude de la réaction sulfatique interne au béton". Thèse de l'école centrale des arts et manufactures, école centrale Paris, 2005.

[11] Leklou N., "Contribution à la connaissance de la réaction sulfatique interne". Thèse de l'université Paul-Sabatier de Toulouse III. 2008.

Influence of Coal Rock Hardness and Confining Pressure on load Fluctuation Characteristics of PDC bit during Gas Extraction Borehole in Soft Coal Seam

ShifengWang[a], XiaomingHan[b]*, QiangqiangZhang[c], Jialiang Li[d], DetuoChen[e],

[a,b,c,d,e] *School of Mechanical and Power Engineering,HenanPolytechnic University, Jiaozuo 454000, China)*

Corresponding author at School of Mechanical and Power Engineering, Henan Polytechnic University, Jiaozuo 454000, China. E-mail addresses: (Xiaoming Han).

Abstract— Load fluctuation characteristics have a great influence on drilling performance. so, study the influence of coal rock hardness and confining pressure on the load fluctuation characteristics of PDC bitbecome more and more important. Gas drainage drilling experiment table was built and Gas drainage drilling experiment was carried out under different coal rock hardness and confining pressure.The results indicate that drilling torque and feed resistance are decreased with the increase ofcoal rock hardness. Vibration amplitude of drilling torque and feed resistance increase with increase of coal rock hardness when the value of coal rock hardnessis larger than 1.3. Vibration amplitude of feed resistance is maximumwhen the value of coal rock hardness is 1.03 and Vibration amplitude of feed resistance is minimum when the value of coal rock hardness is 1.03. Drilling torque and feed resistance are increased with the increase of confining pressure. Vibration amplitude of feed resistance decreases from 3MPa to 7MPa then increases. Vibration amplitude of drilling torque and feed resistance are all minimum when the value of confining pressure is 7MPa. It provides a good basis for setting the appropriate feeding speed and rotation speed in actual work.

Keywords— coal rock hardness, PDC, borehole.

I. INTRODUCTION

All metallurgical and mechanical aspects of failure that can occur for a drill pipeare considered and discussed. And finally, this comprehensive review leads to a conclusion that categorizes the primary sources of drill pipe failure into seven major groups and makes some recommendations to avoid them[1].The ANASYS software was applied to analyze the inherent frequencies of the vertical vibration, horizontal vibration and rotary vibration during the different drilling depth. The excitation frequency to the drilling rod could be changed by the rotary speed adjusted at drilling rig working period. Thus the resonance caused by the vibration could be reduced and could provide the guidance to the success of the geological exploration[2].Transverse vibrations of drillstrings caused by axial loading and impact with the wellbore wall is studied[3].A linear quadratic regulator (LQR) controller is designed based on a linearized model and is shown to be effective in eliminating this type of oscillations. It is also shown that for some operational parameters the control action may excite large bending vibrations due to coupling with the torsional motion[4].With an increase in borehole pressure, the side crack length decrease significantly; furthermore, the main mode of rock failure shifts from tension to shear[5].The fractal dimension of cracks in the coal seam roofing is affected by the thickness of coal seam, spacing of coal seam and the lithological characteristics of overlying rock strata. With the increase of the thickness of coal seam (composite thickness of coal seam), the fractal dimension of cracks increases[6].In orderto increase the drilling performer of PDC bit, lots of research have been done, however, papers aboutinfluence of coal rock hardness and confining pressure on the load fluctuation characteristics of PDC bitis few. So drilling experiment table is built andcarried out underdifferent coal rock hardnessand confining pressure. In this paper, influence of coal rock hardness and confining pressure on drill pipe vibration is researched and some conclusions are obtained.

II. DRILLING EXPERIMENT TABLE IS BUILT

2.1Test bench

According to the theory of rock cutting and breaking, the

establishment of the gas drainage drilling test bench (Fig1) is built. The test bench mainly has two parts, the power system and the testing system. The test rig drilling

experiments is not only used in drilling coal rock with PDC bit ,but also in a variety of types of bits drilling test.
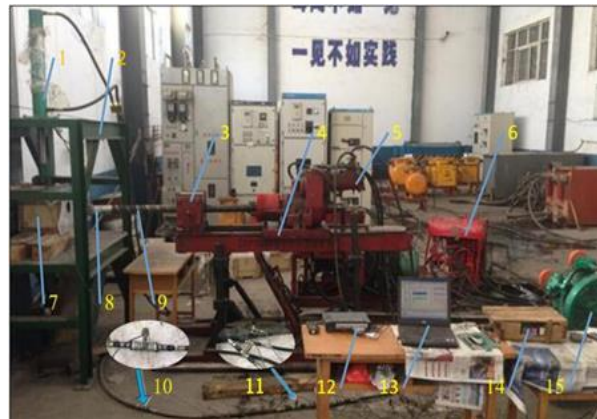
1-fluid cylinder; 2-coal wall support; 3-clamper; 4-advanced gear; 5-gyroscope; 6-control Table; 7-test coal wall; 8-drilling bit; 9-drill pipe; 10-flow sensor; 11-pressure pickup; 12-data acquisition; 13-display interface; 14-flow digital display meter; 15-draught fan
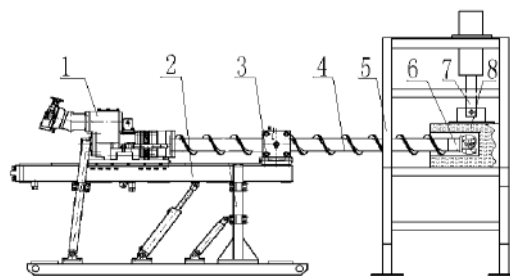
1-clinostat ; 2-feeding device ; 3-clamping device ; 4-drill pipe ; 5-coal wall support ; 6-PDC bit ; 7-hydraulic cylinder ; 8-test coal wall Fig .1. Gas drainage drilling experiment table

2.1.1Power system

The dynamic system of the test bench adopts ZDY1900S full hydraulic drilling machine. The rig is mainly composed of a host machine, pumping station and control station. Pump station is driven by the motor rotation, the hydraulic oil will be transferred to the feed passage and the rotary actuator, the control console on the pole realizes the drill rotation and feed. The drilling machine   not only provides power for the drilling tool, but also provides the confining pressure load for the confining pressure loading device on the top of the coal wall support. At the top of the coal wall support, HSG90/63 engineering hydraulic cylinder is provided, the rated working pressure of the hydraulic cylinder is 16MPa, and the stroke is 640mm, so as to meet the requirement of applying the confining pressure to the coal wall. The hydraulic circuit of the hydraulic circuit is additionallyprovided with two-way hydraulic lock, so as to ensure the stablity of the confining pressure in the operation of the hydraulic cylinder.

2.1.2 Test system

YSV dynamic signal acquisition and analysis software were used in testing system for drilling test data acquisition system; FST800-201G222A-16B pressure sensors are arranged in the hydraulic motor and hydraulic cylinder oil import to drill drilling torque to tests the feed resistance signal. The main performance parameters of the sensor: range: 0-31.5Mpa; sensitivity: 158.73 output voltage: 0-5V; standard engineering unit: mv/Mpa; measurement accuracy: 0.5%FS; the flow of the hydraulic system using the model for the turbine flow sensor LWGY-15A, the nominal pressure 6.4MPa, maximum pressure loss is 0.0035MPa, the turbine flow sensor and the hydraulic motor return oil pressure sensor on the pipeline in series.According to the above power system and the test system composed of drilling test bench, provide the maximum torque of 1900Nm and maximum speed of 300r / min, to the process of 600mm. According to the working performance of the drilling rig, the displacement of the main oil pump in the pump station is changed to change the rotating speed of the drilling machine. The speed range of the drill bit is 85-300r/min. Adjust the displacement of the auxiliary oil

pump in the pump station to change the feed rate of the drilling mechanism. The feed rate range of drilling mechanism is 0-3m/min.

III. INFLUENCE OF COAL ROCK HARDNESS AND CONFINING PRESSURE ON LOAD FLUCTUATION CHARACTERISTICS

3.1 Influence of coal rock hardness on load fluctuation characteristics

To research the influence ofcoal rock hardness（f） on load fluctuation, drilling coal rock experiment is carried out under different coal rock hardness(f=0.65, 1.03, 1.3, 2.4, 3.24). Working condition parameters in the process of drilling coal rock are as follows: confining pressure is 7MPa, feed speed is 0.5 m/min, rake angle of PDC bit is 10 °，rotation speed is 190r/min. Feeding resistance and drilling torque is got under different rotation speed is shown in table1.Fig.2 and Fig.3 show influence of rotation speed on load fluctuation characteristics.

Table1:Drilling torque and feeding resistance under different coal rock hardness

Coal rock hardness （f）	Drilling torque (N·m)			Feeding resistance(KN)		
	Maximum value(N·m)	average value(N·m)	standard deviation	Maximum value(KN)	average value(KN)	standard deviation
0.65	370.7	353.2	18.7	3.9	3.2	0.39
1.03	378.4	364.7	11.6	4.9	4.0	0.65
1.3	417.2	385.5	19.2	4.9	4.8	0.27
2.4	428.6	400.3	21.5	5.3	5.0	0.33
3.24	459.7	420.1	24.8	5.9	5.2	0.53
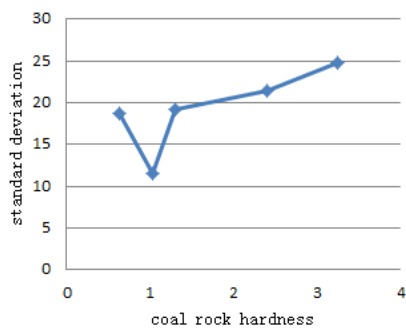
Fig.2: Influence of coal rock hardness ondrilling torque's load fluctuation characteristics
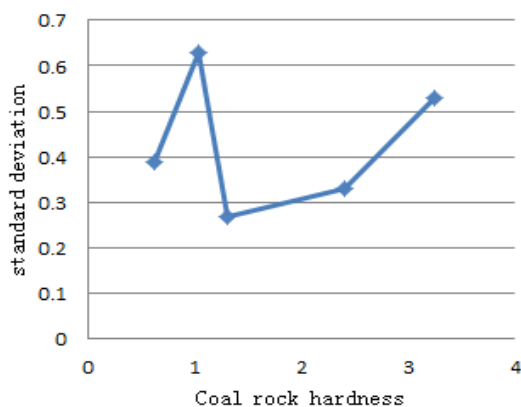
Fig.3: Influence of coal rock hardness on feeding

resistance's load fluctuation characteristics

Table 1 , Fig1 and Fig2showthat drilling torque and feed resistance are decreased with the increase ofcoal rock hardness. Vibration amplitude of drilling torque and feed resistanceincrease with increase of coal rock hardness when the value of coal rock hardnessis larger than 1.3. Vibration amplitude of feed resistance is Maximum value when the value of coal rock hardness is 1.03and Vibration amplitude of feed resistance is Minimum value when the value of coal rock hardness is 1.03.

3.2 Influence of confining pressure on load fluctuation characteristics

To research the influence ofconfining pressure on load fluctuation, drilling coal rock experiment is carried out under different confining pressure (3MPa, 5MPa, 7MPa, 9MPa). Working condition parameters in the process of drilling coal rock are as follows: feed speed is 0.7 m/min, rake angle of PDC bit is 10 °，rotation speed is 190r/min. Feeding resistance and drilling torque is got under different rotation speed is shown in table1.Fig.3 and Fig.4 show influence of rotation speed on load fluctuation characteristics.

Table2:Drilling torque and feeding resistance under differentconfining pressure

confining pressure （MPa）	Drilling torque(N·m)			Feeding resistance(KN)		
	Maximum value(N·m)	average value(N·m)	standard deviation	Maximum value(KN)	average value(KN)	standard deviation
3	335.8	317.2	13.5	3.16	2.50	0.48
5	398.9	351.8	15.9	4.04	3.45	0.42
7	400.1	366.1	12.8	4.61	3.93	0.39
9	422.1	375.3	21.1	5.56	4.74	0.48
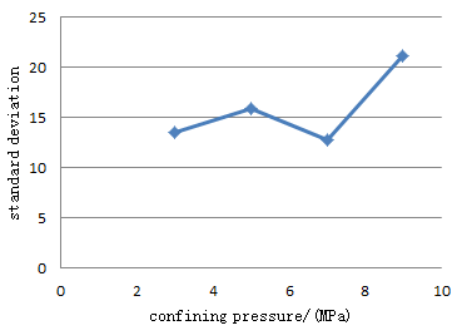
Fig.3(a): Influence of confining pressure ondrilling torque's load fluctuation characteristics
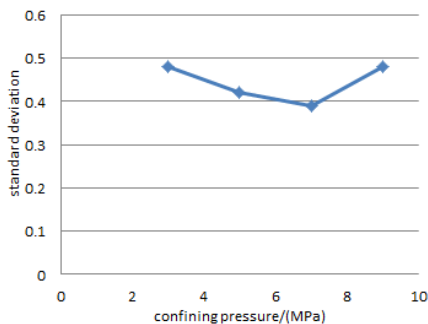
Fig.4: Influence of confining pressure onfeeding resistance's load fluctuation characteristics

Table 2 , Fig3 and Fig4showdrilling torque and feed resistance are increased with the increase of confining pressure. Vibration amplitude of feed resistance decreases from 3MPa to 7MPa then increases. Vibration amplitude of drilling torqueand feed resistanceareall minimum when the value of confining pressure is 7MPa.

IV. CONCLUSIONS

Drilling torque and feed resistance are decreased with the increase ofcoal rock hardness. Vibration amplitude of drilling torque and feed resistanceincrease with increase of coal rock hardness when the value of coal rock hardnessis

larger than 1.3. Vibration amplitude of feed resistance is Maximum value when the value of coal rock hardness is 1.03and Vibration amplitude of feed resistance is Minimum value when the value of coal rock hardness is 1.03.Drilling torque and feed resistance are increased with the increase of confining pressure. Vibration amplitude of feed resistance decreases from 3MPa to 7MPa then increases. Vibration amplitude of drilling torqueand feed resistanceareall minimum when the value of confining pressure is 7MPa. In the paper, vibration amplitude of drilling torque and feed resistance was researched, but many forms of vibration include torsional vibration, longitudinal vibration and lateral vibration during drilling drills coal rock, study these forms is next important task.

V. ACKNOWLEDGEMENTS

REFERENCES

[1] Zamani, S. M., Hassanzadeh-Tabrizi, S. A., &Sharifi, H. (2016). Failure analysis of drill pipe: a review. Engineering Failure Analysis, 59, 605-623.

[2] Zhang, J. C., Duan, L. C., & Wang, H. B. (2009). Analysis on drilling rod vibration mode of coalfield geological exploration based on ansys. Coal Science & Technology.8:64-66.

[3] Yigit, A. S., &Christoforou, A. P. (1996).Coupled axial and transverse vibrations of oilwelldrillstrings. Journal of Sound & Vibration, 195(4), 617-627.

[4] Yigit, A. S., &Christoforou, A. P. (2000).Coupled torsional and bending vibrations of actively controlled drillstrings. Journal of Sound & Vibration,234(1),

67-83.

[5] Shi, X., Cai, W., Meng, Y., Jin, W., Li, G., & Tao, Z. (2014). Numerical study of effects of borehole pressure on bit-teeth induced rock fragmentation. Electronic Journal of Geotechnical Engineering, 19, 4743-4752.

[6] Hu, Y. Z., Liu, C. Y., & Li, J. W. (2015). Fractal analysis of cracks due to mixed mining of coal seam group. Electronic Journal of Geotechnical Engineering, 20(17), 9749-9760.

A Nondestructive Technique for EM-Parameter Determination of Compound Materials using Rectangular Waveguide Sensor and Layered Material Media

Abdulkadhum A. Hassan [1], Janan H. Saadie[2]

[1] Department of Electrical Engineering, Faculty of Engineering, Kufa University, Al-Najaf, Iraq
[2] Department of Material Engineering, Faculty of Engineering, Kufa University, Al-Najaf, Iraq

Abstract— *In this paper, an improved technique of using open-ended rectangular waveguide sensor for simultaneous non-destructive complex electromagnetic parameters determination of compound absorbing materials is developed. The technique is based on employing a layered material medium, which consists of material to be tested and known materials, sandwiched between sensor aperture and perfect conductor plate to obtain two complex reflection coefficients necessary to achieve this purpose. Finite-Difference Time-Domain method is adapted to account for the finite flange size of the sensor and numerically calculate the sensor reflection coefficient under different test conditions. The technique can be employed for cases of single layer and multilayer medium planar sheet measurement. The parameters of the material under test are obtained by fitting both the calculated and measured reflection coefficients using the iterative optimization technique. The details related to the analysis, FDTD modeling and testing procedure of the proposed technique is discussed. The simulations and experimental results are compared with the published data by literatures and companies to validate the proposed technique. The technique is promising for potential applications such as design and fabrication of sheet or layered coating materials and nanocomposite material and bio-medium characterization.*

Keywords— *FDTD; Non-destructive test, Dielectric and magnetic characterization, layered medium, rectangular waveguide sensor.*

I. INTRODUCTION

Radar absorbing materials (RAMs) is essential in a wide range of applications such as radar detection, shielding and electromagnetic compatibility technology [1-5]. These materials are usually designed and fabricated from compound materials as a sheet or coated on metallic structures in order to reduce unwanted reflections or to reduce the radar cross section area of an object. Moreover,

these materials are usually used in a specific application to provide a certain performance of reflectivity over a given frequency range especially at microwave and millimetre wave [6]. The design of radar absorbing materials is constrained by many factors, including thickness, weight, and absorbing properties, which are described by both complex permittivity $\varepsilon_r = \varepsilon' - j\,\varepsilon''$ and complex permeability $\mu_r = \mu' - j\mu''$ over broadband frequency range. These properties are strongly influenced by the frequency at the microwave frequency range [7-8].

For many years, evaluation of electromagnetic properties of materials has been known to be a fundamental aspect of microwave and millimetre-wave technology especially radar absorbing materials [9-11]. It has aroused considerable interests in developing measurement techniques to characterize these materials quickly, accurately, and conveniently. Recently, various techniques are proposed and developed to characterize electromagnetic properties of radar absorbing materials at microwave frequency range with their respective advantages and drawbacks among the others is open-ended rectangular waveguide sensor [12-13]. This technique is widely used to determine both complex permittivity ε_r and complex permeability μ_r over a wide band of frequency range [14] due to its simplicity and openness in its structure. Moreover, it requires less sample preparation. These merits make the technique suitable for characterizing the electromagnetic properties of materials under laboratory and field conditions since the sensor is placed directly against the material under test [15]. Currently, Finite Difference Time Domain (FDTD) method is employed to simulate absorbing ability of radar absorbing materials to electromagnetic waves [16]. Also, with increasing the use of nanocomposite materials, there is a demand for characterization of these materials, starting from the designing process up to the fabrication stage [17] due to its ability to handle complex structures and geometries. In this paper, a technique of using rectangular

waveguide sensor irradiating into a layered material medium in conjunction with FDTD method is proposed to simultaneously determine both complex permittivity and permeability (ε_r and μ_r) of compound absorbing materials. The structure, which consists of material under test backed by known low loss material, is sandwiched between sensor aperture with finite flange and perfect conductor plate to measure two complex reflection coefficients necessary to determine ε_r and μ_r. FDTD method is employed to theoretically calculate the sensor reflection coefficients under different physical test conditions. It is also can be evolved to simulate the design of the electromagnetic wave absorber. The calculated reflection coefficients of the sensor are imposed on the measured values to extract ε_r and μ_r by iterative-optimization technique over an X-band of microwave frequency range. To effectively model these materials, the thickness variation and frequency characteristics of ε_r and μ_r of these materials are studied. The FDTD simulations and measurement results on selected samples of compound absorbing materials are presented and some guidelines for this technique of measurement are highlighted.

II. PRINCIPLES AND ANALYSIS

Figure 1 shows the geometry of the proposed technique used to perform ε_r and μ_r measurement. As shown, the geometry consists of finite flange open-ended rectangular
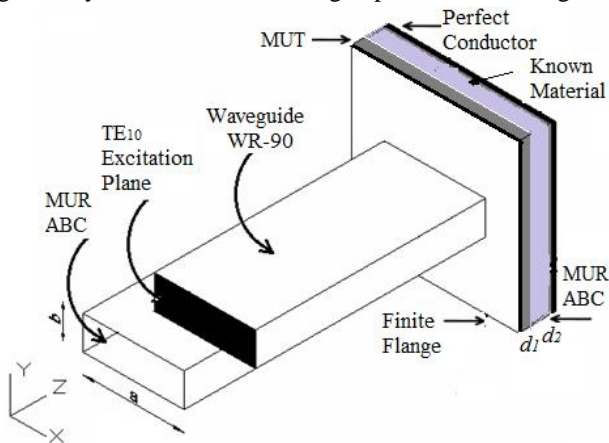
Fig.1: Geometry of the proposed technique:

waveguide sensor in Cartesian coordinates with wide and narrow dimensions (*a* and *b*) placed directly against layered material medium consisting of the material under test with unknown ε_r and μ_r and known thickness d_1, followed by known ε_r, μ_r and thickness material and the whole structure is backed by a perfect conductor to increase measurement sensitivity. The backing known material used should be low loss material to increase measurement accuracy [18]. As shown in Fig. 1, the reflection coefficient symbolized Γ_o (*a, b, ε_r, μ_r, f, d*) is a complicated function of the waveguide sensor dimension

a, b, test frequency *f*, sample thickness *d*, and the parameters of the material under test ε_r and μ_r. The energy radiated from the sensor penetrates through the layered material medium and reflected back into the aperture. Consequently, the reflection coefficient calculated at the sampling point carries the desired information of material under test. The EM-parameter extraction of material under test by the inverse problem process includes finding the values of ε_r and μ_r which minimize the difference between the reflection coefficient theoretically determined (Γ_{th}) and the measured one (Γ_m) obtained under different test conditions. Therefore, for accurate extraction of ε_r and μ_r, the theoretical reflection coefficient of the sensor must be accurately predicted. Using the approximate solution for theoretical reflection coefficient introduces error in the extracted values of ε_r and μ_r. Hence, the problem geometry is formulated using FDTD method to account for the finite size of waveguide flange and accurately predict the reflection coefficient under different test conditions.

1. The Proposed Technique

The main objective of this work is to develop a technique for simultaneous ε_r and μ_r determination of compound absorbing materials during the design phase and fabrication process respectively. In principle, to extract four parameters, two complex reflection coefficients are required. For measurement purposes, in order to determine two complex quantities (ε_r and μ_r) with the assumption that the material under test is backed by conductor, it is necessary to perform a certain experimental procedure to measure the needed two independent complex reflection coefficients under two different test conditions. Physically, the two conditions can be achieved by different ways. Using the proposed technique, the following two ways can be performed to obtain these two conditions as shown in Fig. 2 (*a* and *b*).

(a)   (b)
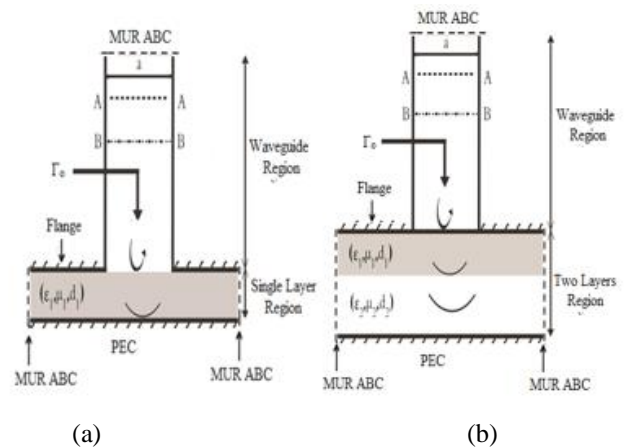
Fig.2: Conditions of reflection coefficient measurement
(a) Single layer test (b)Two layers test
1.1 *Single-Layer Test*

This test is to be performed to obtain one of the two needed reflection coefficients. In this test, the material under test with unknown ε_r and μ_r and known thickness d_1 (only single layer) is sandwiched between the rectangular waveguide sensor and the perfect conductor as shown in Fig. 2 (a). The measured reflection coefficient ρ_{m1} is described using (1):

$$\rho_{m1} = \Gamma_o(\varepsilon_r, \mu_r, f, d) \tag{1}$$

As can be seen in (1), the reflection coefficient is frequency dependent while the frequency is an independent variable. It is to be noted that both complex permittivity ε_r and permeability μ_r of most materials are also frequency dependent and they are slowly varying with frequency.

1.2 *Multilayer Structure Test*

This test is to be performed to obtain the second reflection coefficient. A medium with two layers is used for this purpose as shown in Fig. 2 (b). In this test, the sensor is placed in close contact with a multilayer structure consisting of the material under test with unknown ε_r and μ_r followed by known material and the whole structure is backed by the perfect conductor. The measured reflection coefficient ρ_{2m} is described using (2):

$$\rho_{m2} = \Gamma_o(\varepsilon_r, \varepsilon_r', \mu_r, \mu_r', f, d, d') \tag{2}$$

Where ρ_{m1} and ρ_{m2} are the reflection coefficients measured at different test conditions, ε_r, ε_r', μ_r and μ_r' are relative permittivity and relative permeability of the tested sample and known material, d_1 and d_2' are thicknesses of material under test and known material respectively. It is to be noted that using medium with two layers provides enough information to extract ε_r and μ_r of material under test (using both single layer and two layers tests) while using only single layer test provides the required information if frequency-varying method or thickness-varying method is employed. The proposed technique can be also applied to perform multiparameter measurement (complex permittivity, complex permeability, and thickness) using a medium with *N* different layers. The rectangular waveguide sensor used in the measurement has practically a flange with finite dimension which makes it possible to test high loss sheet samples. For finite flange rectangular waveguide sensor, by using the FDTD method, both electric and magnetic fields distributions are calculated at different physical test conditions. Consequently, the reflection coefficient Γ_0 of the sensor can be determined according to the theory of transmission-line.

2. Numerical Modeling using FDTD Method

The Finite-Difference Time-Domain method has been initially proposed by Yee [19] to numerically solve the Maxwell equations and developed by Taflove [20]. It has been proven to be the most popular numerical technique successfully applied for the solution of electromagnetic problems with complex geometries [21]. In this paper, FDTD method is employed to calculate the sensor aperture reflection coefficient since it is quite difficult, in this case, to apply the analytical approach. Figure 2 (a and b) shows the analytical model of the problem in 3D Cartesian coordinates considering only the dominant TE$_{10}$ mode of the field with sensor dimensions of *a* and *b* respectively. The boundary space of the problem is divided into two regions. The first region is the interior of the waveguide (region 1) while the second region is the multilayer structure backed by perfect conductor. Each region within the geometry is assumed to be linear, isotropic and homogeneous in nature and characterized by both ε and μ. The set of Maxwell's curls equations are given using (3) and (4):

$$\frac{\partial E}{\partial t} = \frac{1}{\varepsilon}\nabla x H \tag{3}$$

$$\frac{\partial H}{\partial t} = -\frac{1}{\mu}\nabla x E \tag{4}$$

Using 3D Cartesian coordinate system (x,y,z), eqs. (3) and (4) are expressed in a system of six coupled Maxwell's differential equation. For x-coordinate of both electric and magnetic fields' components, the differential equations are described using (5) and (6):

$$\frac{\partial H_x}{\partial t} = -\frac{1}{\mu}\left(\frac{\partial E_z}{\partial y} - \frac{\partial E_y}{\partial z}\right) \tag{5}$$

$$\frac{\partial E_x}{\partial t} = \frac{1}{\varepsilon}\left(\frac{\partial H_z}{\partial y} - \frac{\partial H_y}{\partial z}\right) \tag{6}$$

Yee has proposed an approach to numerically solve these equations by which the problem space is divided into a mesh with lattices. A point (i,j,k) in lattice space is denoted as:

$$(i, j, k) = (i\,\Delta x, j\,\Delta y, k\,\Delta z)$$

where Δ is the increment in x, y, z directions. According to Yee procedure, both electric field *E* and magnetic field *H* are distributed to be interleaved with respect to cell whose origin is located at *(i, j, k)*. The components of both electric and magnetic fields are updated in discrete time-steps of Δt interval. Mathematical theorems for the FDTD formulation, concerning issues such as accuracy, convergence, computational complexity and stability is provided in [20]. Following Yee procedure, the x-direction

components of both electric and magnetic fields are described using (7) and (8):

$$H_x^{n+\frac{1}{2}} = H_{x(i,j,k)}^{n-\frac{1}{2}} - \frac{\Delta t}{\mu}\left(\frac{E_{z\,(i,j+1,k)}^n - E_{z\,(i,j,k)}^n}{\Delta y} - \frac{E_{y\,(i,j,k+1)}^n - E_{y\,(i,j,k)}^n}{\Delta z}\right) \qquad (7)$$

$$E_{x\,(i,j,k)}^{n+1} = E_{x\,(i,j,k)}^n + \frac{\Delta t}{\varepsilon}\left(\frac{H_{z\,(i,j,k)}^{n+1} - H_{z\,(i,j-1,k)}^{n-\frac{1}{2}}}{\Delta y} - \frac{H_{y\,(i,j,k)}^{n+\frac{1}{2}} - H_{y\,(i,j,k-1)}^{n-\frac{1}{2}}}{\Delta z}\right) \qquad (8)$$

Following the same procedure, the other field components can be obtained and will not repeat here. It is to be noted that in this formulation the EM parameter ε and μ of material under test can be constant, or they can be changed with frequency. This allows modeling of material properties for lossless and lossy over required broadband analysis. The total space of the problem is discreetized into cubic cells with fine space dimensions to increase the accuracy of calculations. To limit the domain of computational space, the simulation of open problems is usually carried out by placing absorbing boundary conditions (ABCs) in the terminating planes of the grid. In this paper first-order Mur ABC [22] is used for the following reasons:

- It can be applied to the boundary with a dielectric discontinuities

- As compared to other absorbing boundary conditions, It is computationally much easier to implement.

A forward-moving TE$_{10}$ wave is lunched at the excitation plane A-A'. Maxwell's equations solving algorithm involves a continuous sampling of electric and magnetic fields in a finite region at equidistance points in a spatial lattice. The electromagnetic field component distribution (both electric field and magnetic field) is observed within waveguide and multilayer structure until the steady state condition is obtained. The sampling point (B-B') is chosen to be located far away from aperture to avoid higher order modes. The complex reflection coefficient Γ$_o$ of the sensor is calculated by applying transmission-line theory using (9):

$$\Gamma_o = \left|\Gamma_o\right|e^{-j\phi_{\Gamma_o}} = \frac{Y_a - Y_o}{Y_a + Y_o} \qquad (9)$$

where *Ya* is the aperture admittance and *Y$_o$* is the characteristic admittances of sensor aperture.

III. SIMULATIONs AND EXPERIMENTAL RESULTS

1. FDTD Scheme Validation

To verify and validate the FDTD formulation of the problem using the proposed technique, the complex reflection coefficients of X-band rectangular waveguide sensor irradiating into layered material medium is calculated using 3D FDTD code developed for this

purpose. In this work, we passed the developed code by comparing the results of numerical simulations of reflection coefficients with those obtained experimentally using standard WR-90 rectangular waveguide with flange length chosen to be 50 mm [23]. The comparison is made for two cases; the case when only the material under test as shown in Fig. 2 (a) is considered and for the case when a medium of two layers is considered as shown in Fig. 2 (b). In the first case, the sample used is compound absorbing material with ε$_r$ =14.95 - j.0. 3318 and of μ$_r$ = 1.35 – j 1.647 and thickness of 2.8 mm while for the second case, the same sample under test is used followed by the second layer with known ε$_r$ and μ$_r$ and thickness and the whole structure is backed by a perfect conductor. Teflon as low loss material is chosen [18] to be known material with thickness of 8 mm. Simulations and measurements are performed at a frequency of 10 GHz using a HP-8510B automatic network analyzer and the results are shown in table 1. For the two considered cases, the FDTD simulations and experimental results are in good agreement validating the computational tool.

Table 1. Comparison of the sensor reflection coefficient obtained using FDTD modeling versus experimental results for two cases considered. Results are obtained at f = 10 GHz.

Case	Method	|Γ| (Magnitude)	Γ (Phase) (Phase in Degree) dedeDegree)
Single layer	FDTD	0.4391	**-139.38**
	Experiment	0.4424	**-138.17**
Two layers	FDTD	0.4062	**-140.28**
	Experiment	**0.4132**	**-137.98**

2. EM-Parameter Determination

The analysis based on FDTD modeling in the previous sections is to be verified experimentally in order to assess the validity of the proposed technique for simultaneously determination ε$_r$ and μ$_r$ of compound absorbing materials. Several experiments are conducted for this purpose over the given microwave frequency range. Table 2 shows a comparison between the measured results of ε$_r$ and μ$_r$ of a compound absorber sample and corresponding previously published data in [24] where it is seen that they are fairly consistent. The FDTD calculations and measurement are performed at a frequency of 10 GHz with sample thickness of 2.08 mm. The extraction process of both ε$_r$ and μ$_r$ are performed iteratively using numerical optimization technique.

Table.2: Comparison between the measured results of ε_r and μ_r of a compound absorbing material and reference data Results are obtained at f = 10 GHz.

Method	$\varepsilon_r = \varepsilon' - j\,\varepsilon''$		$\mu_r = \mu' - j\mu''$	
	ε'	ε''	μ'	μ''
Proposed Technique	15.21	0.37	1.73	0.87
Reference Data[24]	15.26	0.68	1.71	0.84

As stated in previous sections, the sensor reflection coefficient is sensitive to more than one variables with operating frequency as independent variable while both ε_r and μ_r are frequency dependent (*i.e* $\varepsilon_r(f)$ and $\mu_r(f)$). Also, the sample thickness is another limiting factor in the measurement process. Another test is performed to study the influences of these factors on ε_r and μ_r measurement. The variations of real parts and imaginary parts of both ε_r and μ_r are separately investigated with frequency and sample thickness in this study and the results are illustrated in Fig. 3(a and b). Figure 3-a shows the real parts (ε' and μ')variations of the ε_r and μ_r while the variations of the imaginary parts ($\tan\delta_\varepsilon$ and $\tan\delta_\mu$) of ε_r and μ_r are shown in Fig. 3-b. The measurements are performed on another compound absorbing material with two thicknesses having a ratio of 2. The first sample thickness is chosen to be 2.44 mm and the second one is of 4. 88 mm thickness. Twelve frequency points are selected for the measurement to cover the X-band frequency range. It is clear from the two figures that good agreement is obtained between the measured values (both real parts and imaginary parts for sample of 2.44 mm thickness. For sample with 4.88 mm thickness, a large discrepancy is observed in the results of measurement for both permittivity and permeability. The results obtained showed that the sample thickness has an influence on measurement accuracy and sensitivity. It is quite difficult to obtain accuracy in measurement of thicker sample high loss materials such compound materials. This is due to. that the reflection decreases with increasing the thickness of absorbing material. This is the reason why thickness measurement accuracy becomes poorer for thicker lossy materials. Hence, backing the layered material medium by perfect conductor enhances the measurement sensitivity and accuracy.

(a)

(b)
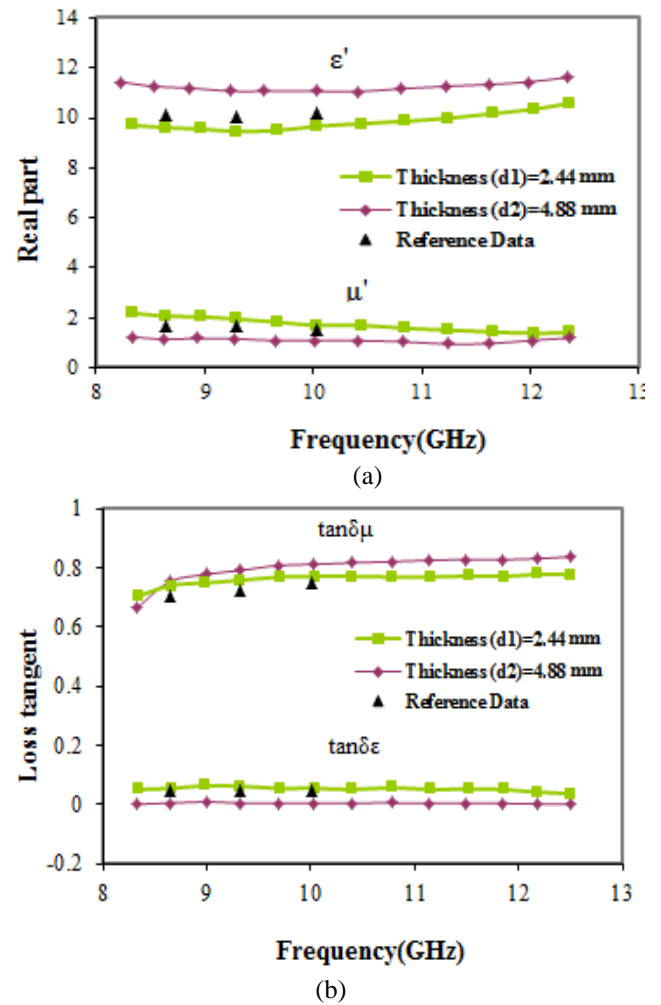
Fig.2: The measured permittivity and permeability of compound absorbing material with two thicknesses compared with reference data. (a) Real parts (b) Loss tangent.

IV. PARAMETERS ε_r, μ_r EXTRACTION

For open-ended rectangular waveguide loaded with material under test, the reflection coefficient (or its equivalent aperture admittance Y_a) is theoretically formulated as a function of sample ε_r and μ_r parameters, sample thickness d and operating frequency f. As with most material characterization methods, there exists no closed form, which relates both ε_r and μ_r to the theoretical reflection coefficient (Γ^{thy}). Hence, in order to simultaneously extract ε_r and μ_r, inverse problem technique must be employed numerically for this purpose using an iterative optimization technique. By using the Γ_0 value, both obtaining from theoretical analysis and experimental under two different test conditions, the complex parameters ε_r and μ_r of the tested sample can be extracted. In this regard, the extracted values of ε_r and μ_r should be those values taken by which the difference between the calculated and the measured values of the sensor reflection coefficient is minimized by inverse

problem. Consequently, an iterative solution using optimization technique is sought to compute ε_r and μ_r for a given value of reflection coefficient Γ_o to optimize the objective function φ using (10).

$$\phi(f_i, \varepsilon', \varepsilon'', \mu', \mu'') = \sum_{i=1}^{N} (\Gamma_m(f_i) - \Gamma_c(f_i, \varepsilon', \varepsilon'', \mu', \mu'', d))^2 \quad (10)$$

where f_i is the operating frequency of the measurement data set measured at N frequency points. It is clear from (10) that by using the values of the measured and the FDTD calculated reflection coefficients, the objective function (φ) can be optimized iteratively. Minimizing process usually starts with initial guess values for ε_r and μ_r. These iterative algorithms are guaranteed in most cases to produce a correct convergence, but this process consumes much time. The technique discussed in this paper is easy to use. It needs only reflection coefficient measurement, then the remaining task is to process the measurement data in a convenient way.

V. CONCLUSION

An improved technique for simultaneous non-destructive EM-parameter of sheet compound absorbing material determination using rectangular waveguide sensor irradiating into layered medium has been numerically investigated and assessed. The FDTD simulations and experiments results of both ε_r and μ_r variations (real and imaginary parts) with the thickness of the sample over an X-band of the microwave frequency range have shown that the sample under test thickness is strongly influencing ε_r and μ_r measurement accuracy. The obtained results suggest that using the proposed technique for ε_r and μ_r measurement is suitable for high loss materials with a thickness of several millimeters. For this reason, the layered structure is backed by a perfect conductor to improve measurement accuracy and sensitivity. The proposed technique can be applied to test a single layer and multilayer material under test where it is quite difficult to use the traditional methods such as thickness-varying method and frequency-varying method for this purpose. The measurement geometry described in this paper is limited to two layer structure, which yield enough information to determine simultaneously electric and magnetic parameters. Since the sensor's reflection coefficient is sensitive to ε_r and μ_r and sample thickness, the technique can be used to perform simultaneous multiparameter measurement (both complex permittivity and permeability and thickness).

REFERENCES

[1] K.J. Vinoy and R.M. Vha, (1996), Radar absorbing materials: from theory to design and characterization, Kluwer ress, Boston, MA**.**

[2] S. M Abbas, A. K. Dixit, R. Chatterjee, and T. C. Goel,(2007), Complex permittivity, complex permeability and microwave absorption properties of ferrite-polymer composite, *J. Magn. Magn. Mater.*, vol. 309, pp. 20-24.

[3] K. Lakshmi, H. John, K. T. Mathew, R. Joseph, and K. E. George (2009), Microwave absorption reflection and EMI shielding of PU-PANI composite, *Acta Materialia*, vol. 57, 371.

[4] D. Zabetakis, M. Dinderman, and P. Schoen (2005), Metal-coated cellulose bars for use in composites applicable to microwave technology, *Adv. Mater.*, vol. 17, no 734,.

[5] H. Bayrakdar (2011), Complex permittivity, complex permeability and microwave absorption properties of ferrite-parafen polymer composites, *J. Magn. Magn. Mater.*, vol. 323, pp.1882-1885.

[6] J.D.C. Dias, I.M. Martin, and M.C. Rezende (2012), Reflectivity of hybrid microwave absorbers based on NiZn ferrite and carbon black, *J Aerosp. Technol Manag*, vol. 4, no. 3, pp. 267-274.

[7] M.C. Rezende*et al*, (2002)., Radar cross section measurements (8-12 GHz) of magnetic and dielectric microwave absorbing thin sheets,, *Revista de Física Aplicada e Instrumentaç*, vol. 1, no. 1, pp. 1-10.

[8] A. M. Gama and M. C. Rezende (2010), Complex permeability and permittivity variation of carbonyl iron rubber in the frequency range of 2 to 18 GHz" *Journal of Aerospace Technology and Management*, vol. 2, no 1, pp. 59-62.

[9] R. Collier, and D. Skinner (2007), Microwave Measurements. Third Edit. IET Eletrical Measurement Series, London, United Kingdom.

[10] G. Roussy, H. Chaabane, and H. Esteban (2004), Permittivity and permeability measurement of microwave packaging materials, *IEEE Tran. Microw. Theory Tech.*, vol. 52, no. 3, pp. 903–907..

[11] K.A.Korolev, S.Chen, and M.N. Asfar (2008), Complex magnetic permeability and dielectric permittivity of ferrites in Millimetre waves, *IEEE Trans. Magn.*, vol. 44, no. 4, pp. 435–437.

[12] C. P. L. Rubinger and L. C. Costa (2007), Building a resonant cavity for the measurement of microwave dielectric permittivity of high loss materials, *Microwave Opt. Tech. Lett.*, vol. 49, pp. 1687-1690.

[13] L. F. Chen, C. K. Ong, C. P. Neo, V. V. Varadan, and V. K. Varadan (2004), Microwave Electronics Measurement and Material Characterization, John Willey and Sons, West Sussex, England.

[14] D. L. Faircloth, M. E. Baginski and S. M. Wentworth, (2006), Complex permittivity and permeability extraction for multi-layered samples using s-parameter waveguide measurements, *IEEE*

Trans. Micro. Theo. Tech. 54(3), pp. 1201–1208.

[15] J. W. Stewart and M. J. Havrilla (2006), Electromagnetic characterization of a magnetic material using an open-ended waveguide probe and a rigorous full-wave multimode model, *J. Electromag. Waves Appl*, vol. 20, no. 14, pp. 2037-2052.

[16] D. H. Kim, D. Kim† and C. M. Choi (2010), A Study on the Design and Fabrication of an Electromagnetic Wave Absorber for the 94-GHz Band, *Journal of the Korean Physical Society*, vol. 56, no. 4, pp. 110-111.

[17] W. Zhang, H. Xiong, S. Wang, Li M. and Y. Gu (2015), Electromagnetic characteristics of carbon nanotube film materials, *Chinese Journal of Aeronautics*, 28(4), pp.1245–1254,.

[18] G. D. Dester (2010), Error Analysis of A Two-Layer Method for the Electromagnetic Characterization of Conductor- Backed Absorbing Material Using an Open-ended Waveguide Probe, *Prog. Electromag.Res*.B, vol.26, pp. 11-21.

[19] K. S. Yee (1966), Numerical solution of initial boundary-value problems involving Maxwell's equations in isotropic media, *IEEE Trans Antenna Propag. AP*, 14, pp. 302-307.

[20] A. Taflove and S. C. Hagness (2005), *Computational electrodynamics,: The Finite Difference Time Domain method*, third ed., Artech-House, Norwood, Massachusetts.

[21] A. Abdulkadhum Hassan , D. Xu, and N. Maode (2000), EM-Properties Measurement of Concave-surface Coating Materials Using a Modifieed Open-ended Coaxial Probe," *Microwave and Optical Technology. Letters*, vol. 27, no. 4, pp. pp 278- 281.

[22] G. Mur (1981), Absorbing boundary condition for the finite-difference approximation of the time-domain electromagnetic field equations, *IEEE Trans. Eectromag. Compat* EMC-22, pp 377-382.

[23] A. Abdulkadhum Hasan (2013), Error Analysis of Rectangular Waveguide Probe with Finite Flange for Non-destructive EM-Properties and Thickness Measurement, *Proceeding of IEEE Symposium on Intelligent Systems* and *Applications*.

[24] N. Maode, S. Yong, Y. Jinkui, F. Chrnpung, and X. Deming (1999), An improved open-ended waveguide measurement technique on parametersε and μ of high-loss materials, *IEEE Trans.Instrum. Meas*., vol. 47, no. 2, pp. 476-481.

Gamma Irradiation Effect of ^{60}Co on the Germination of two subtropical species in the Tehuacán-Cuicatlán Valley

Ernesto Díaz López[1]*, Alejandro Morales Ruíz[1], Arturo Olivar Hernández[1], Patricia Hernández Herrera[1], Juan Antonio Juárez Cortes[1], Jorge Francisco Leon de la Rocha[1], Nazario Francisco Francisco[1], Heliodoro Santiago Santiago[1], Cándido Humberto Bravo Delgado[2], Jesús Manuel Campos Pastelín[2], Humberto Rafael Bravo Delgado[3], Erika Teresa Díaz Oreján[3], Juan Manuel Loeza Corte[3]

[1]Cuerpo Académico "Ecofisiología aplicada a cultivos en zonas áridas". Universidad Tecnológica de Tehuacán (UTT). Prolongación de la 1 Sur No. 1101. San Pablo Tepetzingo, Tehuacán Puebla. C. P. 75859. (*Autor responsable: ernesto.lopez@uttehuacan.edu.mx).

[2]Cuerpo Academíco "Energías sustentables en zonas áridas". Universidad de la Cañada (UNCA). Carretera Teotitlán-San Antonio Nanahuatipam s/n Teotitlán de Flores Magón, Oaxaca. C. P. 68540.

[3]Cuerpo Académico Ingeniería en ProcesosAlimentarios UTTehuacán. Universidad Tecnológica de Tehuacán (UTT). Prolongación de la 1 Sur No. 1101. San Pablo Tepetzingo, Tehuacán Puebla. C. P. 75859.

Abstract—In order to know the influence of ^{60}Co gamma radiation, on the germination of two semitropical species, roselle seeds and sunflower were irradiated at the Transelektro LGI-01 of the InstitutoNacional de InvestigacionesNucleares, At doses 0, 5, 10, 15, 20, 25, 30 and 35 Gy, to determine the radiosensitivity curve and to determine the LD_{50} of both species, under a randomized complete block design with factorial arrangement, Where the study factors were: radiation doses and species. The results indicate that sunflower is more sensitive to gamma radiation than roselle, so the LD_{50} for sunflower and roselle was not reached, because the doses of radiation used, did not achieve 0% germination. Thus, the radiosensitivity curves were fitted to a linear model, with a high coefficient of determination. From the present investigation, It can be concluded that to determine the LD_{50} in the species in question, It is necessary to increase the dose of irradiation, perhaps up to 1000 Gy.

Keywords— LD_{50}, mutation, ionizing radiation, mutagen, mosaic.

I. INTRODUCTION

Sunflower (*Helianthus annuus* L.) and roselle (*Hibiscus sabdariffa* L.), are considered crops of semi-arid zones,and although these present a wide range of adaptability due to their rusticity and phenotypic plasticity,which have been little used to be introduced in tropical areas of the world including Mexico.Sunflower is a plant that originates in northeastern Mexico and southeastern United States (Poverene*et al*., 2002). This species for many years was used as oilseed,since their seeds are obtained fatty acids with high nutritional value (Gallegos *et al*., 2003),but nowadays it has gained importance from the ornamental point of view,due to the great size of its foliage and to the beauty of its chapter which has favored,that is used in flower arrangements and as a cut flower (Melgares, 2001).With regard to roselle,is a plant that belongs to the family malvaceae and has its center of origin in Africa specifically in Sudan,although some authors like Vavilov, mention that its origin is the Abyssinian center (López, 2002).This crop for many years has been used as medicinal because of its diuretic properties,although of its stems also is extracted fiber for the elaboration of ropes which are resistant to the salinity and its seeds,a very fine oil is obtained as the one extracted from *Luffa cylindrical* L.which can be used for the preparation of cosmetics, in addition to possessing antimicrobial properties (Amaya *et al*., 2000).On the other hand, the genetic improvement of plant species has gone through multiple stages,from selection, introgression, crossing, to the use of potent physical and chemical mutagens, a process called Mutagenesis,to obtain cultivars that meet the characteristics

desired by the breeder.This technique is based on the application of physical agents such as gamma radiation emitted by certain radioactive elements such as ^{60}Co (Aros*et al*., 2012).This type of radiation has a very short wavelength of 10^{-12} m, which allows a very high penetration power and is used by geneticists, Causing damage to the DNA molecule causing mutations at the molecular level (Almeida *et al*., 2004), Which will manifest in the phenotype of organisms in the form of somatic mutations known as "Mosaic".This advantage of generating mutations in the plant, can be of great utility since in the same way, resistance to some adverse environmental conditions such as drought,which is of great help in selecting materials that may present the resistance genes to drought,Or even induce this quality to genotypes with the help of gamma radiations (González *et al*., 2007).To achieve this, when irradiating seeds or propagules, It is necessary to do studies on the effect of ionizing radiation on these structures, which is known as radiosensitivity curve,which allows us to determine even the average lethal dose known as LD_{50}.For this reason the main objective of the present study was:determine the radiosensitivity and LD_{50} curve in roselle seeds and sunflower caryopsids under eight ^{60}Co gamma ray levels.

II.   MATERIALS AND METHODS.

2.1 *Location of the experiment.*

The present study was carried out in the laboratory of soils of the Universidad Tecnologica de Tehuacan, during the spring of 2015, located in San Pablo TepetzingoTehuacan Puebla, Mexicoat 18º 24 'north latitude, 97º 20' longitude west and 1409 altitude.

2.2 *Genetic material.*

The germplasm of roselle (Hibiscus sabdariffa L.) was collected from an accession on the coast of Oaxaca, Mexico in PinotepaNacional at a location of 16º 21 'north, 98º 02' west and 28 altitude,whose characteristics are: average postage 0.50 to 1.50 m high and red chalices,the sunflower cariopsides (*Helianthus annuus* L.) cv. Victoria, were donated by the germplasm bank of Ecofisiología de Cultivos of Colegio de Postgraduados,which were irradiated in the Transelektro LGI-01 of the InstitutoNacional de InvestigacionesNucleares (ININ) in Ocoyoacac, Mexico.

2.3 *Determination of radiosensitivity curve.*

This was calculated for both irradiated materials, performing a test of germination,Disinfecting seeds and caryopsids with a solution of 1% sodium hypochlorite and placed in petri dishes with filter paper, depositing 10 seeds per box and equally 10 cariopsides per box, separately for

later incubation in a room of growth at constant temperature at 25ºC,And the percentage of germination was calculated using the following expression PG = (Gs / Ss) * 100 where:PG, Percentage of germination; Gs, Germinated seeds; Ss, seed sown(Gil & Miranda, 2008), After determining the percentage of germination, the rediosensitivity curve was calculated by means of a linear regression plotting the percentage of germination vs radiation dose and obtaining the model of adjustment by least squares.From the obtained model an interpolation was made, taking the dependent variable the value of 50% of germination, and clearing the independent variable to determine the LD_{50} of both species under study (Infante and Zarate, 1990).

2.4 *Experimental design.*

The design used was complete random blocks with three replicates and factorial arrangement following the mathematical model:$Y_{ijk} = \mu + A_j + B_k + \beta_i + (AB)_{jk} + \varepsilon_{ijk}$where: Y_{ijk} is the response variable of the i-th radiation dose in the j-th species of the k-th block;μ, is the true overall mean;A_i, is the effect of the i-th radiation dose;B_j, is the effect of the j-th species under study; B_k, is the effect of the k-th block; $(AB)_{ij}$, is the effect of the interactiondosis of radiation i on the species j under study and ε_{ijk}, is the experimental error of the i-th radiation dose on the j-th species in the k-th block,thus the study factors were integrated by: the radiation dose and the species under study.The experimental unit consisted of a roselle seed and a sunflower.

2.5 *Response variable.*

This was only constituted by the percentage of germination in both study factors and when it was significant, the Tukey test was applied to a level of significance of 5% of probability of error.

III.   RESULTS.

The analysis of variance and the comparison test of means for dose and species, showed highly significant differences for: treatments, both study factors as well as repetitions.Radiation x species interaction was only significant.Regarding the coefficient of variation, this oscillated between 6.34% for radiation dose, whereas for the species it was 10.50%,indicating that the experimental data were very reliable during the development of the experiment (Table 1). For the radiation factor, the highest percentage of germination occurred in the control and the dose of 5 Gy with 96.50 and 92.02%, respectively,being also statistically equal.Levels 10, 15, 20 and 25 Gy of radiation were found to be statistically equal but differ

numerically,In this way the high levels of gamma radiation 30 and 35 Gy presented the lowest values of germination with 81.90 and 79.50%.Regarding the species factor, the highest germination was in roselle with 89.31%, surpassing sunflower that only obtained 80.43%.The radiosensitivity curve for germination with respect to the radiation in roselle, is presented in figure 1.In it is observed that the mathematical model was linearly adjusted in a decreasing way, whose coefficient of determination turned out to be highly significant 0.98 **, and whose slope was -0.37

indicating that for each Gy of radiation, supplied to roselleseeds, there was a decrease of 0.37% germination.On the other hand the germination of sunflower caryopsids, submitted to different levels of radiation, maintained a tendency similar to roselle, keeping the linear model decreasing. For this case the coefficient of determination was 0.92* and slope -0.50, for each unit of radiation the germination of sunflower caryopsids is reduced by 0.50% (Figure 2).

Table.1: Analysis of variance and multiple comparison test, for two study factors based on ^{60}Co gamma radiation, in the Tehuacán-Cuicatlán Valley. 2016.

Radiation factor	G (%)	Species factor	G (%)
T_0	96.50 a	Roselle	89.31 a[¶]
T_5	92.02 a	Sunflower	80.43 b
T_{10}	89.60 ab		
T_{15}	87.17 ab		
T_{20}	86.75 ab		
T_{25}	83.82 ab		
T_{30}	81.90 b		
T_{35}	79.50 b		
HSD	6.40		5.69
CV %	6.34		10.50
ANOVA			
Treatments		**	
Repetitions		**	
Radiation (R)		**	
Species (S)		**	
R x S		*	

[¶]Means within columns with the same literal are statistically the same according to Tukey at (*P≤0.05*). G, germination; HSD, honestly significant difference; CV, coefficient of variation.; *; n.s, significant at 0.01; 0.05 and not significant.**

$$PG = -0.37R + 95.2$$
$$r^2 = 0.95**$$
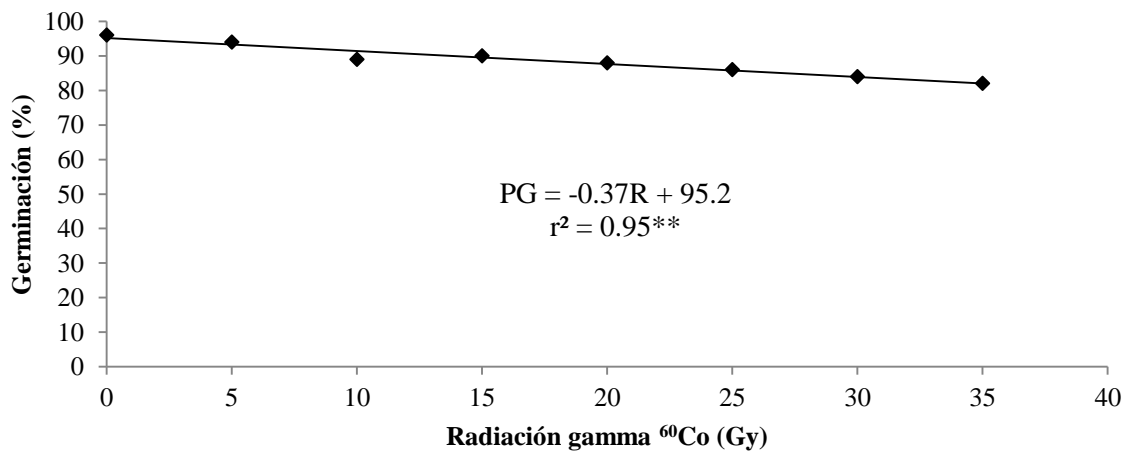
Fig.1: Radiosensitivity curve in Jamaican seeds (Hibiscus sabdariffa L.), subjected to eight levels of ^{60}Co gamma irradiation in the Tehuacán-Cuicatlan Valley. 2016. PG, Percentage of germination; R, radiation.

$$PG = -0.50R + 93.8$$
$$r^2 = 0.92*$$
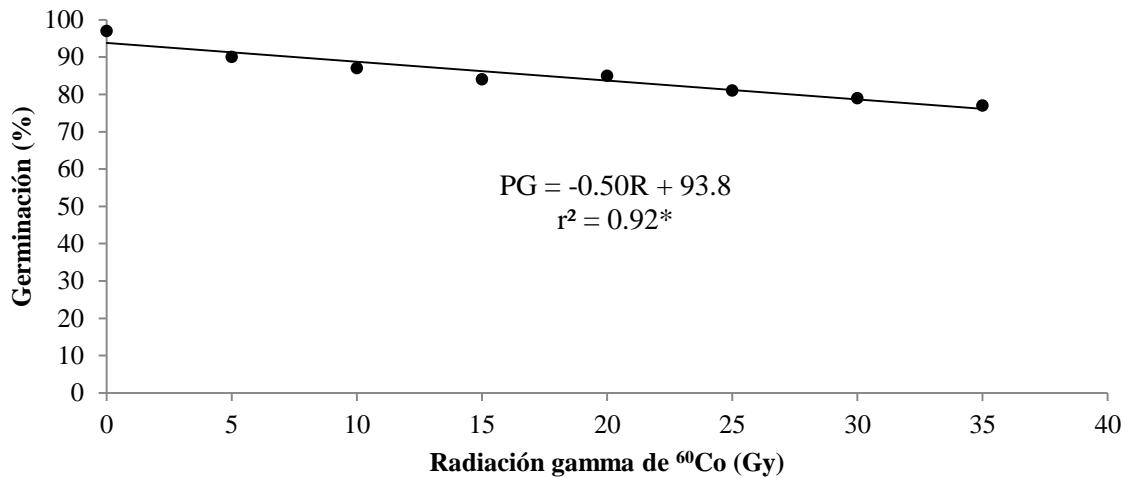
Fig.2: Radiosensitivity curve in sunflower achenes (Helianthus annuus L.), submitted to eight levels of gamma irradiation of ^{60}Co, in the Tehuacán-Cuicatlan valley. 2016.PG, Percentage of germination; R, radiation.

The mean lethal dose,to be derived from the mathematical models of adjustment for both species under study,was not reached,due to the fact that in none of the species did germination reach 0.0%, as can be seen in Figures 1 and 2.Thus in this way,the lowest percentages of germination occurred with 35 Gy,for the species in question with 81.00% germination for roselle and 72.00% for sunflower.This indicates,that roselle has a lower sensitivity to gamma radiation than sunflower,that is to say,11.11% less sensitivity to gamma radiation than 60Co than sunflower (Table 2).

Table.2: Mathematical models of fit, coefficient of determination and mean lethal dose, for roselle (Hibiscus sabdariffa L.) and sunflower (Helianthus annuus L.), subjected to ^{60}Co gamma irradiation.Tehuacan-Cuicatlan Valley. 2016.

Especie	Modelo	r^2	LD_{50} (Gy)
Jamaica	PG=-0.37R+95.2	0.95**	-------------
Girasol	PG=-0.50R+93.8	0.92*	-------------

PG, percentage of germination; R, radiation dose; LD, mean lethal dose.

In the interaction radiation x species, we can see that both species interacted in a decreasing way with respect to radiation,in the range of 0 to 25 Gy,that is to say, as the radiation increased the germination of both decreased,to then decrease drastically from 25 to 30 Gy in sunflower,while roselle does not experience a change of slope keeping the same trend. From 30 at 35 Gy,roselle experienced a steady slope,indicating that in this radiation range,the species presents insensitivity to gamma rays (Figure 3).
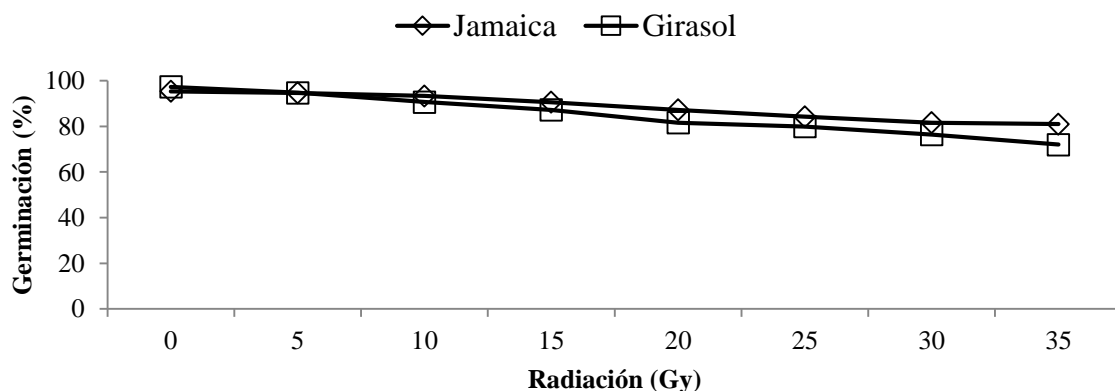
Fig.3: Radiation x species interaction, in a factorial experiment at the Universidad Tecnologica de Tehuacan. San Pablo Tepetzingo, Tehuacán Puebla. Spring 2014.

IV. DISCUSSION

Germination decreased as the radiation dose increased,both in Jamaican seeds and in sunflower caryopsids,the latter presenting a reduction of 11.11% in germination compared to roselle.This response coincides with that observed and reported by Díaz*et al*. (2003),who worked with *Tigridiapavonia* (L.f) D.C. And mention a progressive reduction in the budding of the bulbs of this species,when subjected to gamma rays of ^{60}Co in a range of 5 to 30 Gy despite being different species.On the other hand, Ramírez*et al*. (2006), mention that dose 500 Gy,result in a significant decrease in the germination of tomato hybrids of up to 23%,data that differ from those reported in this present study,the above may be due to the differences between species in which both studies were carried out and the high germination percentage of the tomato hybrids,as well as the different doses of radiation used.The results presented in this study,indicate that both structures are sensitive to gamma radiation of ^{60}Co,and are of great importance for being the basis for establishing doses of radiation,when it is desired to improvement genetic using the mutagenesis technique and thus eliminate the doses that are lethal when killing more than 50% of the study population,which was not reached in this investigation.For this reason the establishment of radiosensitivity curves is of great importance in this type of studies.

V. CONCLUSIONS

From the present investigation carried out, under the conditions of the valley Tehuacan-Cuicatlan, the following conclusions were derived:

- In the low doses of gamma irradiation of ^{60}Co, both species presented an equal germination, statistically speaking.
- Sunflower presented the lowest germination than Jamaican, when applying high dose of gamma rays.
- Sunflower prove be more susceptible to gamma radiation, as it decreased its germination, compared to roselle.
- The germination vs radiation adjustment models were linear with high determination coefficients for both species.
- The LD_{50} could not be determined, because in both species the zero germination percentage was never reached.
- For further studies, where it is intended to establish the LD_{50} of the species in question, it will be necessary to irradiate up to 1 kGy to obtain a positive response.

REFERENCES

[1] Amaya, L., Díaz, F., García, N., Moncada, M. and Guerrero, G. 2007.Obtaining the oil of the seeds of *Luffacylindrica* and evaluation of its potential use in the cosmetic industry.Scientia*et*Technica. 33: 287-289.

[2] Aros, D., Olate, E., Valdés, S. and Infante, R. 2012.Gamma irradiationon*Alstroemeria aurea* G. *in vitro*rhizomes: anaproachtotheappropriatedosageforbreedingpurposes. Revista de la Facultad de Ciencias Agrarias UNCUYO. 44(1): 191-197.

[3] Almeida, E., Fuentes, J. L., Sánchez, A., Carro, S. andPrieto, E., 2004.Effect of gamma radiation on the survival and induction of SOS response in *Escherichia coli* cells deficient in nucleotide cleavage repair and by recombination.Journal Cubana de Investigación Biomédica. 23(4): 242-248.

[4] Díaz, L. E., Pichardo, R. J.C., De la Cruz, T. E.,Normán, M. T., Sandoval, R. F. and Vázquez, G. L. 2003.Induced variability in *Tigridiapavonia* (L.f) D.C var. Sandra. By irradiation of bulbs with gamma rays of ^{60}Co.RevistaChapingoSerieHorticultura. 9(2): 235-241.

[5] Gallegos, I. J.A., Rocha, G. N., González, l. R., Zuno, F. F., and Vidaña, F. S. A. 2003.Characterization of two varieties of sunflower with potential for the production of oil extracted with hexane and isopropanol.Grasas y aceites. 54(3): 245-252.

[6] Gil, C.A.I. and Miranda, L.D. 2008.Effect of temperature, immersion in water and concentration of phytorregulators on the germination of papaya seeds (*Carica papaya* L.).Revista colombiana de ciencias hortícolas. 2(1): 9-20.

[7] González, L. M., Estrada, A., Zaldivar, N. andArgentel, L. 2007.Tolerance to drought in different

wheat varieties, based on some variables of the water regime and concentration of pigments in seedling stay.Revista Ciencias Técnicas Agropecuarias. 16(1): 45-49.

[8] Infante, S. and Zarate, L. P. 1990.Statistical methods: a multidisciplinary approach. 2nd edition.México: Trillas.

[9] López, B. L. 2002.Industrial crops.Ed. Mundi-prensa.

[10] Melgares, J. 2001.The cultivation of sunflower (*Helianthus annuus* L.) for cut flower.Flormarket. 2(2): 55-61.

[11] Poverene, M.M., Cantamutto, M. A., Carrera, A. D., Ureta, M.S., Salaberry, M.T., Echeverría, M.M. and Rodríguez, R. H. 2002.The wild sunflower (Helianthus spp.) In Argentina: characterization for the release of transgenic cultivars.Journal of Investigaciones Agropecuarias. 31(2): 97-116.

[12] Ramírez, R., González, L, M., Camejo, Y., Zaldivar, N. and Fernández, Y. 2006.Radiosensitivity study and selection of the range of stimulating doses of X-rays in four tomato varieties (Lycopersiconesculentum Mill.).Cultivos tropicales. 27(1): 63-67.

Preliminary Studies of Groundwater Potential and It's Distribution Patterns in the Gumuk at Jember

Priyantari N., Supriyadi, Suprianto A., Imbani A.N., Astutik L

Jurusan Fisika, FMIPA, Universitas Jember, Jln. Kalimantan 37, Jember 68121

Abstract— *Gumuk is a natural phenomenon that occurs in East Java, especially in Jember. The existence of gumuk scattered in the district of Jember has mined intensively, causing their numbers have declined dramatically. Collecting data in this study conducted on each of the gumuk using waypoint on GPS device consisting of latitude and longitude coordinates. Waypoint data is modified into shapefile (shp) then it is processed using ArcView Gis 3.3. Based on our preliminary studies in 2 Subdistrict of Pakusari and Ledokombo identified as cumulate gumuk while in the subdistrict of Arjasa as spread gumuk. The groundwater potential in cumulate and spread gumuk need to be investigated so that further confirming the role of gumuks as a water storage. Groundwater potential estimated using self potential methods. The results obtained in the cumulate gumuk have potential value 2 mV to -14 mV, the goundwater potential in the gumuk can be assumed to be dominant. While on the spread gumuk, soil water anomaly uneven, only at some point. The groundwater potential in this gumuk less dominant than the cumulate gumuk. From this study could be concluded that the distribution of cumulate gumuk more abundant groundwater potential than spread gumuk.*
Keywords— gumuk, cumulate gumuk, spread gumuk, groundwater potential, self potential.

I. INTRODUCTION

District of Jember Regency has unique and specific landscape, with the existence of gumuk. Gumuk is small hills composed of rocks and has a varying size (large and height). Gumuk is included in the C category of quarry mining with result stone plates, sand, and stone use as foundation whereas hill mostly consist of soil (Sulistyaningsih, et al,. 1997). The number of gumuk was never officially inventoried, but the number was estimated at more than 1000, so Jember District was also dubbed the "District of a thousand gumuk". According to the theory of Verbeek and Vennema (in Fariha, 2013), the existence of the gumuk in Jember occurred due to the eruption of Mount Raung in the past that drains lava. The lava flows are covered by volcanic material with a thickness of tens meters and erosion occurs on soft parts comprising volcanic sediments of thousands years to produce the topographic shape of the gumuk as it is today.

The existence of gumuk spreaded in Jember now has been much eroded and flattened to the ground. Many of those gumuks have been converted into residential and agricultural areas. In 1990, the housing construction began to proggres quickly in Jember and most of land included gumuk, flatened and use as housing contruction. Besides, gumuk also mostly mined result stone plates causing the number has been reduced drastically. According to Kepel (2000), in macro scale, gumuk numbering thousands plays an important role in the groundwater system in the downstream area because the existence of the gumuk mostly located in the upstream. On a micro scale, the gumuk plays a role for the surrounding area, evidenced by the emergence of springs around a portion of the gumuk, with varying discharges. Springs encountered in the gumuk area are generally seepage.

It is necessary to re-inventory the current number of gumuk with its geological conditions. The distribution can be obtained through GPS (Global Positioning System) used to determine the point of coordinates Latitude and Longitude coordinates in each gumuk. GPS is a navigation satellite system designed to provide three-dimensional position and speed and information about time(Abidin, 2006).

The condition of subsurface structure can be observed using self-potential method. Self potential method is one of the geophysical methods whose basic principle is measure static natural voltage which is in the group of points on the ground surface. This method can be used to determine an area that potentially minerals and metals. Background potentials are formed by the flow of liquids, biolistrik activity in plants and caused by differences in electrolyte concentrations in groundwater as well as other geochemical activities. The value of background potentials depends on the geological resources below the surface shown in table 1 below.

Table.1: Type of SP anomaly from various mineral

Sources	Type of anomaly
Mineral Potentials	
Sulphide (*pyrite, chalcopyrite, pyrrhotite, sphalerite,* galena)	Negative ~ hundreds of mV
Graphite (*magnetite* and other electronically conducting minerals)	Negative ~ hundreds of mV
Coal	Negative ~ hundreds of mV
Manganese	Negative ~ hundreds of mV
Quarrtz veins	Positive ~ tens of mV
Pegmatites	Positive ~ tens of mV
Potensial Background	
Fluid steaming, geochemical reaction, etc	Positive +/- negative ≤ 100 mV
Bioelectric (plants, trees)	Negative ≤ 300 mV
Groundwater movement	Positive or negative up to hunderds of mV
Topography	Negative, up to 2 V

(Source : Reynolds, 1997).

Jardani et al (2006) in their research about self-potential signals associated with preferential groundwater flow pathways in sinkholes state that most of negative anomalies were located along the trend where sinkholes were identified from surface features. The sinkholes are organized along these ridges channel because these ridges high volumes of groundwater flow. Jinadasa and de Silva (2009) do research on resistivity imaging and self-potential applications in groundwater investigations in hard crystalline rocks. from their research, area of negative self potential anomalies correlate well with possibly areas of groundwater accumulations. Base on previous research and table 1, the groundwater potential in the gumuk can be identified using a negative self-potential anomaly.

There are two kinds of data acquisition technique in self-potential method that is fixed base and leap frog technique. In fixed base technique, one of the electrodes is fixed at one point and the other electrode is moved at each measurement, whereas in leapfrog technique the two electrodes are moved at each measurement. Both techniques are very effective for knowing subsurface structures, but leapfrog techniques are more cost-effective and time-efficient than fixed base techniques (Sharma, 1997). Goto et.al (2012) using leapfrog method in SP observation for investigation groundwater flow system in a nonvolcanic mountain slope. Onojasun (2015) also using leapfrogging approach in delineating groundwater contaminant plums using self-potential surveying method in Perth Area, Australia.

II. METHODS

The data were collected in 3 sub-districts, i.e. Ledokombo, Pakusari and Arjasa. Gumuk choosen as research location at those sub district are gumuk that still intact and had not been mined at all. Data acquisition in the using GPS to determine Latitude and longitude coordinates of the location and elevation of each gumuk. GPS survey data in the form point is usually processed by converting into segment data such as topographic contour data before further processing in the GIS. Latitude and longitude coordinat obtained from GPS device as waypoint. Waypoint data is converted to shapefile (shp) then processed futher using ArcView GIS. Last result as map of gumuk distribution in 3 sub-distrik which will become the reference in knowing the current position and condition of the gumuk.

Meanwhile, to know the potential of groundwater in the gumuk area is done by taking the line along the 200 m in the gumuk with each spacing 5 m for each line. The data acquisitin location for groundwater potential in Ledokombo sub district, taken in Lembengan Village with coordinates 8º09'50" S dan 113º43'054" E. While in Pakusari sub district taken in Subo Village with coordinates 8º09'56,2" S dan 113º46'16,5" E. The last location in Arjasa sub District, Biting Village with coordinates 8º06'46,5" S dan 113º46'09,4" E. Location taken, is expected to represent the area of the gumuk. Technique of data acquisition using leap frog technique. The data acquisition technique can be seen in Figure 1.
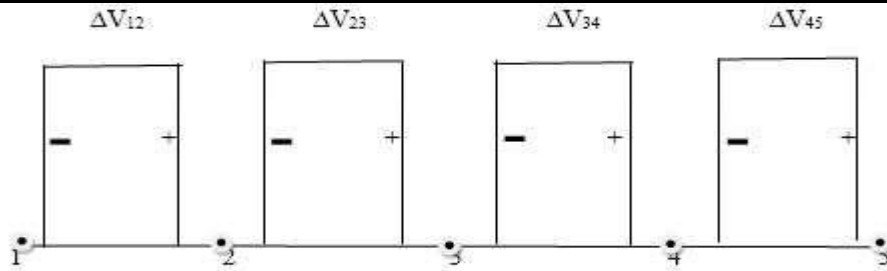
Fig.1: leapfrog technique in SP acquisition

where

ΔV_{12} : Potential difference value between point 1 and point 2

ΔV_{23} : Potential difference value between point 2 and point 3

ΔV_{34} : Potential difference value between point 3 and point 4

ΔV_{45} : Potential difference value between point 4 and point 5

In this research, we get the value of voltage in mV unit. The data is then processed in surfer 12 software so that it becomes a self potential contour map (equipotential map) that describes the groundwater potential of the research area.

III. RESULTS AND DISCUSSION

The maps of gumuk distribution patern done in 3 sub district in Jember shown di figure 2, 3 and 4 using ArcView GIS 3.3. GPS data survey generated in waypoint formulated by converting the data in the form of shapefile (shp). Data processing is done by combining the map of the location of the study area with the point coordinates of each gumuk by using the GIS method. From these data

will be obtained map distribution of gumuk with a certain scale. In the map of gumuk distribution, the area of research is imaged with different colors., the road symbolized by the red colored lines and the village boundary symbolized by the black line that can be seen on the legend. The intact gumuk is imaged with blue dots while the gumuk being mined is imaged with red dots. The first research location is located in Ledokombo subdistrict consisting of several villages, namely Sukogidri, Sumberanget, Ledokombo, Lembengan, Lesung Source, Slateng, Suren, Sumberbulus, Karang Paiton, and Sumbersalak. Figure 2 is a map of gumuk distribution in Ledokombo subdistrict with scale 1: 125.000 with area of 146.92 km^2.
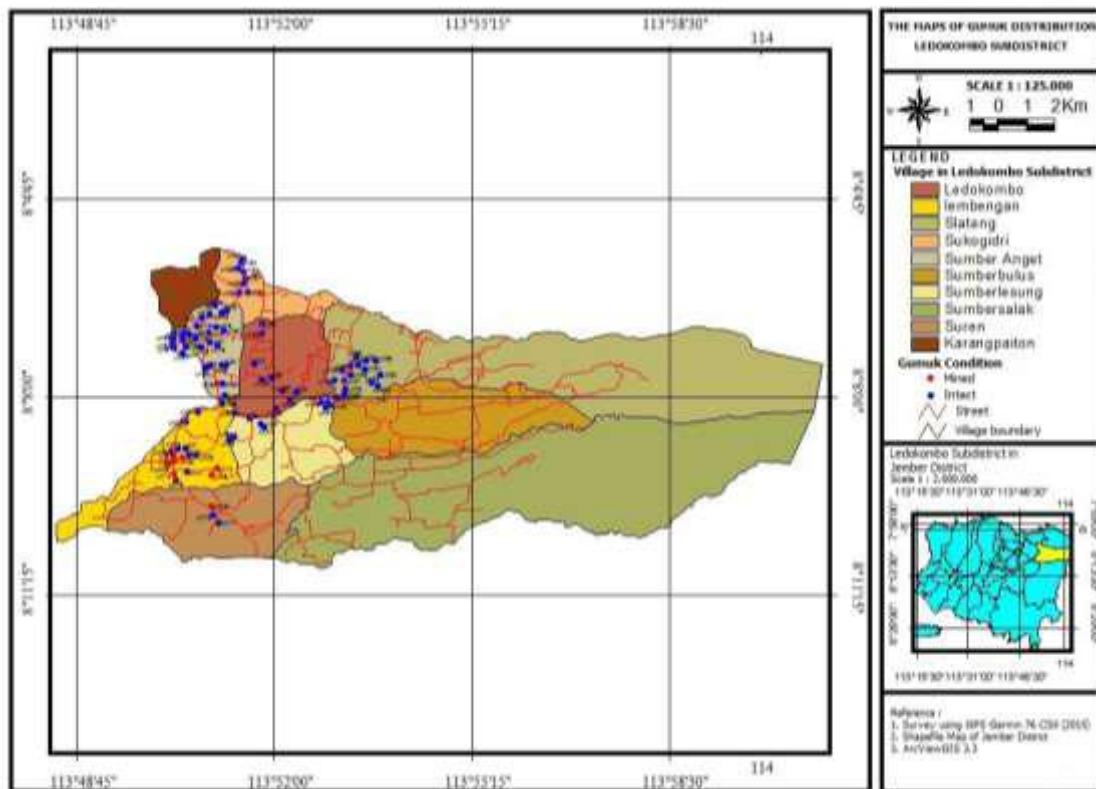
Fig.2: Map of Gumuk Distribution in Ledokombo Sub District

Based on the results of the research described in table 2, the number of gumuk in Ledokombo subdistrict as 92 gumuk, consisting of 83 gumuk in intact condition and 9 gumuk being mined. The largest number of gumuk in this sub-district is in Sumber Anget Village which is 29 gumuk, consist of 28 gumuk in intact condition and 1 gumuk is being mined. While the fewest gumuk in Suren the village as 3 gumuk, consisting of 2 gumuk in intact condition and 1 gumuk being mined. Based on the geological map of Jember district, the rock formations in Ledokombo sub district consist of Raung rock, Argopuro Tuff, and Bagor Form.

Table.2: Number of Gumuk in Ledokombo Subdistrict

	Village	intact	mined	Rock formation
1	Sukogidri	8	-	Batuan Raung & Tuff Argopuro
2	Sumber Anget	28	1	Batuan Raung & Tuff Argopuro
3	Ledokombo	10	-	Tuff Argopuro
4	Lembengan	10	7	Tuff Argopuro
5	Sumber Lesung	9	-	Tuff Argopuro
6	Slaten	16	-	Form Bagor & Tuff Argopuro
7	Suren	2	1	Tuff Argopuro
8	Sumberbulus	-	-	-
9	Sumbersalak	-	-	-
10	Karang Paiton	-	-	-

The measured groundwater potency in the study location can be shown in the form of contour maps. The result of the potential contour of gumuk in Lembengan Village of Ledokombo SubDistrict is shown by figure 3 below:
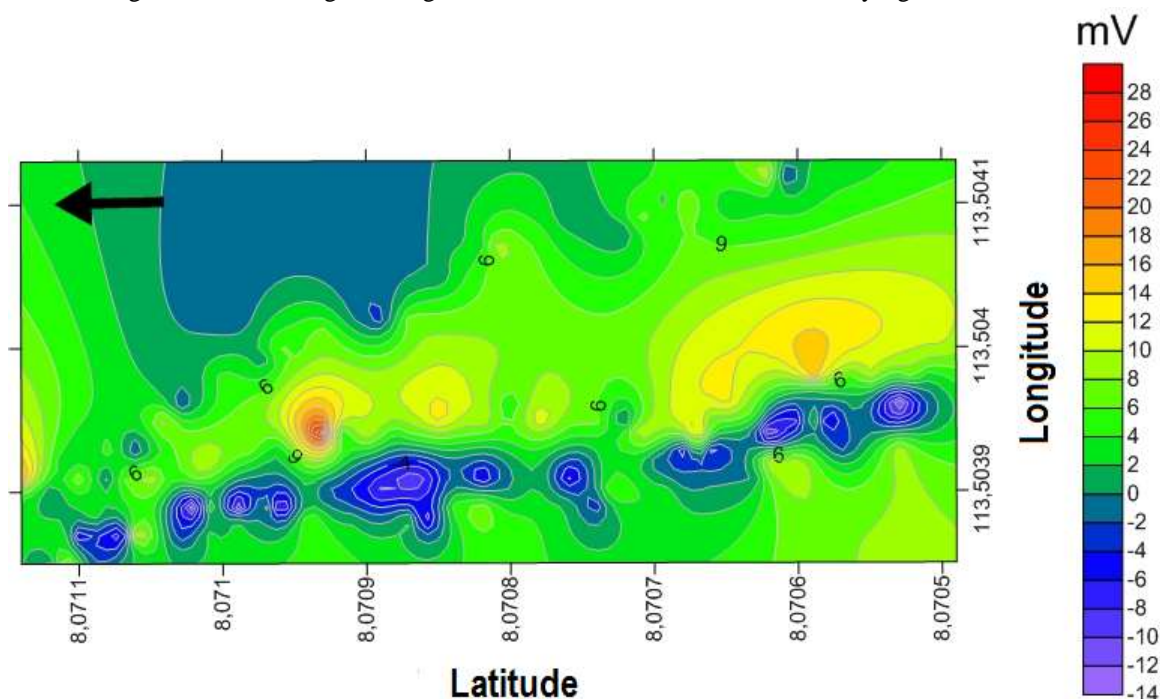
Fig.3: Map of contours potential distribution of gumuk in Lembengan Village, Ledokombo Sub District

Anomalies of groundwater potential in line 1 and 2 with coordinates 08º07'05" to 08º07'11" S and 113º50'39" E With a range of values from 0 mV up to -14 mV. Then there is also an anomaly of groundwater potential on line 4 with coordinates 08º07'09" to 08º07'10" S and 113º50'41" E potential value of -2 mV to -8 mV. The amount of groundwater potential in the research area is 15% of the research area.

The second research is located in Pakusari sub-district consisting of Bedadung, Patemon, Sumberpinang, Subo, Jatian, Pakusari and Kertosari villages. Figure 4 is a map of the gumuk distribution in Pakusari Sub District with scale 1: 60.000 and the area 29,11 Km^2. In Figure 4, can be seen that the distribution of gumuk in Pakusari sub-district is evenly distributed and the condition of the gumuk that is being mined is less than the gumuk under intact condition.
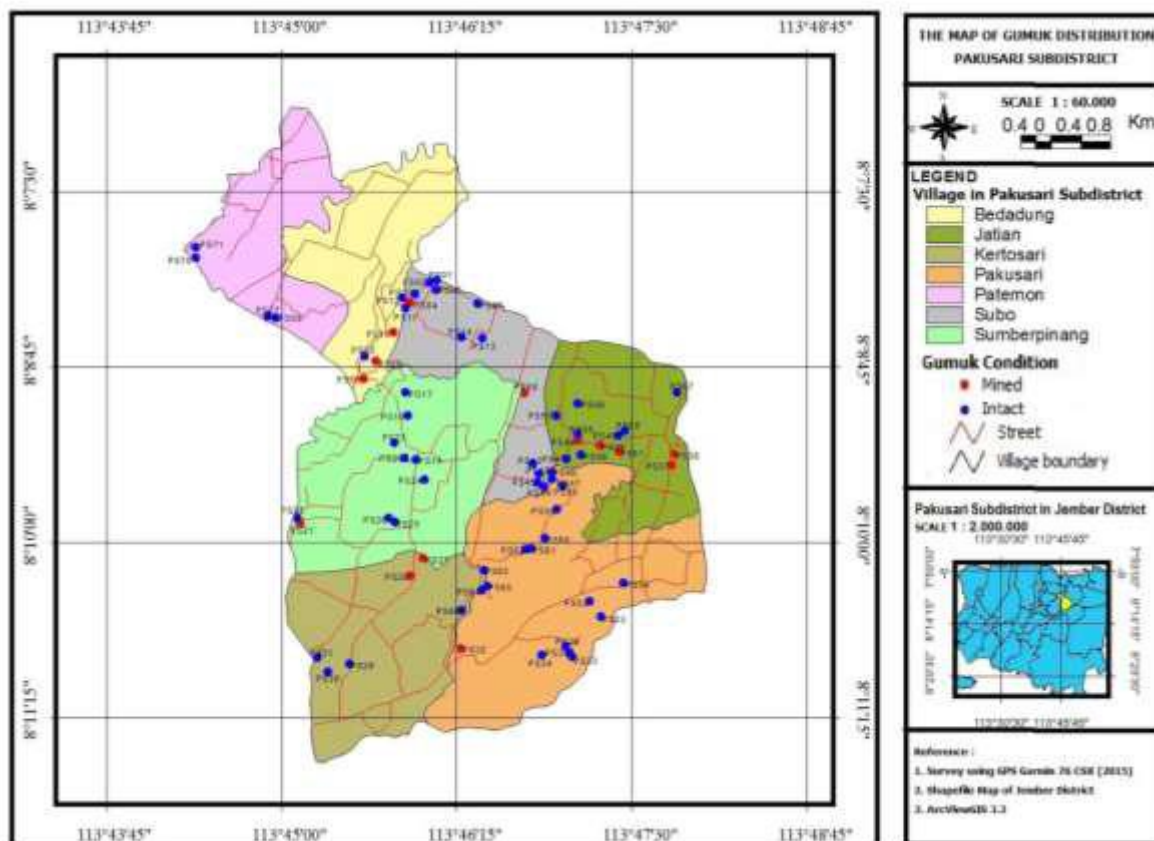
Fig.4: Map of Gumuk Distribution in Pakusari Subdistrict

The number of gumuk in Pakusari Sub-district is 71 gumuk, consisting of 56 gumuk in intact condition and 15 gumuk in mining process. In table 3 is seen that the largest number of gumuk in Pakusari Village is 18 gumuk consisting of 17 gumuk in intact condition and 1 gumuk in mined condition. While the fewest guduk in Patemon Village as 4 gumuk and in intact condition. Based on the geological map of Jember District the rock formations in Pakusari sub-district consist of Tuff Argopuro and Bagor Form.

Table.3: Number of Gumuk in Pakusari Sub District

No	Village	intact	mined	Rock Formation
1	Bedadung	2	3	Tuff Argopuro
2	Patemon	4	-	Tuff Argopuro
3	Sumberpinang	9	1	Tuff Argopuro
4	Subo	12	2	Tuff Argopuro
5	Jatian	8	6	Tuff Argopuro & Fom Bogor
6	Pakusari	17	1	Tuff Argopuro
7	Kertosari	4	2	Tuff Argopuro

The measured self potential at the research site can be displayed in the form of contour maps. The result of the potential contour of the spreading of dune in Subo Village of Pakusari District is shown by figure 1.5 below:
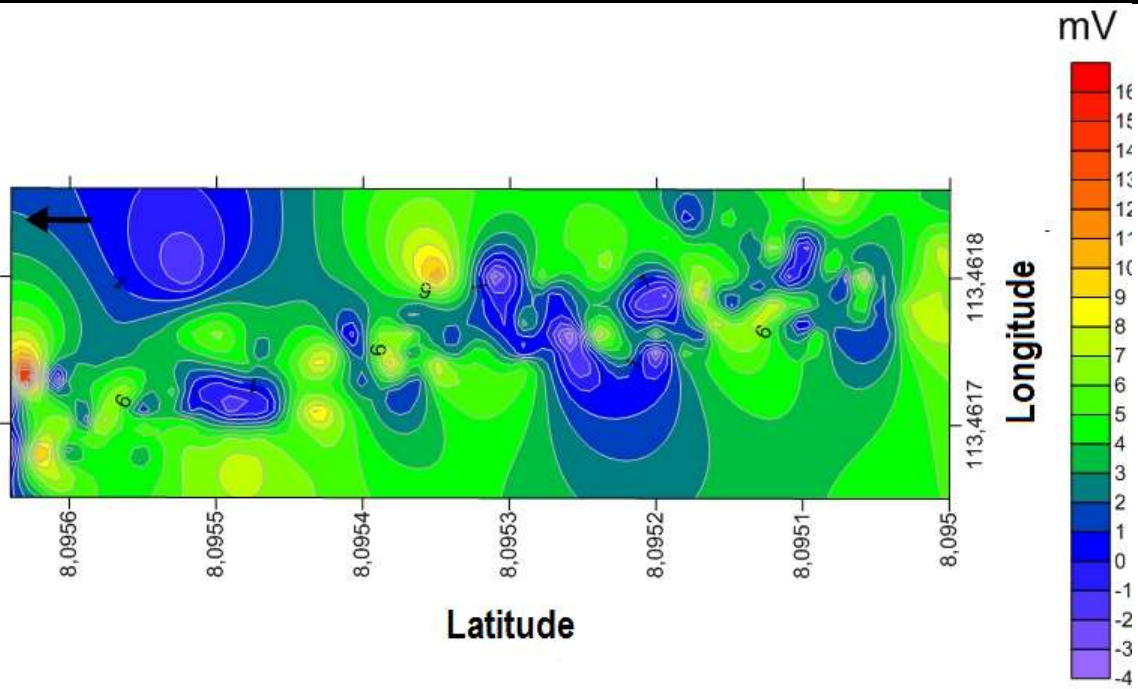
Fig.5: Map of potential contour distribution of gumuk in Subo Village Pakusari SubDistrict

At the gumuk in Subo Villages, pakusari subdistrict, some potensial groundwater potency were shown in 08º09'52" sampai dengan 08º09'53" S dan 113º46'18" E with range of potential value 2 mV to -4 mV. Groundwater potential areas is 24% of this research area.

The third location is in Arjasa Subdistrict, the result of its gumuk distribution is seen in Figure 6 with the scale of 1: 75.000 and the area of 43.75 Km^2.
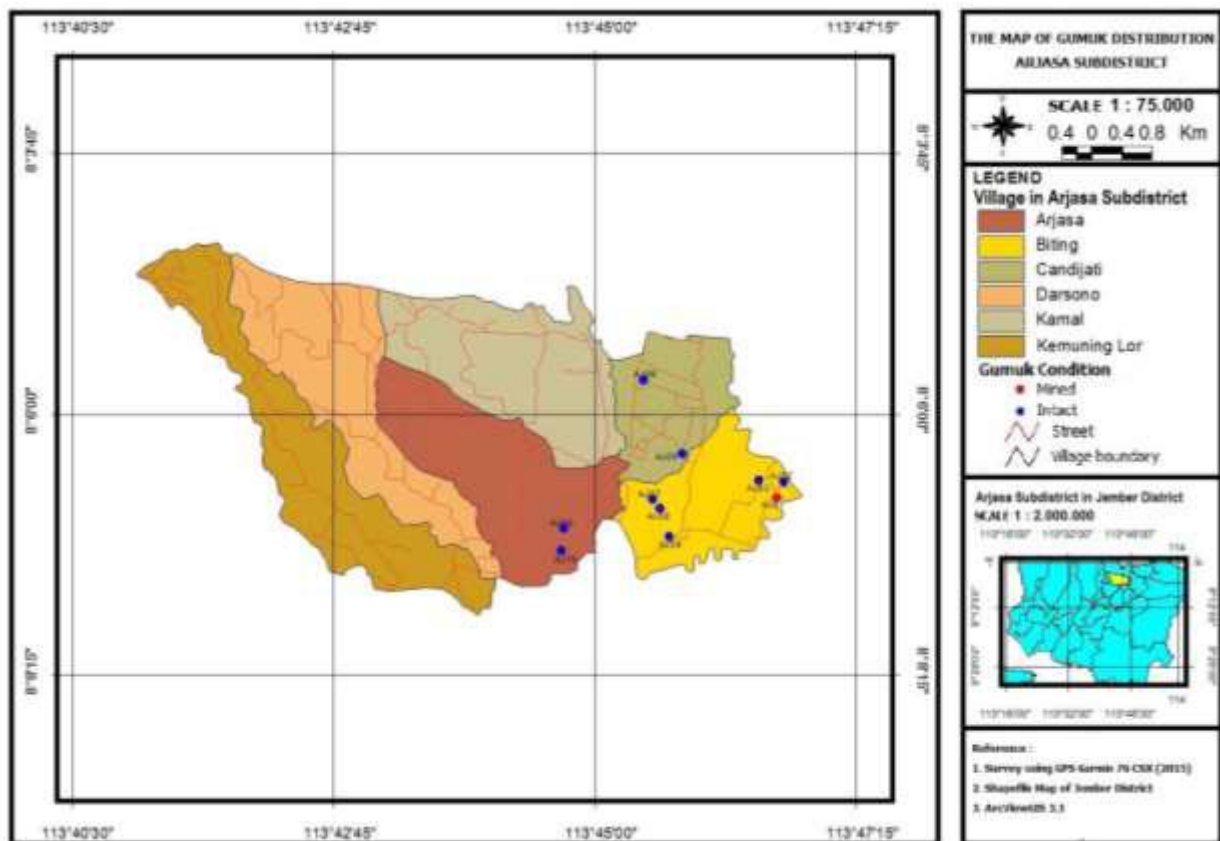
Fig.6: Map Distribution of Gumuk in Arjasa Sub District

Based on table 4. the number of gumuk that is in District Arjasa as 10 gumuk, consisting of 9 gumuk in intact condition and 1 gumuk is being mined. The area where the distribution of the gumuk is located in 3 villages, Biting, Candijati, and Arjasa. This sub-district is a subdistrict that has the least number of gumuk compared to other sub-districts, this is because the gumuk in this region many have been mined, so the number of gumuknya decreases. Rock formations contained in the region are the formation of Bagor Form Stone, Argopuro Breccia, and Argopuro Tuff.

Table.4: Number of Gumuk in District Arjasa

No	Village	intact	mined	Rock Formation
1	Biting	5	1	Form Bagor, Breksi Argopuro, dan Tuff Argopuro
2	Candijati	2	-	Breksi Argopuro
3	Arjasa	2	-	Breksi Argopuro
4	Kamal	-	-	-
5	Darsono	-	-	-
6	Kemuning Lor	-	-	-

The results of the self potential contour of gumuk distribution in Biting Village, Arjasa Sub District is shown by Figure 5 below:)
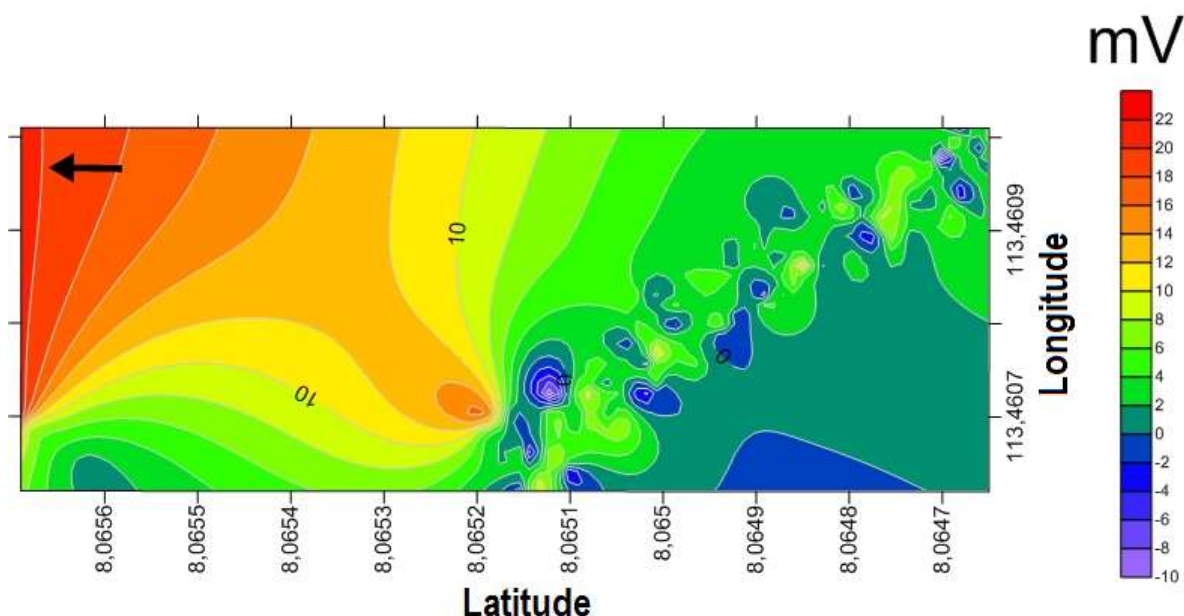

Fig.5: Map of potential contour distribution in Biting Village, Arjasa Sub District

The potential of groundwater in the spread of gumuk spread in the village of Biting Arjasa District has a range of values 0 mV to -10 mV, groundwater anomalies shown uneven in the gumuk area only at some point. The area of groundwater potential is 4% of the research area.

The number of gumuk in Jember district decreases due to switching function to residential areas and most of them have been mined. This lead to decreasing of spring water which are generally found around gumuk. Gumuk ecosystem, functionally play big role for human life, i.e forming a local hydrologic cycle that has an important role in creating a microclimate for agricultural landscape and preserve the water cycle. The hydrological cycle of the gumuk can be likened to a water reservoir capable of storing rainwater as an input and then drain to the area under it continuously. Therefore, Jember District Government should make spatial planning for non-existent of gumuk and can be developed into productive economic activities without destroying its formation

IV. CONCLUSION

Based on the measurement results of the gumuk distribution and the potency of groundwater obtained pattern of gumuk distribution divide into cumulate gumuk and spread gumuk. Gumuk is assumed to have a cumulate pattern if the distance between the gumuk not too far away and when viewed from a distance it will be seen forming a single gumuk. This type of gumuk based on

research results are in Sub District Ledokombo and Pakusari. While the gumuk is assumed to have spread pattern if the distance between gumuk far enough and its position is not seen as one unity. This type of gumuk based on research results are in Sub District Arjasa. The results obtained on the cumulate gumuk have a potential range of 2 mV to -14 mV, so that the potency of groundwater in the cumulate gumuk can be assumed to be dominant. Whereas in the spead gumuk anomalous groundwater shown unevenly, in the gumuk area only at some point. Potency soilwater in gumuk spreads less dominant compared with cumulate gumuk.

REFERENCES

[1] Abidin, H. Z. 2007. Penentuan Posisi dengan GPS dan Aplikasinya. Jakarta: PT. Pradnya Paramita.

[2] Fariha, H. 2012. Aplikasi Metode Geolistrik Resistivitas 2 Dimensi (2D) Untuk Mendeteksi Struktur Bawah Permukaan Pada Daerah Gumuk Di Kabupaten Jember. *skripsi.* Jember: Universitas Jember.

[3] Goto,T, Kazuya Kondo, Rina Ito, Keisuke Esaki, Yasuo Oouchi, Yutaka Abe, and Maki Tsujimura, 2012, Implications of Self-Potential Distribution for Groundwater Flow System in a Nonvolcanic Mountain Slope. International Journal of Geophysics, Volume 2012

[4] Jardani,A., J.P.Dupont, and A.Revil. 2006. Self-potential signals associated with preferential groundwater flow pathways in sinkholes. Journal of Geophysical Research, Volume 111, Issue B9

[5] Jinadasa, S.U.P. and R.P. de Silva. 2009. Resistivity imaging and self-potential applications in groundwater investigations in hard crystalline rocks, Journal of the National Science Foundation of Sri Lanka, 37 (1)

[6] Kepel (Kelompok Peduli Lingkungan). 2000. *Program Konservasi Ekosistem Gumuk*. [serial on line]. http://kepel.itgo.com/gumuk/index.htm [3 Maret 2015].

[7] Onojasun, Okan Evans. 2012. Delineating Groundwater Contaminant Plums Using Self-Potential Surveying Method In Perth Area, Australia, INTERNATIONAL JOURNAL OF SCIENTIFIC & TECHNOLOGY RESEARCH VOLUME 4, ISSUE 11, NOVEMBER 2015,ISSN 2277 -8616

[8] Reynolds, J.M. 2011. *An Introduction to Applied and Enviromental Geophysics 2nd edition*. New York: John Wiley & Sons.

[9] Sulistyaningsih N., Sutikto T., Bowo C., Regar A.F.C., dan Sudibya J. 1997. *Sumbangan ekologis Formasi Gumuk di DATI II Kabupaten Jember*. Jember: Universitas Jember

[10] Sharma, P.V. 1997. *Environmental and Geophysics*. New York: Cambridge University Press.

Impact of GST on E-Commerce

Ms. Priti Jadhav, Ms. Manjushree Yewale, Ms. Trupti Kalyankar, Mrs. Vandana Nemane

Dr. D. Y. Patil ACS College, Pimpri, India

Abstract— *E-commerce as anything that involves an online transaction. E-commerce provides multiple benefits to the consumers in form of availability of goods at lower cost, wider choice and saves time. The general category of e-commerce can be broken down into two parts: E-merchandise: E-finance. E commerce involves conducting business using modern communication instruments: telephone, fax, e-payment, money transfer systems, e-data interchange and the Internet. Online businesses like financial services, travel, entertainment, and groceries are all likely to grow. Forces influencing the distribution of global e-commerce and its forms include economic factors, political factors, cultural factors and supranational institutions.*

Goods and Service Tax or GST as it is known is all set to be a game changer for the Indian economy. Overall it is known to be beneficial to both the consumer, business and the Government. In India, there are different indirect taxes applied on goods and services by central and state government. GST is intended to include all these taxes into one tax with seamless ITC and charged on both goods and services. Thus excise duty, special additional duty, service tax, VAT to name a few will get repealed and will be added into GST. For this, GST will have 3 parts CGST, SGST and IGST. The central taxes like excise duty will be subsumed into CGST and state taxes like VAT into SGST. This going to be forward on all transactions of both goods and services, only one tax will apply which is GST comprising of CGST and SGST. IGST would be applied instead of SGST for interstate transactions. Input credit of all these taxes will be available against all the respective outputs.

This paper is outcome of a review of various research studies carried out on Impact of GST on E-commerce. This paper examines different aspects like No threshold for GST registration, No Benefit under Composition Scheme, Tax Collection at Source by Marketplace Operator. Finally in the conclusion one country and one tax will help Indian Economy to grow Rapidly.

Keywords— E-commerce, GST, Traditional business, Opportunities.

I. INTRODUCTION

India's e-commerce market is estimated to have crossed Rs. 211,005 crore in December 2016 as per the study conducted by Internet and Mobile Association of India. The report further claim that India is expected to generate $100 billion online retail revenue by the year 2020.

The uprising of Electronic Commerce in India has also resulted in conception of online marketplaces. A Marketplace is an e-commerce platform owned by the E-commerce Operator such as Flipkart, Snapdeal and Amazon. Some of the features of a marketplace model are:

- Marketplace enables third-party sellers to register and sell online on their platform.
- Marketplace charges a subscription fees/ commission on sale value from listed sellers.
- Third-party sellers under this model gain access to a larger customer base, registered with marketplace.
- Customer on the other hand gain access to multiple sellers and competitive prices for desired products.
- Items purchased on such marketplaces are either shipped by Merchant/Third-party seller directly or through the fulfillment center managed by Marketplace Operator.

Government has also allowed Foreign Direct Investments under such model to promote e-commerce marketplace business model in India.

Marketplaces has provided retailers with additional channel of sales and reach which was unimaginable for an offline seller. Major marketplaces claim to have lacs of sellers affiliated with their platform with millions of SKUs. While the number of sellers and their business have increased significantly, GST has specifically taken up marketplaces and has come out with rules & regulations specific to this segment.

Introduction of these regulations requirements has compelled the online seller community to embrace GST regime. Some of these compliance are:

No threshold for GST registration: Government has specified a threshold limit for all the businesses. A business is liable to register under Goods and Services Tax once such threshold limit is breached. However such limit is not

applicable in case of E Commerce sellers. All the businesses carrying out e-commerce activity are required to get registered under GST irrespective of their turnover.

No Benefit under Composition Scheme: Most of these sellers registered with marketplace operators are small and medium businesses. Government has introduced composition scheme under GST law. This scheme is primarily aimed to reduce the burden of compliance for small and medium businesses. Under this scheme, businesses are required to file returns quarterly instead of monthly and pay taxes at nominal rates up to 2%. To know more about Composition Scheme, However GST law has explicitly excluded e-commerce businesses from this scheme.

Tax Collection at Source by Marketplace Operator: Under the new tax regime, marketplace operators are mandatorily required to deduct a percentage amount as the GST liability of seller and deposit it with government. This mechanism is being termed as "Tax Collection at Source (TCS)" under the GST law. Eventually the marketplace seller will have to file monthly return under GST to claim the credit of TCS collected by the marketplace operator. This will also impact the liquidity and cash flow of these sellers.

While all the marketplace operator have already completed the first level analysis of impact of GST on their operations, marketplace sellers are still unaware of these rules.

Need of the hour is to keep themselves aware of the changes that are going to come. Also such sellers should now start planning their transition strategy for GST regime.

Some of the key points that should be kept in mind are:
1. Get your **GST enrollment** done on time. To read more about the enrollment process and its relevance.
2. Plan your logistics and warehousing requirement carefully. To read our detailed guide on impact analysis on logistics and warehousing,
3. Adopt such platforms, technologies which will enable your business to be GST compliant.

Although we are at a very initial stage for GST implementation. But marketplace sellers may not have much luxury of time and it is advised to be proactive in your business decisions for GST transition.

What is considered as e-commerce according to GST rules?

E-Commerce is defined like this in Section 43B(d) of the MGL (Model GST Law) – Electronic Commerce to mean the supply or receipt of goods and/ or services, or transmitting of funds or data, over an electronic network, primarily the internet, by using any of the applications that rely on the internet, like but not limited to e-mail, instant messaging, shopping carts, web services, universal description Discovery and integration (UDDI), File Transfer Protocol (FTP) and Electronic Data Interchange (EDI) whether or not the payment is conducted online and whether or not the ultimate delivery of the goods and/or services is done by the operator.

E-Commerce Operator	Not an Ecommerce Operator	Not an Ecommerce Operator
Amazon and Flipkart are e-commerce Operators because they are facilitating actual suppliers to supply goods through their platform (popularly called Market place model or Fulfillment Model)	Amazon and Flipkart will not be treated as e-commerce operators in relation to those supplies which they make on their own account (popularly called inventory Model).	Titan 78 supplying watches and jewels through its own website would not be considered as an e-commerce operator for the purposes of this provision.

With the inclusion of retail entrepreneurs in the ambit of GST and the introduction of specific provisions for e-commerce companies, certain areas of GST will impact the e-commerce sector.

Every company in India, be it a multinational company or a small/medium enterprise, is gearing up for the implementation of GST. The e-commerce sector would follow suit in its preparation by focusing on provisions specific to this sector in the GST law. The success of the e-commerce sector is largely dependent on the increasing number of retail entrepreneurs, who fall in the unorganized retail sector category. The government has included such players in the ambit of GST with an intention of broadening the tax base and has introduced specific provisions for the e-commerce companies. Here are some of the key areas of GST that impact the e-commerce sector:

1. **No trade barriers—one nation one tax**
    (i) In the present regime, there is no uniformity in the tax rates among the different states and therefore every state determines its own tax rates specific to the products. For example, a mobile phone in state 1 is taxed under VAT at five percent and in state 2

at 14.50 percent. As a result, the sellers in state 2 would not want to sell locally but would prefer to sell from state 1, resulting in loss of revenue for state.

(ii) E-commerce operators have set up distribution centres only in certain locations and collect the VAT applicable on sales made from such centres. In order to compensate for the loss of VAT revenue, many states have recently imposed entry tax on goods coming from other states, which discourages sales made from other states. The entry tax acts as a trade barrier, restricts free movement of goods from one state to another and increases the cost for traders.

(iii) However, such trade barriers will cease to exist as GST is inclusive of entry tax. The destination state earns the revenue from GST on sales regardless of where the sale was made. Further, there is no rate arbitrage under GST because the classification of goods and rate of GST is common across states.

2. **Tax collection at source (TCS)**

It is mandatory for all e-commerce operators to collect tax at the rate of two percent as TCS on the net value of sales made by suppliers through e-commerce operators. Such TCS has to be deducted in each state and deposited accordingly. This brings in significant compliance challenges to sellers and may discourage sales through marketplace model. However, this may not be applicable for inventory based models, where the e-commerce operator makes the sale from its own inventory. The key purpose of this provision is to encourage compliances under GST and provide a mechanism for the government to track suppliers who sell through e-commerce operators.

3. **Increase in compliances for e-commerce operators**

The e-commerce operators should report all supplies made by the seller and the TCS collected thereof on a monthly basis. The sales reported by the e-commerce operator will have to match with the sales declared by the supplier himself at the end of every month, and any difference will be added to the turnover of the supplier and consequently be liable to discharge GST on such additional turnover.

The e-commerce operator has to report the product/service code and the applicable rates for each item level individually. This requires them to map every sale done by the dealer and ensure TCS is deducted at the right value. The implementation of compliance is cumbersome for both e-commerce operator and the supplier.

Additionally, the e-commerce operators will have to register in each state and file the reports separately on a monthly

basis. This process increases the challenges in compliance and costs of running the business.

4. **Mandatory registration of sellers and unavailability of composition scheme**

GST mandates that all sellers supplying through an e-commerce operator need to be registered under GST irrespective of the threshold limit of Rs 20 lakh. These sellers cannot opt for composition scheme, where they pay a flat tax at the rate of two percent and do not maintain details of each product sold. In this scenario, it is not feasible for small businesses to maintain a detailed record of purchases and sales and pay higher rate of tax. Because of this, many small retailers may not prefer to work with an e-commerce company, which impacts the business for e-commerce operators.

5. **Increase in credits**

The GST law has extended the meaning of 'input tax' to cover any goods/services used by the company in the course of business, which has widened the ambit of input GST credits. This has removed the requirement to establish the direct nexus of inputs/input services with the final product/service provided by companies. For e-commerce operators and sellers, the unavailability of credit towards excise duty and VAT on goods and service tax on certain services adds to the cost of running the business, which would be avoided under GST on account of increase in credits.

II.   CONCLUSION

As we can see, the GST law may have a negative impact on the e-commerce sector. Given that e-commerce sector in India is one of the most rapidly advancing sectors and the government is vigorously promoting digitised economy, the introduction of such cumbersome compliances cringes the growth of this sector.

Statutory framework introduced by the government should be towards the advancement of business rather than creating obstacles. The GST law should provide an enabling environment that encourages e-commerce operators and suppliers

In the run-up to one of the biggest tax reforms in the country, the market is abuzz with new rules and guidelines about the Goods and Services Tax (GST). How will GST really impact your business? How will your financial reporting change? Find out the answers to all this and more, directly from industry and tax experts who will share their expertise on Your Story's new series 'India on GST'.

REFERENCES

[1] https://cleartax.in/s/impact-of-gst-on-e-commerce-marketplace-sellers

[2] http://www.profitbooks.net/gst-impact-on-ecommerce-business/

[3] https://yourstory.com/2017/06/gst-india-benefit-barrier-e-commerce-sector/

[4] http://economictimes.indiatimes.com/industry/services/retail/gst-impact-on-e-commerce-marketplaces-put-an-embargo-on-non-compliant-merchants/articleshow/59431750.

[5] https://www.legalraasta.com/gst/impact-of-gst-on-e-commerce/

[6] https://www.zoho.com/books/guides/gst-for-ecommerce.html

Block Transformation for Encrypted Image through RDH

Pavana K P[1], Mrs. Aritri D.Ghosh[2]

[1]Student M.Tech Digital electronics, Dept. of ECE, CMR Institute of technology, Bengaluru, India
[2]Assistent Professor Dept. of ECE, CMR Institute of technology, Bengaluru, India

Abstract—For a greater amount of ubiquity of information outsourcing to cloud, it may be vital to preserve those security of information furthermore empower those cloud server should handle the information effortlessly toward same period. With accomplish such requirements, "Reversible Data hiding by Encrypted image (RDH EI)" makes enormous challenge for analysts. In this novel, proposed a framework for "Block transformation for EI through RDH". Contrasting with past Encryption based schemes, RDH EI based framework let the user to transmit the semantic of original image into semantic of target image with similar size. The transmitted picture or image looks similar as target image, which is utilized as Encrypted image (EI), and will outsource to Cloud server. Hence, Cloud server can embed the data into EI through RDH technique for Plain text image. Also image can retrieve back as original without any degradation. Data hiding will be done by least significant bit replacement, also RIT mainly includes block pairing and block transformation process which satisfies image quality.

Keywords— Reversible image transformation (RIT), Encrypted image (EI), LSB, Reversible data hiding (RDH).

I. INTRODUCTION

These days outsourced capacity through cloud gets more mainstream service, particularly to media files such as images, videos, which have huge storage room. On deal with the outsourced images, those cloud server might implant A percentage extra information under the images, for example, picture classification Also documentation data and utilization such information should identify those ownership alternately check the integument from claiming pictures. Also reversible data hiding technology is needed, by which the original image can be losslessly restored after the embedded message is extracted. Data security basically means protection of data from illegal users and provides high security to check data medication. This area of data security has gained more attention over the recent period of time due to the huge increase in data transmission rate over the network. In order to recover the security types in data transfers over the internet, many techniques have been developed like: cryptography, steganography. Also cloud service for outsourced storage makes it interesting to protect the privacy of image contents. For instance, recently many private photos of actress leaked from cloud. For this RDH is helpful for managing the outsourced images, it cannot protect the image content, encryption is the most popular technique for protecting privacy. So it is fascinating to implement RDH in encrypted images but will not get any information about the image contents. Inspired by the needs of privacy protection, many methods have been presented to extend RDH methods to encryption domain. From the viewpoint of compression, these methods on RDH-EI belong to the frameworks [14] "vacating room after encryption (VRAE)" and "reserving room before encryption (RRBE)"

For both frameworks, VRAE and RRBE the image owner will send a cipher text formed image to the cloud. However the cipher texts with the special form of messy codes are easy to cause the attention of the cloud server who may try to dig out information on the encryption users. In fact the cloud server is assumed to be curious to collect information from the outsourced files [15], and obviously the encrypted images are more attractive to a curious cloud server. Therefore, the fact that the user is outsourcing encrypted images, itself is also a kind of privacy of the user, which should be protected.

II. LITERATURE REVIEW

There are many techniques available for reversible data hiding in encrypted image as follows Lai et al. [2] propose an image transformation technique, which selects a target image similar to the secret image, then replaces each block of the target image by a similar block of the secret image and embeds the map between secret blocks and target blocks; it forms an Encrypted image of the secret image. A greedy search method is used to find the most similar block. Although Lai et al.'s method is reversible, it is only suitable for a target image similar with the secret image, and the visual quality of encrypted image is not so good.

In 2003 J Tian proposed the "reversible data embedding (RDE) utilizing of difference expansion" [7]. He presented a max-capacity with high-quality, RDE technique for digital-images. This technique can apply for both digital-audio & for digital-video also. He evaluates the dissimilarity between neighboring pixel-values. In this paper author considered only grayscale images. The author explored the redundancy in digital-images, which achieved a high embedding capacity, and remain the distortion law. This correspondence [3] proposed a lossless, reversible and data hiding schemes for public-key-encrypted images probabilistic and homomorphic properties of cryptosystems. With these schemes, the pixel reorganization is avoided and the encryption/decryption is performed on the cover pixels directly so that the amount of encrypted data and the computational complexity are lowered. Due to data embedding on encrypted domain may result in a little bit distortion in plaintext domain due to the homomorphic property, the embedded data can be extracted and the original content can be recovered from the directly decrypted image. With the combined technique, a receiver may extract a part of embedded data before decryption, and extract another part of embedded data and recover the original plaintext image after decryption This technique [5] Z Qian et al proposed a "Distributed Source coding (DSC) with RDH in EI". After Encryption of 0riginal image by content user, the Data Hider compress the elected bits series considered from encrypted image which makes the room for secret-data/message. From the receiver side, secret bit sequence can be withdraw if the receiver know unique embedding key. If receiver knows encryption-key then he can recuperate original image exactly with higher-quality by using image estimation algorithm. Finally if receiver knows "Embedded key" & "Encryption-key", then receiver can embed the secret message and perfectly recover the actual image by utilizing of "Distributed source decoding method". The aim of author is to enhance the embedding payload in encrypted-images. So he applied the separable RDH methodology for encrypted images through "Slepian-wolf source encoding" mechanism. He concludes that his work achieves the great embedding payload with good image recovery quality, and avoids the room reserving operations by the sender.

The reversibly embed the message into the host sequence by modifying its histogram with methods like histogram shifting [6]. Recently, Zhang et al. proposed the optimal histogram modification algorithm [8], for RDH by estimating the optimal modification probability. Zhang divided the encrypted image into several blocks. By flipping 3 LSBs (least significant bits) of the half of pixels in each block, room can be vacated for the embedded bit. The data extraction and image recovery proceed by finding which part has been flicked in one block. This process can be recognized with the help of spatial association in the decrypted image. The decoder side by further exploiting the spatial correlation using a dissimilar estimation equation and side match technique. For both methods in [10] and [11], decrypting image and extracting data must be jointly executed. Recently, Zhou et al. [12] proposed a novel RDH-EI method for joint decryption and extraction, in which the correlation of plaintexts is further exploited by distinguishing the encrypted and non-encrypted pixel blocks with a two-class SVM classifier. To separate the data extraction from image decryption, Zhang [13] emptied out space for data embedding by directly using the typical manner of cipher text compression that is, compressing the encrypted pixels in a lossless manner by using the syndromes of parity-check matrix of channel codes. Recently Weiming Zhang, Hui Wang, Dong dong Hou, and Nenghai Yu propose a novel context [1], for RDH-EI based on reversible image transformation (RIT). Dissimilar from all preceding encryption-based frameworks, in which the encryption texts may attract the notation of the curious cloud, RIT-based context allows the user to transform the contented of original image into the content of another cover image with the same size. The transformed image that looks similar as the cover image is used as the "encrypted image," Reversible data hiding in images is a technique that hides data in digital images for secret communication. It is a method to hide other missive into cover media with a revocable manner so that the innovative cover content can be perfectly restored after extraction of the hidden message. In this paper will be using the method as [1] for transformation where the concept of mosaic image for data security, dividing the image into blocks with respect to cover and will be doing data hiding using LSB replacement with less complexity also achieved exact recovery by extracting the hidden data.

III.   PROPOSED SYSTEM

Here in this we proposed framework for RDH-EI by using reversible image transformation (RIT). RIT transforms the content of original image I into the content of another target image J, with equal size and the transformed image looks similar as target image or cover image which will be used as "encrypted image" and which will be outsourced to cloud. And cloud server can embed data into the encrypted image using RDH method that is least significant bit replacement with less complexity and gives high quality of image also original image can be retrieved back in lossless way through encryption key.
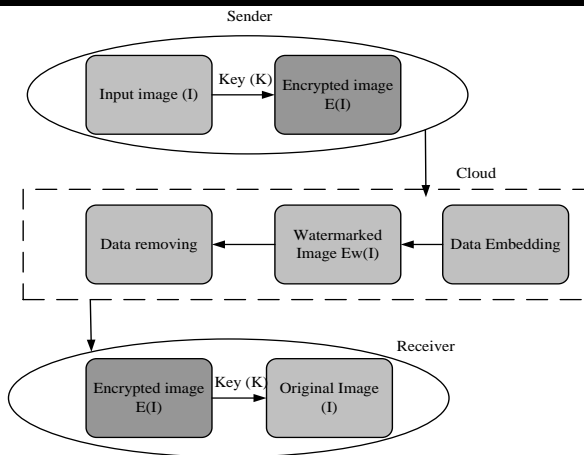
Fig.1: Proposed system

For color images, we transform the color channel R, G, and B respectively in the same manner. So we just take gray images (one channel) as an example to describe the method. For an original image I, we randomly select a target image J having the same size with I from an image database. Firstly, we divide the original image I and the target image J into N non-overlapping blocks respectively, and then pair the blocks of I and J as a sequence such that $(B_1,T_1),...,(B_N,T_N)$, where B_i is an original block of I and T_i is the corresponding target block of J, $1\leq i \leq N$. We will transform B_i toward T_i and generate a T_i' similar to T_i. After that, we replace each T_i with T_i' in the target image J to get the transformed image J'. Finally we embed some accessorial information (AI) into J' with an RDH method and generate the ultimate "encrypted image" E(I).These AI is necessary for recovering I from J'. Before being embedded, these AI will be compressed and encrypted with a key K shared with the receiver, so only a receiver having K can decrypt E(I). the proposed transformation process consists of three steps: block pairing, block transformation and AI embedding.

A. BLOCK PAIRING

To make the transformed image J' look like target image J, we hope, after transformation, each transformed block will have close mean and standard deviation (SD) using equation (1) and (2) with the target block. So we first compute the mean and SD of each block of I and J respectively. Let a block B be a set of pixels such that B = {p1, p2,..., pn}, and then the mean and SD of this block is calculated as follows:

$$u = \frac{1}{n}\sum_{i=1}^{n} p_i,$$

(1)

$$\sigma = \sqrt{\frac{1}{n}\sum_{i=1}^{n}(p_i - u)^2}.$$

(2)

When matching blocks between original image and target image, we hope two blocks with closest SDs to be a pair. In Lee et al.'s method, the blocks of original image and target image are sorted in ascending order according to their SDs respectively, and then each original block is paired up with a corresponding target tile in turn according to the order. To recover the original image from the transformed image, the positions of the original blocks should be recorded and embedded into the transformed image with an RDH method. If the image is divided into N blocks, N log N bits are needed to record block indexes. Obviously, the smaller the block size is, the better the quality of transformed image will be, but which will result in a large N. therefore, the amount of information used to record the index for each block may be so large that it will cause much distortion when embedding these information into the transformed image. In fact there may not exist enough redundant space to store these additional information. For instance, if we divide a 1024×1024 image into 4×4 blocks, $2^{16} \times 16$ bits are needed to record the positions of blocks. To compress the block indexes, we first classify the blocks according to their SD values before pairing up. In fact, we found that the SD values of most blocks concentrate in a small range close to zero and the frequency quickly drops down with the increase of the SD value from boss base image database. Therefore we divide the blocks into two classes with unequal proportions class 0 for blocks with smaller SD, and class 1 for blocks with larger SD and pair up the blocks belonging to the same class. By assigning the majority of blocks to the class 0, we can avoid the large deviation of SDs between a pair of blocks and efficiently compress the indexes at the same time. In this paper, we propose to divide both the original and target images into non-overlapping 4× 4 blocks and calculate the SDs of each block. We first divide the blocks of original image I into 2 classes according to the quantile of SDs. Denote that the %α quantile of SDs by N_α, We assign the blocks with SDs $\in [0, N_\alpha]$ to "Class 0," and blocks with SDs $\in (N_\alpha, N_{100}]$ to "Class 1." And then we will scan the blocks in the raster order, i.e., from left to right and from top to bottom, and assign a class label, 0 or 1, to each block. Next, we label the blocks of target image based on the classes' volumes of original image. Assuming that the ith class in the original image includes n_i blocks for i= 0 or 1, we scan the target image in the raster order, and label the first n_0 blocks with the smallest SDs as Class 0, and the rest n_1 blocks as Class 1. As a result, each class in the target image includes the same number of blocks as the

corresponding class in the original image. We pair the original block up with target block in the following manner. Scan the original image and target image in raster order respectively and pair the jth block of the class i in the original image up with the jth block of the class i in the target image for i = 0, 1 and j= 1, . . . , n_i. For each pair of blocks (B,T), as will see later section, the original block *B* will be transformed to target block *T* by mean shifting and block rotation, yielding T. By replacing each T with T' in the target image, the sender will generate the transformed image. Note that both operations of mean shifting and block rotation will not change the SD value, so T' has the same SD as B. Therefore, the SDs in transformed image is only a permutation of those in original image. When classifying the blocks of transformed image according to %α quantile of SDs, the receiver can get a CIT that is same with the CIT of target image. Therefore to restore the original image from the transformed image, the receiver only needs to know the CIT of the original image.

B.   BLOCK TRANSFORMATION

Let the original block B = {p_1, p_2,···, p_n}, and the corresponding target block T = {p_1',p_2'….,p_n'}. And calculate the means of B and T and denote them by u_B and u_T respectively. The transformed block T'= {p_1", p_2",…..p_n"} is generated by the mean shifting as follows:

$$p_i" = p_{i+} u_T - u_B \qquad (3)$$

Where ($u_T - u_B$) is the difference between the means of target block and original block. We want to shift each pixel value of original block by amplitude ($u_T - u_B$) and thus the transformed block has the same mean with the corresponding target block. However, because the pixel value $p_i"$ should be an integer, to keep the transformation reversible, we round the difference to be the closest integer as

$$\Delta u = round (u_{T-} u_B) \qquad (4)$$

And shift the pixel value by Δu, namely, each $p_i"$ is gotten by

$$p_i" = p_{i+} \Delta u \qquad (5)$$

Note that the pixel value $p_i"$ should be an integer between 0 and 255, so the transformation may result in some overflow/underflow pixel values. To avoid such transformed blocks abstained by (5), we assume that the maximum overflow pixel value is OVmax for $\Delta u \geq 0$ or the minimum underflow pixel value is UNmin for $\Delta u < 0$. If overflow/underflow occurs in some blocks, we eliminate them by modifying Δu

$$\Delta u = \begin{cases} \Delta u + 255 - OV_{max}, & \text{if } \Delta u \geq 0 \\ \Delta u - UN_{min}, & \text{if } \Delta u < 0 \end{cases}$$

(6)

We use the modified Δu to shift the pixels of block B, and thus all the pixels' values are controlled into the range of [0,255]. However the range of Δu's value is still very large which cannot be efficiently compressed. Thus we further modify Δu as

$$\Delta u = \begin{cases} \lambda \times round(\frac{\Delta u}{\lambda}), & \text{if } \Delta u \geq 0 \\ \lambda \times floor(\frac{\Delta u}{\lambda}) + \frac{\lambda}{2}, & \text{if } \Delta u < 0 \end{cases}$$

(7)

In which the quantization step, λ, is an even parameter. Then it just needs to record Δu'=2 $|\Delta u|/\lambda$, by which it has the advantage of not to record the sign of Δu. Because when Δu' is an even number it means $\Delta u \geq 0$ and when Δu' is an odd number it means $\Delta u < 0$. Since when λ is large the amount of information recording Δu' will be small but the offset between the modified Δu and the original Δu will be large, a tradeoff must made by choosing λ. We set λ =8 in the following experiments. Finally, to maintain the similarity between the transformed image and target image as much as possible, we further rotate the shifted block into one of the four directions 0^0, 90^0, 180^0 or 270^0. The optimal direction is chosen for minimizing the root mean square error (MSE) between the rotated block and the target block. After shifting transformation and rotation, we get a new block T'. With these new blocks, we replace the corresponding blocks in the target image and generate the transformed image J'. The parameters, Δu' and rotation directions, will be compressed, encrypted and then embedded into the transformed image J' as AI to output the "encrypted image" E (I).

C.   REVERSIBLE DATA HIDING
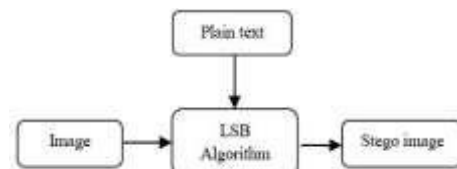
Fig.2. Embedding data
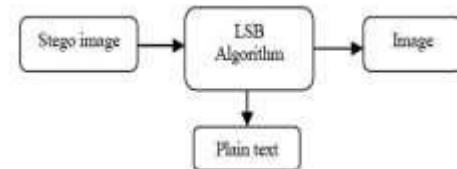
Fig.3. Reverse data hiding

Message encoding on an image can be divided in to two parts, one portion is data hiding other is reversible data hiding. In data hiding part there is a digital image in which we encode secret message by removing LSB of image pixel and add our secret message on corresponding LSB position, then the output image is called stego image. For retrieve the secret message program splits the image into its channels and applies the inverse lifting

scheme to each channel to the level specified by the user. When the transformation is completed, the program retrieves the message out of the pixels of the cover image. Different streams of digital media can be used as a cover stream for a secret message. Stegnography is the art of writing secret message so that only the sender and the intended recipient are aware of the hidden message. A successful information hiding should result in the extraction of the hide data from the image with high degree of data integrity. Current trends favor using digital image files as the cover files to hide another digital file that contains the secret message or information.

IV. RESULT

The experimental result for the method block transformation, embedding the data, restoration achieved through MAT lab tool using GUI, MAT lab implements GUIs as figure windows containing various styles of control objects, there we must program each object to perform the intended action when activated by the user of the GUI, all of these tasks are simplified by GUIDE, The process of implementing a GUI involves two tasks that is

- Layout the GUI components
- Programming the GUI components

GUIDE primarily is a set of layout tool. Which generates an M-file that contains code to handle the initialization and launching GUI also this file provides a frame work for the implementation of the callbacks the functions that execute when users activate components in the GUI, and FIG- file contains a complete description of the GUI figure

Let us show complete result analysis, by taking original image as lenna image and target image or cover image as baboon image which is shown below of equal size as 1024x1024 and done reversible image transformation process as explained and data hiding will gives the following outputs,

(a)   *(b)*

Fig.4. (a) Original image. (b) Cover image

Once we select with the images, will be doing block pairing step where can see the plots for SD value distribution as shown below
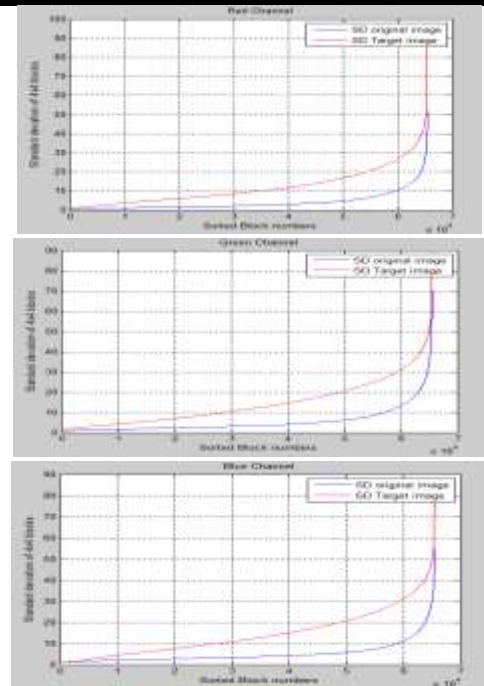
Fig.5. Plots of SD values for R G B channel

Later will do transformation step by considering several mathematical steps as explained above and embed the data into the transformed image using LSB replacement, corresponding transformed and embedded image will be shown below

(a)   *(b)*
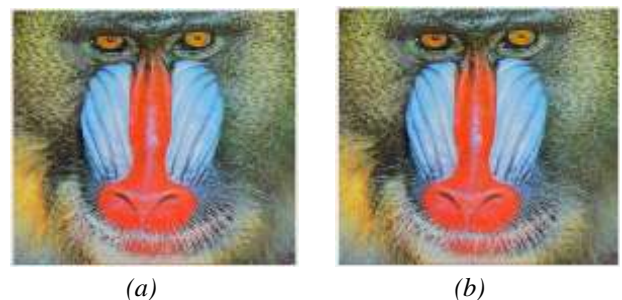
Fig.6. (a) Transformed image. (b) Embedded image

To recover image back, we need to extract the hidden data and do anti transformation gives the recover image which is as same as original that is called lossless recovery. Which will be shown in below figures

(a)   *(b)*

Fig.7. Recover image. (a) Wright key. (b) Wrong key

V. CONCLUSION

The proposed work formulates the novel for "RDH EI" which allows the secure block transmission for EI. "RIT" based "RDH - EI" changes the content of original image into content of another target image where secure the original image contents by transforming entire original to target and the outcome looks target image which is also the encrypted image. Since an EI contains plaintext image fo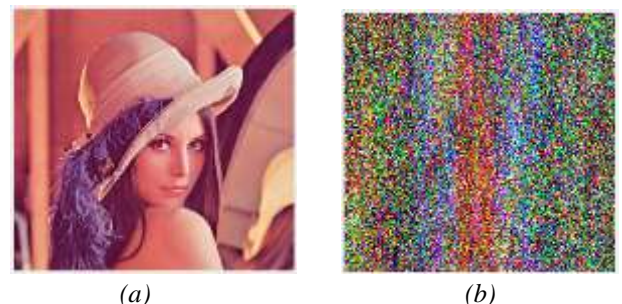rm, which neglect the annotation of cloud server. That will free from cloud server to select any conventional RDH method for plaintext image to implant watermark. Here the reversible image transmission based scheme will be used to restore as the original image in lossless fashion hence it achieves reversibility. From this technique, user can transmit the actual image to randomly selected cover image with equal size. Also the method fulfill the requirements on image quality with embedding capacity. Since the method works with key, gives back original image with maximum accuracy hence the method most helpful for all secured communication systems.

REFERENCES

[1] Weiming Zhang, Hui Wang, Dong dong Hou, and Nenghai Yu propose a novel framework for RDH-EI based on reversible image transformation IEEE Trans on Multimedia, vol.18, no.8, aug 2016.

[2] I.-J. Lai and W.-H. Tsai, "Secret-fragment-visible mosaic image–a new computer art and its application to information hiding," IEEE Trans. Information Forensics and Security, vol. 6, no. 3, pp. 936–945, 2011.

[3] Xinpeng Zhang, Jing Long, Zichi Wang, and Hang Cheng, "Lossless and Reversible Data Hiding in Encrypted Images with Public Key Cryptography," IEEE Trans. on Circuits and Systems for Video Technology, 2015.

[4] X. Hu, W. Zhang, X. Li, and N. Yu, "Minimum rate prediction and optimized histograms modification for reversible data hiding," IEEE Trans. Inf. Forensics Security, vol. 10, no. 3, 653–664, Mar. 2015.

[5] Z. Qian, and X. Zhang, "Reversible data hiding in encrypted image with distributed source encoding," IEEE Trans. on Circuits and Systems for Video Technology, vol. 26, no. 4, pp. 636-646, Apr. 2016.

[6] Z. Ni, Y .Shi, N. Ansari, and S. Wei, "Reversible data hiding," IEEE Trans. Circuits Syst. Video Technol., vol. 16, no. 3, pp. 354–362, Mar. 2006.

[7] J. Tian, "Reversible data embedding using a difference expansion," IEEE Trans. Circuits Syst. Video Technol., vol. 13, no. 8, pp. 890–896, Aug. 2003.

[8] W. Zhang, X. Hu, X. Li, and N. Yu, "Recursive histogram modification: Establishing equivalency between reversible data hiding and lossless data compression," IEEE Trans. Image Process., vol. 22, no.7,pp.2775–2785, Jul. 2013.

[9] X. Zhang, "Reversible data hiding in encrypted images," IEEE Signal Process. Lett., vol. 18, no. 4, pp. 255–258, Apr. 2011.

[10] W. Hong, T. Chen, and H. Wu, "An improved reversible data hiding in encrypted images using side match," IEEE Signal Process. Lett., vol. 19, no. 4, pp. 199–202, Apr. 2012.

[11] J. Zhou et al., "Secure reversible image data hiding over encrypted domain via key modulation," IEEE Trans. Circuits Syst. Video Technol., vol. 26, no. 3, pp. 441–452, Mar. 2016.

[12] X. Zhang, "Separable reversible data hiding in encrypted image," IEEE Trans. Inf. Forensics Security, vol. 7, no. 2, pp. 826–832, Apr. 2012.

[13] K. Ma, W. Zhang, X. Zhao, N. Yu, and F. Li, "Reversible data hiding in encrypted images by reserving room before encryption," IEEE Trans. Inf. Forensics Security, vol. 8, no. 3, pp. 553–562, Mar. 2013.

[14] S. Yu, C. Wang, K. Ren, and W. Lou, "Achieving secure, scalable, and fine-grained data access control in cloud computing," in Proc. IEEE INFOCOM, Mar. 2010, pp. 1–9.

A Multi-Agent Systems Contribution for Audit and Change Management

Nabil Benanbaar[1], Laila Moussaid[2,] Hicham Medromi[3]

(EAS- LRI) Systems Architecture Team, ENSEM, Hassan II University, BP.8118, Oasis Casablanca, Morocco

Abstract— *The progress made in Information Technology and the popularity of best practices have grown to give rise to new applications such as IT GRC. the good use of these applications requires communication and exchanges between these architectures. In front for a high number of standards and best practices, the model of management in Information system department becomes very dynamic. In this model, audit and change management are two problematics that are rarely automated in the function of information systems. These systems must adapt to new management methods and practices in order to improve innovation and management within companies. The major challenge of these standards and best practices is to adapt the target processes to the existing context and to have automatic mechanisms for auditing and generating a plan of evolution in an application.*

In this paper we propose an approach for Audit and Change Management in IT GRC tools. Our approach uses multi-agent systems to give the evolution plan in order to generate a road map for implementation the IT governance framework.

Keywords— *IT Governance, Audit and Change Management, best IT framework, IT GRC, Multi–Agent.*

I. INTRODUCTION

The evolution of information systems since the 1960 has enabled the profound changes having evolved the needs of management tools in information systems. The appearance of the term Information System is indicative of the changes in attitudes: this stems resulted the emergence of new actors and new management entities of information systems. This management approach reveals the challenge of the evolution of the information system, which must be managed and controlled by strategic alignment.

Strategic alignment is an approach to align the strategy of information system on the business rules of company. This approach has purpose of enhancing the value in use of the information system and makes it an asset to the company. To do this, a new system design was passed; this system is based on modeling a multi-Architecture environment, the aim of this practice is to define how organizations can align Information Technology (IT)

strategy with business strategy ensures that companies can measure their performance.

Today, this mode of management is called IT Governance.

IT Governance describes how an Information System (IS) is directed and controlled by defining approaches and good principles to implement the search for performance and reducing costs and risks. It can also define the relationship between IS users, the key processes and the common points between technical and functional architectures [1].

In this paper, we will focus on IT GRC architectures.

GRC is the acronym for "Governance, Risk and Compliance". It is a concept that describes the integration of activities to improve the efficiency and effectiveness of many functions of organizations.

By way of explanation, IT Governance, IT Risk and IT Compliance, ensures that enterprise objectives are achieved by evaluating stakeholder needs, conditions and options, setting direction through prioritization and decision making, and monitoring performance, compliance and progress against agreed-on direction and objectives [2].

Currently, implementing the techniques and tools of Audit and change management becomes a key element of the innovation and management system within companies.

II. STAT OF ART

Like Enterprise Resource Planning (ERP), GRC is becoming one of the most important business requirements of an organization [3], mainly due to rapid globalization, increasing regulation and growing demand for transparency for companies, [4], [5], and [6].

The GRC methods are based on the process approach.

A. IT Processes

IT Governance, IT Risk and IT Compliance are based on a set of processes to ensure that the objectives assigned to the IS are well considered. There are a variety of processes to meet the needs of the activities of an IS department. These processes can be divided as follows:

• **Management planning:** is the process of definition and assessing an organization's goals and creating a realistic detailed plan of action for meeting those goals. The basic

steps in the management planning process involve creating a road map that outlines each task the company must accomplish to meet its overall objectives.

• **Service Management:** refers to the entirety of activities that are performed by an organization to plan, design, deliver, operate and control information technology (IT) services offered to customers.

• **Project Management:** is the discipline of initiating, planning, executing, controlling, and closing the work of a team to achieve specific goals and meet specific success criteria.

• **Cost Management:** is the process of planning and controlling the budget of a business. Cost management is a form of management accounting that allows a business to predict impending expenditures to help reduce the chance of going over budget.

• **Software Management:** is the process of planning and leading software projects. It is a sub-discipline of project management in which software projects are planned, implemented, monitored and controlled. Realizes software and implements them using programming languages.

• **Security Management:** This is a broad field that encompasses several aspects; these processes protect by appropriate measures and detect as soon as possible the security problems that could threaten the information system of an organization.

• **Provider Management:** the processes that give specialist advice and support with contracts between customers and provider in order to get more value in the customer-provider relationship.

• **Resource Management:** The process of using a company's resources in the most efficient way possible. These resources can include goods and equipment, financial resources, and human resource.

• **Quality Management:** Set of activities allowing the determination of the quality policy and its implementation in order to maintain and improve the services and products of an IT organization.

B. IT GRC Processes

Today, there are several best IT frameworks in the IT market to implement the IT GRC concept, each standard is specialized in a specific field. In the following, we will cite the main best practices and standards used by companies in the IT domain.

• **COBIT (Control Objectives for Information and related Technology):** is a framework developed and delivered by ISACA (Information Systems Audit and Control Association), he Allows to control the objectives and to manage the IT processes, to do this, COBIT provides a set of practices to manage the levels of control that must be applied on IT processes and resources.

• **ITIL (Information Technology Infrastructure Library):** is a set of detailed practices for IT service management (ITSM) that focuses on aligning IT services with the needs of business. The main goal of ITIL is to improve service to the customer.

• **CMMI (Capability Maturity Model Integration):** was developed by a group from industry, government, and the Software Engineering Institute (SEI). CMMI models provide guidance for developing or improving engineering processes of an organization. A CMMI model may also be used as a framework for appraising the process maturity of the organization. The main goal of CMMI is to ensure to customers of a certain level of maturity of the company's engineering processes.

• **PMBOK (Project Management Body of Knowledge):** developed by the Project Management Institute (PMI), PMBOK is a guide and global standards provide guidelines, rules and characteristics for project, program and portfolio management. The PMBOK Guide is process-based, meaning it describes work as being accomplished by processes. The main goal of PMBOK is to improve life cycle management of any project, program and project portfolio.

• **ISO 27001(International Standard Organization):** specifies the requirements for establishing, implementing, maintaining and continually improving an information security management system within the context of the organization. It also includes requirements for the assessment and treatment of information security risks tailored to the needs of the organization. The main goal of ISO 27001 is to protect the information asset and to comply with legal and regulatory requirements.

• **ISO 20000:** Is a service management system (SMS) standard. It specifies requirements for the service provider to plan, establish, implement, execute, monitor, review, maintain and improve an SMS. Requirements include design, transition, provision and improvement of services to meet service requirements.

C. Overview of EAS-IT GRC

The IT GRC assures the alignment of the objectives of the organization as regards needs defined by the stakeholders. This is illustrated by the progress strategic of a given organization and also by the taken decisions. The proposed solution supplies a high-level model for the IT GRC who will allow the implementation of the IT GRC in an intelligent way. We give a brief description of every layer of the platform EAS-IT GRC (figure 1) for a good understanding of the global architecture [7].

IT GRC platform is composed of four principle layers:

• **Strategic layer:** based on COBIT framework; ensuring permanent alignment of IT and Business with

stakeholders' participation. Its role is to propose new processes of management for the IT department.

• **Decision layer:** assures making a comparative analysis between the best frameworks for each IT process in order to make a decision for the best reference to set up.

• **Processing layer:** This layer is composed of different systems, which can be implemented; it defines the processes and actions to be deployed according to the chosen framework.

• **Communication layer:** It is responsible for all communications between layers of the IT GRC platform.
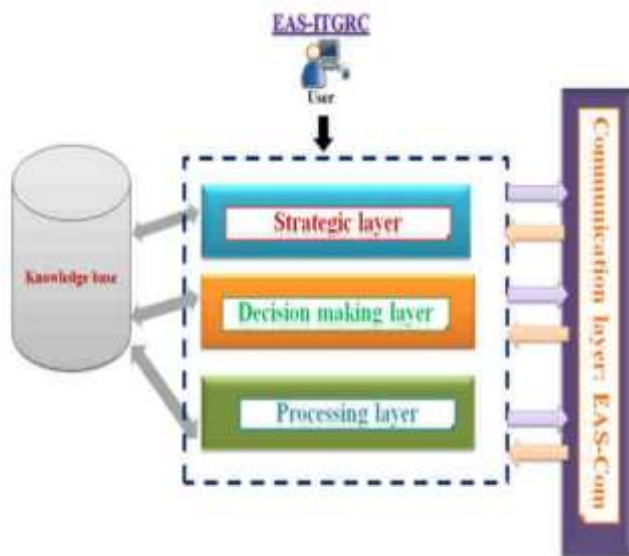

Fig.1: EAS-IT GRC solution

III. PROPOSED ARCHITECTURE EAC-ACM

The bibliographic study on IT solutions GRC enabled us to identify several architectures and solutions of IT governance for companies. The analysis of these solutions allowed us to identify limitations of the IT GRC relative to the actual needs of different companies. Among these limitations we quote:

• The company's IT strategic plan changes after 3 to 5 years because of the new vision of the company, the current IT GRC platforms do not offer solutions for aligning the IS with the strategy business.

• The change in the company's IS strategy directly implies a change in practices of users IT system, which requires auditing existing activities to propose new solutions, the current IT GRC platforms do not allow auditing of existing practices based on best practices and standards.

• The change in IS governance requires new actions to be taken; the current IT GRC platforms cannot generate an IT action plan to implement the new solutions.

In this paper, we focus on the following issue: How can we audit existing practices and plan changes automatically in IT governance in order to implement a new actions and recommendations?

A. Proposed Architecture

Our approach based on EAS-IT GRC allows the audit and generation an IT planning in order to assist the change management.

Our proposal proposes a new layer for audit and change management using Multi-Agent Systems (MAS) in order to automate the link between the actions to be implemented and the roadmap for IT planning towards the implementation of the IT governance.

This proposal is structured in two phases: Audit and Gap Analysis, and change management.

The phase of ensuring Audit and Gap Analysis involves the following steps:

• **Information gathering:** this step allows to list the processes to be implemented communicated by the communication layer and explore the current practices in order to update the knowledge base of the information system.

• **GAP Analysis:** this step allows GAP Analysis between the existing and the proposals of improvements.

• **Proposal for recommendations:** this step allows the identification of actions to be realized within the framework of the change brought by the new governance.

• **Prioritization of actions:** this step allows the identification of the urgency and impact of every action to be realized within the framework of the change brought by the new governance.

The phase of change management involves the following steps:

• **Classification of actions:** this step allows the classification for every action by using the priority of each action.

• **Identification of position:** this step allows identifying the position of each action in the IT planning.

• **Identification of duration:** this step allows the identification of duration of implementation of every activity.

• **Generation of IT action plan:** This step allows the generation and display of the action plan.

EAS-ACM (figure 2) is composed of two multi agent systems (MAS): Audit and GAB analysis and change management.

We believe that developing an expert system will bring significant advantages such as the statistics calculated from the facts base and the use the tools for analysis.

Our system is also based on multi agent systems because agents exhibit a high level of autonomy and function successfully in situations with a high level of uncertainty.
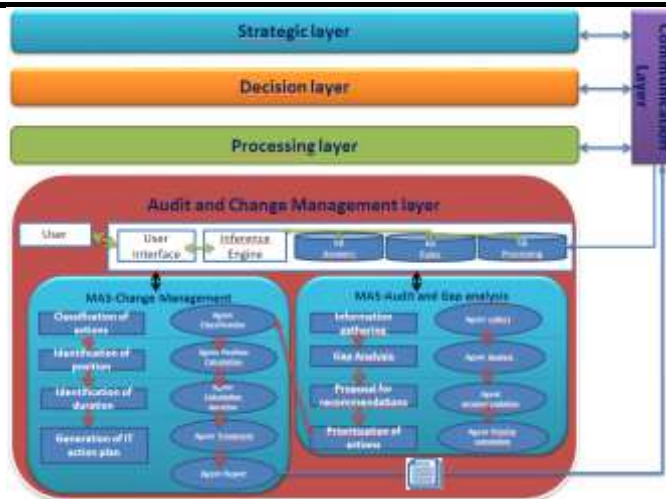
Fig.2: EAS-ACM architecture

B. System Expert

Expert system is one of the areas of artificial intelligent. An expert system also known as knowledge based system is a computer program that contains the knowledge and analytical skills of one or more human experts in a specific problem domain. The goal of the design of the expert system is to capture the knowledge of a human expert relative to some specific domain and code this in a computer in such a way that the knowledge of the expert is available to a less experienced user [8].

It is divided into two sub-systems: The inference engine and the knowledge base

The Knowledge base contains accumulated experience and a set of rules.

The inference engine applies the rules to the known facts to deduce new facts.

This process would iterate as each new fact in the knowledge base could trigger additional rules in the inference engine.

Inference engines work primarily in one of two modes: Forward chaining and backward chaining. Forward chaining starts with the known facts and asserts new facts. Backward chaining starts with goals, and works backward to determine what facts must be asserted so that the goals can be achieved. Four main characteristics distinguish an expert system from a conventional program are as the following:

Expertise: Expert systems use a large amount of knowledge about a particular domain, this knowledge is often subjective, possibly incomplete and subject to change. However, expert systems must have the skills to use this knowledge efficiently in order to solve complex problems quickly.

Symbolic reasoning: In an expert system, the knowledge is explicitly represented in symbolic form, in a structure called the knowledge base.

The inference engines manipulate this knowledge using a set of heuristic rules appropriate to the given domain.

Depth: Expert systems operate in a narrow domain, dealing with hard and challenging problems. They have to use complex rules.

Self-knowledge: An expert system has the feature of explanation capability. It should be able to explain how it has arrived at a particular conclusion.

Besides to that, an expert system can advise, modifies, update, expand and deals with uncertain and irrelevant data

C. Agent and Multi Agent System

An agent is a computer system within an environment and with an autonomous behavior made for achieving the objectives that were set during its design [9].

A multi-agent system (MAS) is a system that contains a set of agents that interact with communications protocols and are able to act on their environment. Different agents have different spheres of influence, in the sense that they have control (or at least can influence) on different parts of the environment. These spheres of influence may overlap in some cases; the fact that they coincide may cause dependencies reports between agents [10].

Starting from the definitions cited above, we can identify the following agent types [11]

• **The reactive agent** is often described as not being "clever" by itself. It is a very simple component that perceives the environment and is able to act on it. Its capacity meets mode only stimulus-action that can be considered a form of communication.

• **The cognitive agent** is an agent more or less intelligent, mainly characterized by a symbolic representation of knowledge and mental concepts. It has a partial representation of the environment, explicit goals, it is capable of planning their behavior, remember his past actions, communicate by sending messages, negotiate, etc.

• **The intentional agent** or BDI (Belief, Desire and Intention) is an intelligent agent that applies the model of human intelligence and human perspective on the world using mental concepts such as knowledge, beliefs, intentions, desires, choices, commitments. Its behavior can be provided by the award of beliefs, desires and intentions.

• **The rational agent** is an agent that acts in a manner allowing it to get the most success in achieving the tasks they were assigned. To this end, we must have measure of performance, if possible objective associated with a particular task that the agent should run.

• **The adaptive agent** is an agent that adapts to any changes that the environment can have. He is very intelligent as he is able to change its objectives and its knowledge base when they change.

• **The communicative agent** is an agent that is used to communicate information to all around him. This information can be made of his own perceptions as it may be transmitted by other agents.

IV.   EAC-ACM FUNCTIONALITIES

In our proposal, we are interested in the study of the two main components of our system that is the Audit and change management.

The main objective of EAC-ACM is to generate the IT planning to meet the needs of the new politic of IT Governance.

In the following, we will present two integrated multi-agent systems constitutes the EAS-ACM toolkit: "MAS-audit and Gap analysis" and "MAS change management".

A.   MAS-Audit and Gap Analysis

This System asks the users of the practices existing, analyses the answers to questions using its knowledge base, and calculates the difference in order to generate the recommendations. Our system displays the recommendations and asks the user to define the urgency and the impact of each action.

Our expert system is based on the data collection and analysis of the environment by the agents.

Its knowledge base contains the best practices communicated by the processing layer as well as the rules of calculation of the mathematical formulas.

Data collection is carried out by agents by means of questionnaires, and the answers are recorded, and analyzed by the expert system of our architecture.

The answers to the questionnaire should give a view on the priority of the actions to be implemented in the company. A. MAS-Audit and Gap Analysis consists of four agents which are:

• **Agent collect:** After receiving all the activities and processes from layer communication, this agent has the role of displaying a survey to the user in order to gather the current practices.

• **Agent Analyst:** This agent analyzes the difference between the existing and the practices recommended by the communication layer in order to discover changes.

• **Agent recommendations:** At this level, this agent generates the list of new activities and updates the knowledge base of expert system.

After this all, this agent is responsible of gathering the impact and urgency of every action to be realized within the framework of the change brought by the new governance

• **Agent Priority Calculation:** This agent allows the calculation of the priority of each action with this formula:

$$Priority = Impact * urgency$$

B.   MAS-Change Management

The major goal of this agent system is to generate the IT action plan in order to deploy the new practices.

To achieve this goal, we must calculate the position and duration of each action; for it, we propose two formulas mathematics which use the value of the priority to be able to calculate the date of starting up of the implementation of the activity as well as the duration estimated to deploy all the actions.

The MAS-Change Management of our platform is responsible of producing a report concerning the IT action plan.

Agents involved in the running of this agent system are:

• **Agent Classification:** based on the priority of each action, this agent allows displaying activities with a chronological order.

• **Agent Position Calculation:** this calculates the value of position of every action with formula:

$$Position = 1/Priority * Q$$

Q represents a number from 1 to 3

Q is equal to 1 if the activity is concerning an organization

Q is equal to 2 if the activity is relative to a tool

Q is equal for three if the activity is relative in the implementation of a new management method.

• **Agent Duration Calculation:** in order to draw the road map, this calculates the value of duration of implementation of every action according to the following rule base

An activity bound to an Organizational change must be realized in a deadline 1 month

An activity bound to a Technological change must be realized in a deadline 2 months

An activity bound to a change Methodology must be realized in a deadline 3 months

The duration is represented by a bar which defined the week number or month to realize the recommendations.

• **Agent Treatment:** The calculation of position and duration for the set of the activities will allow us to take out with a detailed action plan of the implementation of the best practices of IT governance; this allows the generation and display the road map.

• **Agent Report:** it produces a report containing an overview of the road map in question, this will give a visibility onto the projects with short, average and long term relative to the implementation of best practice IT within a department of Information systems.

V.   CONCLUSION

In this paper, we proposed the use of a Multi-Agent System in a multi-system architecture to discover and set up the new practices brought by IT framework. The objective is to generate the road map for change

management in order to deploy new IT governance processes. The use of a knowledge base containing all the information about the company IT framework is required to explore the changes and thus be able to propose an IT action plan for the implementation of new practices.

Future work involves developing a simulation of our prototype based on multi-agent systems.

REFERENCES

[1]. Gary Hardy Using IT governance and COBIT to deliver value with IT and respond to legal, regulatory and compliance challenges information security technical report11 2006 page 55-61

[2]. M.N. Kooper, R. Maes, E.E.O. Roos Lindgreen "On the governance of information: Introducing a new concept of governance to support the management of information". International Journal of Information Management: The Journal for Information Professio-Professionals, Volume 31 Issue 3, June, 2011, Pages 195-200

[3]. Gill, S., & Purushottam, U. (2008). Integrated GRC-is your organization ready to move. Governance, risk and compliance. SETLabs Briefings, 37-46.

[4]. Frigo, M. L., & Anderson, R. J. (2009). A strategic framework for governance, risk, and compliance. Strategic Finance, 90(8), 20.

[5]. Tarantino, A. (2008). Governance, risk, and compliance handbook: technology, finance, environmental, and international guidance and best practices. John Wiley & Sons.

[6]. Wagner, S., & Dittmar, L. (2006). The unexpected benefits of Sarbanes-Oxley. Harvard business review, 84(4), 133.

[7]. Aziza Chakir, Meriyem Chergui, Soukaina Elhasnaoui, Hicham MEDROMI, Adil Sayouti, Intelligent Plateform to Select The Best IT-GRC Framework For Treatment The Needs Of Stakeholders (International Journal of Applied Engineering Research ISSN 0973-4562 Volume 11, Number 12 (2016) pp 7829-7835)

[8]. Dennis Ritchi (1996), artificial Intelligent, Tata McGraw-Hill, New Delhi.

[9]. M. Wooldridge, Intelligent Agents, Multi agent systems, In The MIT Press, "A modern Approach to Distributed Artificial Intelligence", (England Massachutts London: MIT Press Cambridge, 1995, p. 27-78)

[10]. M. Wooldridge, An Introduction to Multi-Agent Systems, Wiley & Sons, 2000.

[11]. S. Maalal, M. Addou, "A practical application of a method of designing multi-agent systems based on the AUML language and the MDA approach", Proceedings of the Fourth Workshop on Information Technologies and Communication WOTIC"11, Casablanca, Morocco, p.104, 2011.

Potential of Egg shell powder as replacement of Lime in soil stabilization

Anoop S P[1], Hizana Beegom[1], Jwoleena P Johnson[1], Midhula J[1], Tharis Muhammed T N[1], Prasanth S[2]

[1]Under graduate students in Civil Engineering, UKF College of Engineering & Technology, Kollam, Kerala, India
[2]Assistant Professor in Civil Engineering, UKF College of Engineering, Kollam, Kerala, India

Abstract— *This paper presents a study on the properties of soil stabilized by using lime and egg shell powder. Tests were conducted to assess the potential of egg shell powder in replacing lime, which can make the overall stabilization process economical and eco-friendly. Results obtained show that all the treated mixes gave much better strength than untreated soil. Egg shell powder was introduced in quantities of 0.5%, 1%, 1.5% and 2% of the weight of soil. Tests were conducted replacing up to 50% of the lime used for stabilization. It was observed that 25% replacement of lime by egg shell powder gave better strength properties and can be adopted for practical purposes.*

Keywords— *Lime, Soil stabilization, Egg shell, improvement, Geotechnical, replacement*

I. INTRODUCTION

Improvement of soil properties is necessary in the modern scenario as soils with the required properties are not readily available for construction activities. There have been a lot of issues reported when structures were constructed on weak and soft soils like problems of shear failure, excessive settlement, differential settlement etc. The alternatives left with us are making the soil at site suitable for the expected load by improving its properties or adopting a deep foundation. Adoption of deep foundation is not at all an economically viable solution. Hence improvement of soil properties and in-situ treatment of soil are gaining importance these days. Soil stabilization is an economically feasible solution to one of the major construction problems. Researchers all over the world have studied various materials which can be used in conjunction with soil to improve soil properties. (Basha, 2005) studied the stabilization of soil with Rice husk ash and cement. (Brooks, 2009) conducted stabilization studies on stabilization using fly ash and rice husk ash. (Kamon, 1991) conducted researches on stabilization of soil using lime and industrial wastes. (Paul, 2014) conducted studies on soil stabilization using egg shell powder and quarry dust. (Anoop S P, 2017) conducted studies on improving soil using lime and elephant dung

strips. Of all the various studies conducted around the world, the most commonly used and effective stabilizer was found to be lime. Lime is a not an industrial waste or a by-product, the manufacture of lime requires heating in the order of 750° C, which contribute to the fact that stabilization of large areas of soil with lime alone will increase the cost required for stabilization. In this study an attempt is made to replace lime with egg shell powder and to find out the extent up to which lime can be replaced by egg shell powder without compromising on the strength.

Egg shell powder is an ideal material to replace lime in the stabilization process due to its similar chemical composition. The chief ingredient in egg shell powder is calcium carbonate as in the case of lime. Egg shells are disposed from hotels, restaurants etc in huge quantities and they are currently facing disposal problems. Use of egg shell powder in soil stabilization reduces the disposal problems associated with egg shell generations. Moreover, powdering of egg shell can be done easily. Egg shell powder generation does not involve generation of CO_2 as in the case of lime where heating is done up to 750°C. Hence use of egg shell powder in soil stabilization will make the overall stabilization process economical, sustainable and eco-friendly.

II. MATERIALS AND MIXES

The materials used for this study consist of Soil, Lime and Egg shell powder. Soft clayey soil from Chathanoor area of Kollam district in Kerala was used for the study. Lime was purchased from the local markets and Egg shells were collected from hotels and restaurants in Parippally. The egg shells, thus collected were crushed and made into powder form. This was then sieved through 75 micron IS sieve so as to bring it to the size range of fine grained soil. The egg shell powder used for the study is shown in Fig 1

Fig.1: Egg shell powder

The materials mentioned above were mixed in various proportions for studying its effect on the soil stabilization process. First of all, the untreated soil was tested and its strength was obtained to understand whether there is need for stabilization. To this untreated soil mix, optimum lime content calculated as per ASTM D 6276 standards was added. The optimum lime content was found to be 4% of the weight of soil. Then egg shell powder was introduced as a replacement to lime in the stabilization process. The proportions of lime and egg shell powder were varied keeping the total replacement amount a constant. The various mixes used in this study are mentioned in table 1.

Table.1: Mixes used in this study

Mix designation	Details
C	Untreated soil
C + 4L	Clay + 4% weight of soil replaced by lime
C+3.5L+0.5ESP	Clay + 3.5% lime replacement and 0.5% weight replaced by egg shell powder
C+3L+1 ESP	Clay + 3% lime replacement and 1% weight replaced by egg shell powder
C+2.5L+1.5ESP	Clay + 2.5% lime replacement and 1.5% weight replaced by egg shell powder
C+2L+2 ESP	Clay + 2% lime replacement and 2% weight replaced by egg shell powder

III. TESTS CONDUCTED

Experimental tests were conducted on untreated soil as well on lime and egg shell powder modified mixes in order to study the effect of addition of egg shell powder. The various tests conducted were atterberg limits, compaction and unconfined compression test. All these tests were carried out as per IS 2720 standards.

IV. RESULTS AND DISCUSSIONS

The soil mixes mentioned above were tested and the results obtained are summarized in table 2. Unconfined compressive strength of in situ soil was found to be only 0.45 kg/cm^2 which indicate the necessity for soil stabilization. When the soil was mixed with optimum lime content, there was a drastic change in the strength of soil sample. The strength almost doubled upon introduction of lime.

Table.2: Results of experimental tests on untreated and modified soil mixes

Sample	Liquid limit (%)	Plastic limit (%)	OMC (%)	γ_d (g/cc)	Mean UCC (kg/cm^2)
Untreated soil	24	11	18	1.76	0.45
C+ 4L	30	12.41	20	1.8	0.88
C+3.5L+0.5ESP	33	12.71	20	1.83	0.85
C+3L+1ESP	34	13.08	22	1.87	0.92
C+2.5L+1.5ESP	35	13.1	22	1.77	0.81
C+2L+2ESP	35	13.01	22	1.77	0.68

There were not much variations in the atterberg limits of the soil sample on addition of egg shell powder. Egg shell powder was not found to alter the flow and consistency behavior of the soil sample. The variation of atterberg limits with the addition of egg shell powder is shown graphically in Fig 2.
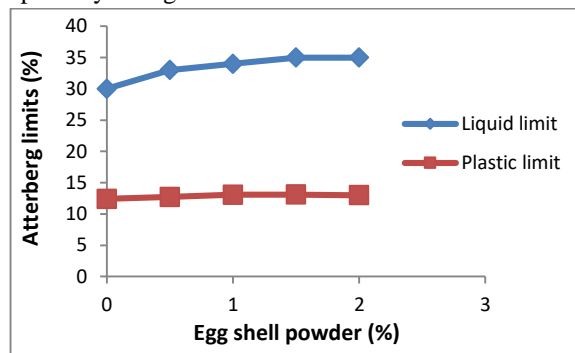

Fig.2: Variation of atterberg limits with Egg shell powder

Compaction tests showed an increase in the dry density upto 25% replacement of lime by egg shell powder. Above 25% replacement of lime by egg shell powder, dry density started to decrease. Egg shell powder is not that compatible a material as lime and hence when added in large quantities to replace lime, soil properties could not be improved. The variations in dry density on the addition of egg shell powder to lime modified mix is shown in Fig 3.
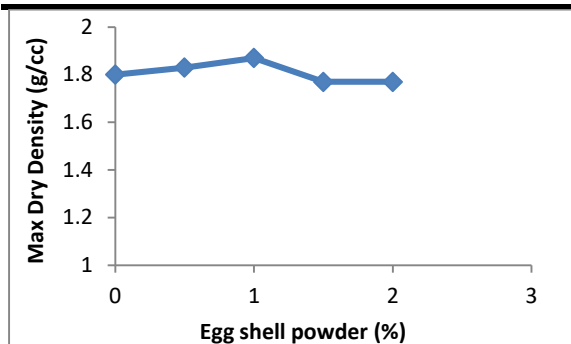
Fig.3: Variation of dry density of soil on adding egg shell powder

All the soil mixes were tested for their unconfined compressive strength. The results show that there is an increase in unconfined compressive strength upto 25% replacement of lime by egg shell powder. Above this level of replacement, the strength was found to decline. Addition of small dosages of egg shell powder improved the strength of lime modified mix. As the replacement percentage increased, the strength started to fall as shown in figure 4. This may be due to the fact that egg shell powder is not an efficient material as lime and increasing egg shell powder will reduce the total lime content. Addition of small dosages of egg shell powder increased the rate of pozzolanic reaction occurring and hence gave a higher strength. All the modified mixes gave much better strength than untreated soil as shown in Fig 4.
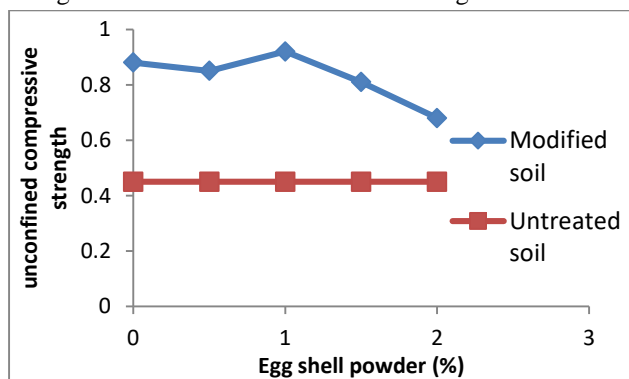

Fig.4: Variation of UCC with Egg shell powder

V.   CONCLUSIONS

Egg shell powder was found to be a very good alternative in replacing the costly lime used for soil stabilization. The use of egg shell powder in soil stabilization will reduce the disposal problems of egg shell as well as make the stabilization process economically and sustainable. From the study, it was seen that egg shell powder can replace upto 25% of the lime used for stabilization process. This replacement also increased the strength of treated soil. Thus it can be concluded that egg shell powder is an ideal material to replace lime in the soil stabilization process owing to its similar chemical compositions and properties

REFERENCES

[1] Amu, O. O., A. B. Fajobi, and B. O. Oke. "Effect of eggshell powder on the stabilizing potential of lime on an expansive clay soil." Journal of Applied Sciences 5.8 (2005): 1474-1478.

[2] Bowles, Joseph E. "Physical and geotechnical properties of soils." (1979).

[3] Petry, Thomas M., and Dallas N. Little. "Review of stabilization of clays and expansive soils in pavements and lightly loaded structures—history, practice, and future." *Journal of Materials in Civil Engineering* 14.6 (2002): 447-460.